ACTA Mineralogica Petrographica

ACTA MINERALOGICA-PETROGRAPHICA, FIELD GUIDE SERIES, VOL. 16, PP. 1–51.

Mineral deposits of the Fore-Carpathian region and weathering processes of monuments in polluted atmosphere in Kraków (SW Poland)

Edited by MAREK MICHALIK*

Institute of Geological Sciences, Jagiellonian University, Kraków, Poland; marek.michalik@uj.edu.pl (*communicating author)

Written by WANDA WILCZYŃSKA-MICHALIK[1a], MAREK MICHALIK[2b], ANDRZEJ ŚLĄCZKA[2c] AND HARRY KUCHA[3d]

[1] Institute of Geography, Pedagogical University, Kraków, Poland; [a]wmichali@up.krakow.pl
[2] Institute of Geological Sciences, Jagiellonian University, Kraków, Poland; [b]marek.michalik@uj.edu.pl; [c]slaczka31@tlen.pl
[3] Faculty of Geology, Geophysics and Environmental Protection, AGH University of Sciences and Technology, Krakow, Poland; [d]kucha@geol.agh.edu.pl

Table of contents

0. General introduction

During the field trip building stones used in historical monuments in Kraków will be presented and weathering processes in polluted urban atmosphere will be discussed. Historical salt mine in Wieliczka situated in the Carpathian Foredeep and a Mississippi Valley-type (MVT) lead and zinc deposit in the Pomorzany Mine will be visited. Environmetal problems related to lead and zinc mining will be discussed during the presentation of the flotation waste and metallurgical slags dumps.

The Upper Jurassic limestones form characteristic forms in the Kraków area landscape *i.e.* narrow and relatively deep valleys and white limestone crags and cliffs. Older rocks (Middle Jurassic, Triassic, Permian, Carboniferous and Devonian) crop out in the western part of the Kraków area. Cretaceous rocks are exposed mainly in the eastern part of the area. Miocene deposits are present in the young tectonic depression in the southern part of the area Upper Paleozoic form the foreland of the Variscan orogen zone situated further west (Gradziński, 2000). Details of the local geology will be discussed in relation to objects presented.

Day 1 (Part A)

1. Route from Budapest to Kraków

ANDRZEJ ŚLĄCZKA

Budapest is located in the northern part of the Pannonian Basin (Fig. A1), a young, deep Neogene depression filled by a sedimentary succession. The basement of this basin is built up of Paleozoic to Lower Tertiary formations representing the sedimentary cover of the Apulian Plate.

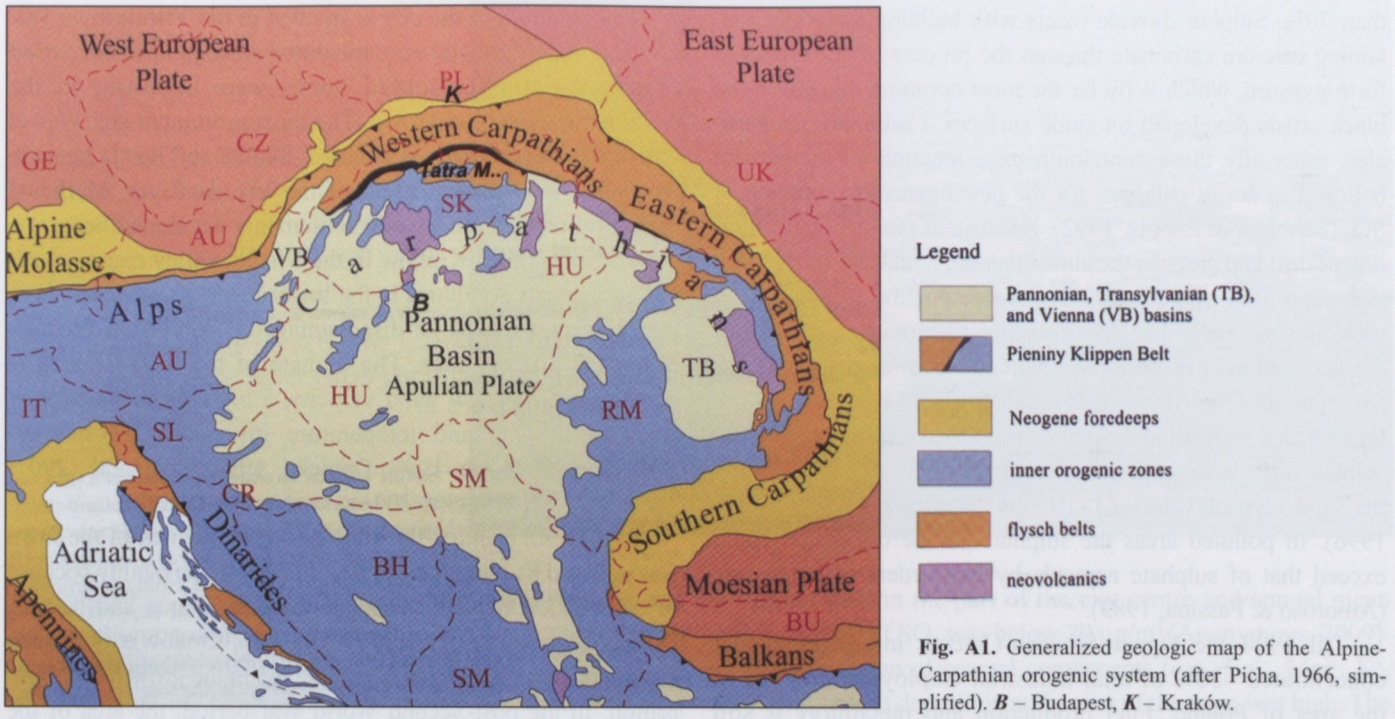

Fig. A1. Generalized geologic map of the Alpine-Carpathian orogenic system (after Picha, 1966, simplified). ***B*** – Budapest, ***K*** – Kraków.

Along the road to Kraków, the field trip route crosses at first the Transdanubian Central Range built up mainly of Triassic limestones representing a fragment of uplifted basement within the Pannonian Basin, and later on enters the Carpathians, the eastern prolongation of the Alps. This part of the Carpathians, due to differences in their depositional and structural history, is divided in two parts: the Inner and Outer Carpathians, separated by the narrow zone of the Pieniny Klippen Belt. The Inner Carpathians, which constitute a sedimentary cover of the northern part of the Apulian Plate, are built up of Permian/Lower Triassic to the mid-Cretaceous sedimentary successions and were deformed and thrusted in the Late Jurassic up to Late Cretaceous. In the northern part, the Tatra area, a post-tectonic depression was formed and filled up mainly by flysch deposits of the Late Tertiary age. The Pieniny Klippen Belt is a complex suture, which was affected by both the Late Cretaceous and Tertiary tectonic phases.

The Outer Carpathians, also known as the Northern or Flysch Carpathians, developed on the thinned continental crust of the southern margin of the Northern European Plate. They are built up by flysch deposits of the Late Jurassic to Early Miocene. As a result of intense Miocene orogeny, the sediments were folded and detached from their substrate, and several uprooted nappes were created. The whole Outer Carpathians are overthrusted onto the European plate and the inner part of the Miocene foredeep basin for a distance of more than 100 km. Along the northern margin of the Carpathians a narrow belt of folded Miocene deposits occur. Leaving the Carpathians Mts. and approaching Kraków, the field trip route crosses narrow depressions, filled by Miocene deposits, which represent the outer part of the foredeep basin. Hills around Kraków are horsts built up of Upper Jurassic limestones.

Day 2 (Part B)

2. Kraków: presentation of the monuments and weathering processes of building stones

WANDA WILCZYŃSKA-MICHALIK
& MAREK MICHALIK

2.1 Introduction

Human influences on the composition of the atmosphere are harmful to cultural heritage. Recent anthropogenic emissions of sulphur dioxide (SO_2), carbon oxides (CO, CO_2), and nitrogen oxides (NO_x) have a much larger acid-generating capacity than natural fluxes. Irrespective to pH value, high concentration of atmospheric pollution and high load of contamination in atmospheric precipitation is also an important factor of decay of building stones. Pollution by the products of fossil fuels combustion remains a major environmental issue, with well-documented health and material damage effects.

Coal is the basic fuel utilised in Poland, both for industrial energy production and for individual domestic use by high percentage of the population. Combustion of coal in power plants and home furnaces is a source of sulphur dioxide, nitrogen oxides, fly ash and soot. Relatively low temperature of burning of coal in home furnaces causes emission of compounds containing a lot of soot and tarry material. Such material contains potentially toxic compounds of which benzo(α)pyrene is an example (Clarke, 1996).

Relative humidity influences sulphur dioxide oxidation rates. Generally, the rate of conversion increases sharply as the relative humidity increases above 70% (Amoroso & Fassina, 1983). The relative humidity of the atmosphere in Kraków is usually higher

than 70%. Sulphur dioxide reacts with building materials containing calcium carbonate through the process of sulphation to form gypsum, which is by far the most common mineral in the black crusts developed on stone surfaces. Carbonaceous particles, especially those containing trace amounts of metals, are believed to act as catalysts for the heterogeneous oxidation of SO_2 (Sabbioni & Zappia, 1992). Because of the high concentration of dust and gases in the atmosphere in Kraków, both dry and wet deposition of pollutants is a cause for the weathering of rocks in stonework. The dry deposition phenomenon consists of the accumulation of airborne pollutants from atmosphere on a stone surface (*e.g.* Amoroso & Fassina, 1983; Livingston, 1989). Overall dry deposition velocities measured experimentally for sulphur dioxide range from below 5×10^{-3} ms^{-1} to nearly 2×10^{-2} ms^{-1} and a typical value of 1×10^{-2} ms^{-1} is often assumed (Clarke, 1996). In polluted areas the sulphur dioxide deposition could exceed that of sulphate aerosols by two orders of magnitude (Amoroso & Fassina, 1983).

Till 1994 the Upper Silesian-Cracow industrial district concentrated ~30% of total industrial employment on 6% of the area of Poland. Fuel production and metallurgy is still important in the branch structure of industry in the majority of the centres in the Upper Silesian Industrial District. Hard coal is the most important energy carrier in this region and its combustion causes air pollution with toxic substances such as: sulphur dioxide, benzo(α)pyrene, nitrogen dioxide and dusts. Generally, in the last twenty years of the 20th century, the emission of atmospheric pollutants in the Upper Silesian Region has been reduced (Oleś, 2001).

2.2 Kraków area

Kraków is one of the largest cities of southern Poland located upon the Vistula River. The earliest human settlements in the Kraków area date back to the Stone Age. The town is rich in historic monuments unique in a world scale from each epoch of its over thousand-year history. History of Kraków and its architectural monuments is a synonym of Polish identity. At present, Kraków has a population of 930,000 out of which more than 170,000 are students of universities.

In 1978, UNESCO decided to register Kraków as one of the world's most precious paradigms of cultural heritage. Extensive conservation works in Kraków began at the end of the seventies of 20th century. Kraków as the city of exceptional significance for Polish and European culture requires special treatment during preservation and renovation work on its monuments. Numerous monuments have been heavily damaged because of the aggressive atmosphere. In 1994, the local government created new plans of city spatial development and the preservation and renovation of cultural sites was set among the main objectives. In recent years, most of the historical buildings have been renovated (Fig. B1) and recovered their former splendour.

The old town of the city is situated in the Vistula river valley. The upper terraces were inhabited since prehistoric period (Tyczyńska, 1968). Isolated horsts were important in the development of the old town. The most prominent are: Wawel where the Royal Castle is situated, Skałka and horsts beneath the centre of the town north of the Vistula River. Medieval town originated from several settlements developed here.

The location of Kraków in the Vistula valley causes accumulation of air pollutants in the lower layer of the atmosphere that in turn is a cause of disadvantageous conditions for residents and historic sites. The climate of the Kraków area is characterized by low wind velocity, a high number of foggy days and nights and temperature inversions (Morawska-Horawska & Lewik, 1997; Dębicka, 1999; Brzeźniak, 2001; Trepińska & Skublicka, 2001).

In the 19th century, the atmosphere of the area of the town was polluted by coal smoke and sulphur dioxide mainly because of combustion of solid fuels in industrial plants and houses. During the second part of the 19th century, Kraków experienced rapid industrialisation that was reflected in the growth of urbanisation. In the post-Second World War period, the area of the city has become increasingly industrialised, with metallurgical and chemical sectors as the most important. Multiple threats to the historic substance of Kraków became evident already in the early seventies of 20th century. The priority of development of heavy industry shook the ecological balance and caused violent destruction of the city's environment (Fig. B2).

The pH value of individual and average monthly precipitation in Kraków varied in broad limits. The average pH for the period 1994–1998 fluctuated between 4.47 in the western part of the town, through to 5.09 in the city centre, and up to 5.6 in the eastern part of Kraków (Chmura & Godzik, 1996; Godzik, 1999). A tendency of increase in the alkalinity of precipitation in the eastern part of the town is related to particulate emission of the ArcelorMittal Steelworks (formerly Lenin Steelworks and later Sendzimir Steelworks) and other industrial plants situated nearby (Fiszer, 1990; Turzański, 1991; Godzik, 1999). The relative humidity (RH) of the atmosphere in Kraków is high. The average monthly RH value in the town often

Fig. B1. City walls of Kraków before renovation (right) and after renovation (left).

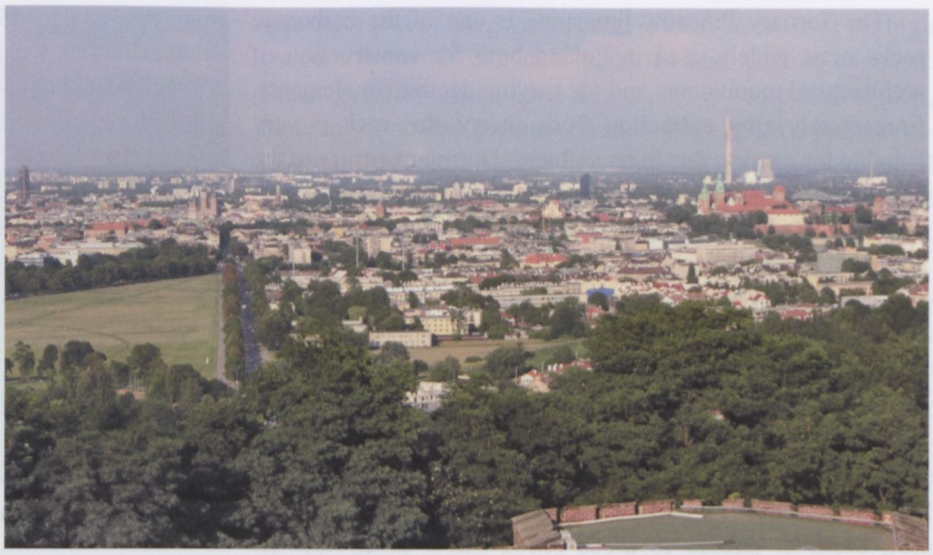

Fig. B2. Historical centre of Kraków (Royal Castle, Market Place) and industrial plants (Power Plant, Steelworks) in the background.

exceeds 80%. The influence of strong industrialisation and urbanization on climate in the city is marked by thermic pollution (Lewińska, 1979, 1996), high frequency of occurrence of inversion of temperature, lowering of wind velocity, decrease in sunshine and reduced air transparency (Matuszko, 2007). In the 1970s, the duration of insolation in the city of Kraków was less by about 10% in the whole year period, and up to 30% in winter in comparison with the surrounding area (Olecki, 1975). Kraków is a poorly ventilated city, with many "canyon"-like narrow streets with high building along them. The average wind velocity range about 1.8 m/s and is often lowered in the centre of the town because of buildings. At night, inversion of temperature in the urban area occurs nearly permanently (Walczewski & Łukaszewski, 1986).

A higher reduction of emissions of industrial dust in the town compared to gaseous emissions caused the shift of average pH of rains in Kraków to lower levels in the last few years of the 20th century because of the decrease in the effect of neutralisation of sulphur and nitrogen compounds by alkaline dusts. A gradual acidification of wet deposition may be expected in the near future.

In the city centre of Kraków, the highest average annual concentration of suspended dust (PM10; particulate matter <10 μm) and sulphur dioxide were noted in the period from 1968 to 1987. For that period, the average annual concentration of sulphur dioxide (SO_2) varied from 83 μg/m³ (1971) to 122 μg/m³ (1985), concentration of suspended dust varied from 143 μg/m³ (1977) to 195 μg/m³ (1979) (Lach *et al.*, 1996). The average annual concentration of sulphur dioxide (SO_2) and suspended dust in the city centre of Kraków during the period from 1982 to 1992 varied significantly. The highest average annual concentration of SO_2 was noted in 1985 (122 μg/m³) and the lowest (75 μg/m³) in 1990 and 1992. In the centre of the town, the average annual concentration of suspended dust (PM10) during the period from 1982 to 1992 varied from 116 μg/m³ in 1986 to 52 μg/m³ in 1992. In 2008 the annual concentration of suspended dust (PM10) was noted at level above 60 μg/m³ only in the part of the city centre and annual mean concentration of SO_2 was below 20 μg/m³ (Anonymous, 2009).

Concentration of several components (*e.g.*, Ca^{2+}, Mg^{2+}, K^+, Cl^-, SO_4^{2-}) in wet deposition at the area of the town was high. The average annual wet deposition of SO_4^{2-} was 2034 mg/m² in 1994 and 2036 mg/m² in 1998. For Ca these values were 6054 mg/m² and 2488 mg/m², respectively (Anonymous, 1995; Anonymous, 1999). In the 21st century, deposition of various components with atmospheric precipitation decreased. In 2008 wet deposition of most components was lower comparing with averages values for the period 1999–2007 (Anonymous, 2009).

2.3 Building stones used in Kraków

Numerous types of building stones of different origin were used during the long history of the town, most commonly sedimentary rocks quarried relatively close to the town. The Upper Jurassic limestone from the Silesian-Cracow Monocline, the black bituminous Devonian limestone well known as Dębnik marble, the Middle Triassic dolomite (the Libiąż dolomite), the Tertiary Pińczów limestone, and different sandstones of the Carpathians were the main raw materials used in the construction of monuments in Kraków (*e.g.* Kuźniar, 1918; Dobrowolski, 1950; Tatarkiewicz, 1951; Skalmowski, 1956; Grabski & Nowak, 1957; Weber-Kozińska, 1967; Fabryczek, 1973; Michalik, 1981; Małecki *et al.*, 1988, 1991b; Rutkowski, 1996; Pietrzyk-Sokulska, 2001; Rajchel, 2002, 2004; Wilczyńska-Michalik, 2004). During the field trip we will discuss weathering processes of these rocks in polluted urban atmosphere.

The Upper Jurassic limestone have been quarried in some places near the old town and exploited from the Vistula River alluvia. It was commonly used as building material in historical monuments of Kraków since the Romanesque period. The Upper Jurassic limestone was also commonly used as material for pavements. Limestones excavated near Kraków area was also used for lime production (Rutkowski, 1996).

The Tertiary Pińczów limestone is one of the carbonate rocks most widely used in Poland both for construction of architectural monuments and for carving decorative elements. Immediately after extraction from quarry, this rock is very suitable for carving due to its softness. During exposure to the atmosphere, the material dries and hardens considerably, preserving perfectly the sharpness of the carved features. A rapid expansion of the use of this material in Kraków occurred in the 13th century after the establishment of the Gothic city. The Pińczów limestone became very popular during the Renaissance period. In the 16th century, Santi Gucci, architect of Florence, established a workshop in Pińczów specialised in the prefabrication of architectural and sculptural elements, which were transported to different places, often to quite distant ones (Ahmed & Płuska, 2000; Chrzanowski, 2000).

The black Dębnik limestone (so-called "Dębnik marble") was well known as a building stone since Medieval time but its use for building decoration in Kraków and its environs started during the 17th and 18th centuries. The stone has been excavated in Dębnik near Krzeszowice since 1630. During 17th and 18th centuries, a lot of quarries and also stone-cutting workshops existed in the Dębnik area (*e.g.*, the oldest quarry called "Carmelitan"). Having been polished, the Dębnik limestone acquires black colour but exposed to the atmospheric influence, its colour changes from black into steel-grey. The Dębnik limestone exhibits good physical properties, gives a good polish and shows the original design.

The Middle Triassic (Muschelkalk) dolomite known as the Libiąż dolomite was most extensively exploited in 19th and 20th centuries and was transported from about 40 km distance to Kraków. It was used for example for construction of revetment walls of the Vistula River, bridges, and monumental buildings. Limited scale exploitation of this stone has been started earlier (*e.g.*, stone used in façade of the baroque St. Peter and Paul church).

Among the Carpathian sandstones, only a few types are suitable raw materials for production of block stones, plates and geometric elements (Bąk *et al.*, 1998). Carpathian sandstones were used in the whole history of the Kraków architecture. The most widely used in architecture is the Istebna sandstone (Rajchel, 2002). According to Tatarkiewicz (1951), the Dobczyce sandstone (a sandstone of the Istebna type) was the favoured for works by Italian architect and sculptor Bartolomeo Berrecci. For a long time, Lgota beds Cretaceous sandstones were exploited near Kalwaria. The Godula sandstones were used in construction of churches in Kraków (*e.g.* St. Andrew church).

2.4 Weathering of building stones in polluted atmosphere in Kraków

Weathering of building materials in historical monuments in Kraków was studied intensively by numerous authors since the nineties of 20th century (*e.g.*, Andrzejewski *et al.*, 1992; Florczyk *et al.*, 1998; Haber *et al.*, 1988; Kozłowski & Magiera, 1989; Kozłowski *et al.*, 1990; Magiera & Kozłowski, 1995; Małecki *et al.*, 1991; Manecki *et al.*, 1982, 1995, 1996a, 1996b, 1998a, 1998b, 1999; Marszałek, 1992, 1995, 1999, 2000, 2001, 2004, 2008; Marszałek & Skowroński, 2010; Marszałek *et al.*, 2006; Michalik & Wilczyńska-Michalik, 1998; Pawlikowski, 1959; Rembiś & Smoleńska, 2003; Smoleńska & Rembiś, 1999a, b; Wilczyńska-Michalik, 1997, 1998, 1999, 2004; Wilczyńska-Michalik *et al.*, 1994, 2008; Wilczyńska-Michalik & Michalik, 1991a, 1991b, 1993, 1998a, 2006). A large number of studies were related to disastrous conditions of monuments in the town characterized by exceptionally high level of atmospheric pollution.

2.4.1 Upper Jurassic limestone

Presence of strongly contrasted white and black zones on rock surfaces is the most characteristic feature of weathered Upper Jurassic limestone (Fig. B3). Intense development of black zones is typical of surfaces sheltered against direct rain-washing (Fig. B4). Especially intense blackening on humid surfaces exposed to the north is well visible on vertical walls of monuments in Kraków. White zones are typical of intensively rain-washed surfaces. In Kraków, the development of white surfaces is higher on walls of western exposition. In numerous buildings, each building block is white at the upper side (the washed surface) and black on the lower side (the sheltered surface). Grey zones in deep hollows between building blocks are related to dry deposition. Black zones are covered by black gypsum crust. The surface of black gypsum crust is uneven with subparallel folds on vertical walls (Fig. B4) and mushroom-shaped forms on overhanging surfaces. Formation of folded gypsum crust is related probably to the downward movement of gypsum crystals in water suspension during evaporation after precipitation.

Fig. B3. Black zone covered by gypsum crust (on the surface sheltered against direct rain-washing) and white zone (on the surface intensively washed by rain-water) on a block of the Upper Jurassic limestone; Kraków, City Walls.

Fig. B4. Folded surface of black gypsum crust on the Upper Jurassic limestone; Kraków, City Walls.

Fig. B5. Cross-section of the black gypsum crust on the surface of the Upper Jurassic limestone; gypsum veinlets and nests below the rock surface. Optical microscope, crossed polars.

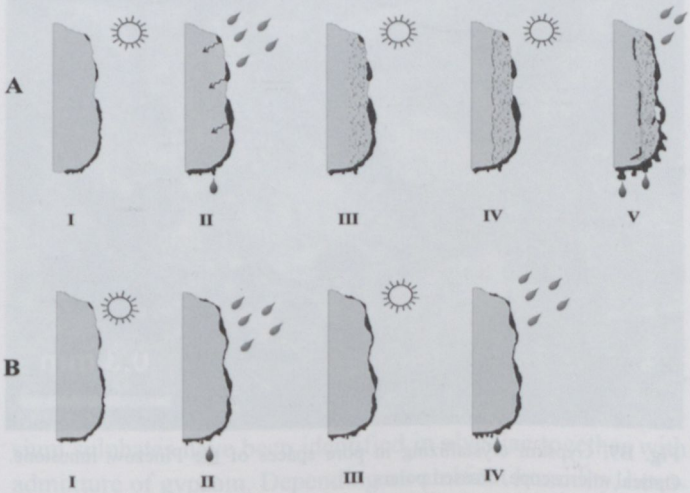

Fig. B6. Different mechanisms of formation of the black gypsum crust on the surface of the Upper Jurassic limestone in urban (A) and rural (B) areas (from Wilczyńska-Michalik, 2004).
A: I – dry deposition of pollutants, II – crystallization of gypsum on the surface, reaction of precipitation with calcite ($CaCO_3$) on the surface, penetration of the solution into the rock, III – crystallization of gypsum nests inside the rock, IV – formation of fissures between the gypsum-rich layer and gypsum-devoid limestone, V – growth of gypsum veinlets inside the limestone, gypsum nests and superficial gypsum crust, VI – exfoliation and disintegration of rock;
B: I – dry deposition of pollutants, II – reactions of rainwater with calcite ($CaCO_3$) on the surface, III – Crystallization of gypsum from the evaporating solutions, IV – partial dissolution of the former gypsum crust, reaction of solution with calcite, crystallization of gypsum.

The outer part of the gypsum crust is black because of the high concentration of dark dust particles and organic pigment. Black gypsum crust (0.5–3 mm thick) is composed of fine, randomly oriented gypsum crystals (Fig. B5). Gypsum crystals on the outer surface are anhedral and contain small amounts of Na, Cl and other elements. Filamentous fungal hyphae, bacteria or algae are often present on the surface. Halite and neomorphic, nonstoichiometric dolomite are sometimes present on the black crust surface. Locally, blistering of the black gypsum crust occurs. In the Upper Jurassic limestone in Kraków, gypsum veinlets and nests are present below the surface of the rock in the outermost, up to 5 mm thick, layer of the rock (Fig. B5).

Black and white zones are also present on surfaces of the Upper Jurassic limestone in outcrops or in old quarries in rural environments. Black zones could be similar to those from urban area *i.e.* covered by black gypsum crust or related to the presence of black organic pigment or dark coloured calcite. Gypsum nests and veinlets are absent below the rock surface in rural areas. Black gypsum crust in rural environment contains usually less dark pigment. On the crust surface, gypsum crystals are euhedral, often with dissolution voids. The differences in black gypsum crust from urban and rural area (Fig. B6) are related to differences in concentration of various components in atmospheric precipitation (lower in rural areas) and to differences in pH values (lower in rural areas) (Wilczyńska-Michalik & Michalik, 1998; Wilczyńska-Michalik, 2004).

2.4.2 Pińczów limestone

Effect of exposition of the Pińczów limestone to the influence of polluted atmosphere is strongly related to the time of reaction. Surfaces exposed for relatively short period of time became grey. It can be observed in replicas of statues of Apostles in front of the St. Peter and Paul church, which were prepared in the early 1980s. Discontinuous, rather thin (less than one mm) and tightly connected layer of dusts is observed at the grey surface.

The Pińczów limestone exposed for a longer period of time to the influence of polluted atmosphere exhibits granular disintegration. Gypsum-rich black crusts can be developed on the Pińczów limestone only locally. The disintegration and flaking of black crusts is often the reason of heavy decay of the stone structure. Some of the carved elements show deep disintegration, loss of material and crumbling of stone fragments from surface and subsurface layer. Sometimes the fine-carved details became unrecognisable because of deep granular disintegration (Figs. B7, B8).

In the Pińczów limestone, gypsum is present in numerous voids inside and between the organic remains (skeletal grains) or in other pore spaces of the rock (Fig. B9). Usually pore spaces are not completely filled with gypsum. Gypsum is finely crystalline and the crystals do not exhibit any preferred orientation. In some samples, one can find more or less continuous veinlets of gypsum in the rock parallel to the surface, causing disintegration of the rock. The resistivity of the Pińczów limestone is strongly related to the texture, *i.e.* grain size and porosity (Haber *et al.*, 1988; Kozłowski *et al.*, 1990).

Beside gypsum, dolomite (identified using EDS method) was found in the crust of secondary minerals on the rock surface. Dolomite is present in form of irregular aggregates. Dolomite is nonstoichiometric ("protodolomite"). Celestite (also identified using EDS) is relatively common in several samples of gypsum crusts on the Pińczów limestone (Wilczyńska-Michalik, 2004; Wilczyńska-Michalik & Michalik, 2006). Crystallization of protodolomite is related to increasing concentration of ions during rainwater solution evaporation. The process is described as the "urban model for dolomite precipitation" (Rodríguez-Navarro *et al.*, 1997). Celestite (with small content of Ba) is noted only in the weathering crust on the Pińczów limestone, indicating that Sr is derived from the rock (Wilczyńska-Michalik & Michalik, 2006). Relatively high concentration of celestite in the gypsum crust on the Pińczów limestone can be explained by lower solubility of celestite in comparison to gypsum.

Fig. B7.
Deep disintegration of the Pińczów limestone; an Apostel statue from the St. Peter and Paul Church, Kraków. The statue is now sheltered under a roof, which results in deposition of grey dust on the rock surface.

Fig. B8.
Deep disintegration of the Pińczów limestone; head of an Apostel from the St. Peter and Paul Church, Kraków.

2.4.3 Dębnik limestone

Surfaces of black bituminous Dębnik limestone exhibit strong discolouration (whitening) (Fig. B10). In Kraków, on surfaces well sheltered against rainwater, gypsum crust can be observed (Fig. B11). The morphology of the gypsum crust is very similar to that developed on the Jurassic limestone (folded or mushroom-like morphology). On the surface of the Dębnik limestone not covered by gypsum crust, small gypsum crystals forming irregular aggregates are present. Among gypsum crystals, some dust particles have been found (Wilczyńska-Michalik, 2004).

2.4.4 Libiąż dolomite

Cavernous and honeycomb weathering (alveolar pattern) is the most characteristic feature on the surfaces of architectural elements constructed from the Libiąż dolomite in Kraków.

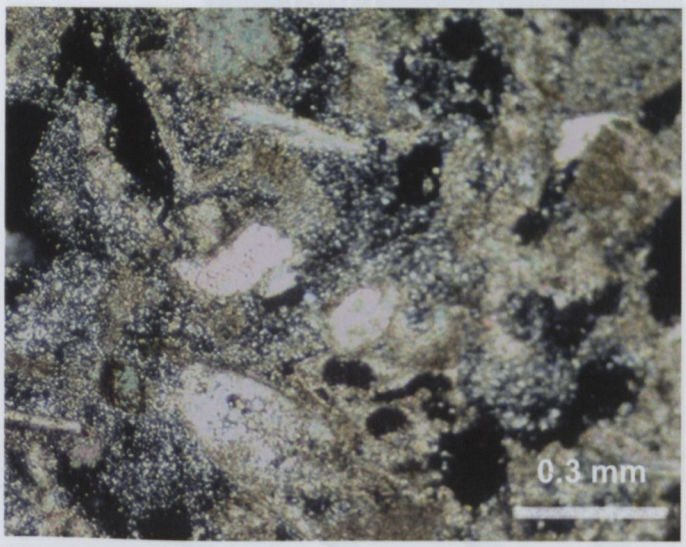

Fig. B9. Gypsum crystallizing in pore spaces of the Pińczów limestone. Optical microscope, crossed polars.

Fig. B10. Whitening of black Dębnik limestone after long exposition in the wall of the Carmelitan church, Kraków.

Fig. B12. Alveolae formed during weathering of the Libiąż dolomite. The surface of the rock is partly covered by black gypsum crust.

Fig. B11. Black gypsum crust on the Dębnik limestone (folded surface of the gypsum crust); Carmelitan church, Kraków.

Fig. B13. Alveolae in the Libiąż dolomite, filled during renovation; wall around the Wawel Cathedral (Kraków).

Alveolae range in size from 1 cm^2 up to 30 cm^2 and are few cm (from 1 cm to 4 cm) deep. Alveolar pattern develops mostly on the surfaces exposed to rain and wind action. The distribution of alveolae is related to sedimentary structures of the dolomite. Efflorescence of secondary salts is common inside the alveolae. At the bottom of alveolae, white pulverulent material is often accumulated. The filling of alveolae during renovation often produces a "patchy" appearance of the rock surface (Fig. B13).

Four mineral assemblages have been distinguished in the outer layer developed on the Libiąż dolomite building stones in Kraków: hexahydrite–gypsum assemblage; gypsum-dominated assemblage; halite with minor amounts of gypsum, assemblage of nitrates and other sulphates; halite-dominated assemblage.

Hexahydrite–gypsum assemblage is related to surfaces rich in alveolae. Rock surfaces within the cavities related to honeycomb weathering are soft, crumbly and scaly. Magnesium sulphates have been identified in alveolae together with admixture of gypsum. Depending on ambient humidity, hexahydrite or epsomite is the dominant component among pulverulent salts.

Surfaces of the Libiąż dolomite used in buildings that are sheltered against rain are commonly covered by a black gypsum crust. The crust is not very tightly bound to the substratum. Blistering and exfoliation can often be observed. Intense blistering causes development of cavities on the rock surface. The gypsum crust on the vertical walls is built up of fine crystalline gypsum crystals. The gypsum crust on overhanging surfaces form a few mm thick aggregates of mushroom-like forms composed of gypsum crystals of various habits. Elongated crystals forming branched aggregates are common in crusts on overhanging surface. In the Libiąż dolomite (rock of medium porosity and of relatively inhomogeneous texture) the outermost layer of the rock is rich in newly formed gypsum, which is present between dolomite crystals (Fig. B14). Gypsum crystals are often oriented relative to the rock (the elongation of crystals is perpendicular to the surface). Gypsum crystals on the surface of the gypsum crust on the Libiąż

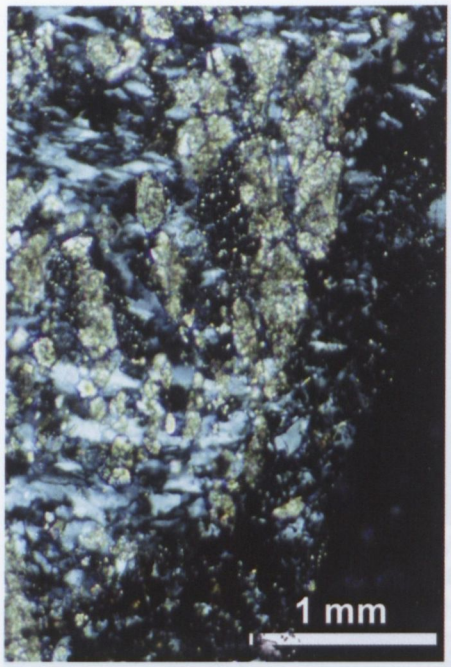

Fig. B14. Gypsum-rich outer layer of the Libiąż dolomite; wall near the Vistula River (Kraków).

dolomite are usually euhedral or subhedral (Wilczyńska-Michalik & Michalik, 1991a; Wilczyńska-Michalik, 2004).

The halite–gypsum–nitrates–other sulphate assemblage occurs near the ground level, where moisture can rise up in the rock from ground. The proportions of the main constituents in this assemblage are variable. It comprises a lot of salt minerals like halite, gypsum, nitrammite, nitronatrite, syngenite, langbeinite and also ankeritic dolomite and dust grains.

The halite-dominated assemblage occurs on walls protected from rainwater and insolation. The crust is up to few mm thick and is composed of densely packed cubic halite crystals with rounded edges.

Common usage of the Libiąż dolomite in technical constructions (*e.g.*, bridges) gives an opportunity to compare dark zones developed in environments of dry deposition and in environments exposed to wet and dry deposition. In both environments, dark crusts are composed of gypsum with subordinate dolomite and calcite. On walls subjected to wet and dry deposition, the crust is black, compact and brittle (Fig. B15) and on walls subjected to dry deposition, it is greyish and pulverulent (Fig. B16). Gypsum in the black crust from environment subjected to wet and dry deposition forms rosette-like intergrowths (Fig. B17). In samples sheltered against rainwater washing, gypsum crystals form loosely packed aggregates (Fig. B18) and soil-derived dust (quartz, micas, feldspars) or anthropogenic dust particles are abundant (Fig. B19). Abundance of dust is the reason of significantly higher con-

Fig. B15. Black crust on the wall surface subjected to dry and wet deposition (Kamienna Street, Kraków).

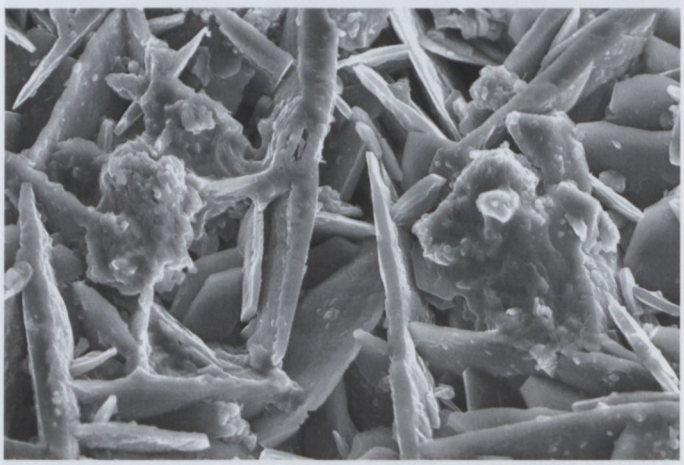

Fig. B17. Rosette-like intergrowths of gypsum crystals in the black crust on the wall surface subjected to dry and wet deposition, SEM photo (Kamienna Street, Kraków).

Fig. B16. Grey crust on the wall subjected to dry deposition (Łokietka Street, Kraków).

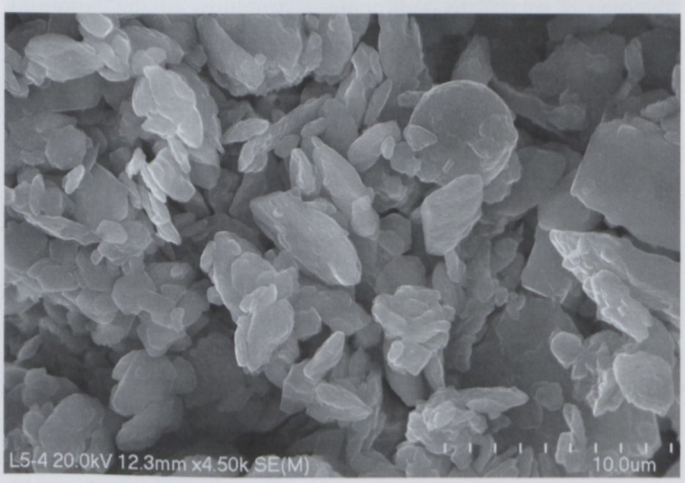

Fig. B18. Loosely packed gypsum crystals on the surface of gypsum crust from the wall sheltered against rainwater, SEM photo (Łokietka Street, Kraków).

Fig. B19. Soil-derived and anthropogenic dust between gypsum crystals on the surface of crust from the wall sheltered against rainwater, SEM photo (Łokietka Street, Kraków).

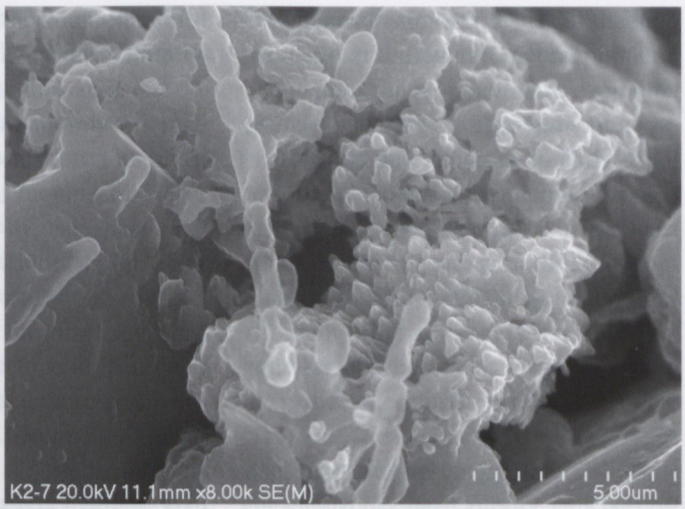

Fig. B21. "Protodolomite" on the gypsum crust on the wall surface subjected to dry and wet deposition (Kamienna Street, Kraków).

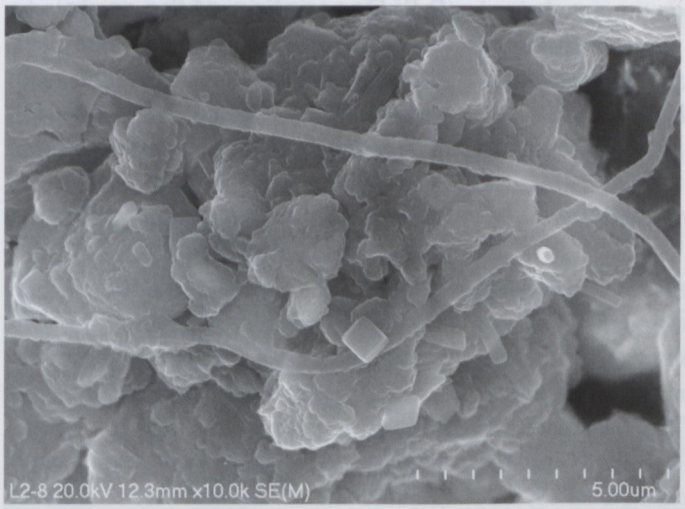

Fig. B20. Aluminosilicate dust, halite crystals and fungal hyphae on the surface of crust from the wall sheltered against rainwater, SEM photo (Łokietka Street, Kraków).

Fig. B22. Gypsum-rich crust on the surface of sandstone blocks (Lubicz Street, Kraków).

centration of several elements (*e.g.* Fe, Ti, Zr, Zn, Pb, Ni) in this crust in comparison to dark crust developed on surfaces subjected to rainwater washing (wet and dry deposition environments). Calcite, halite and whewellite occur in small amount in crust developed in dry deposition environment (Fig. B20). In samples from rainwater-washed surface, authigenic, non-stoichiometric dolomite ('protodolomite') is also present (Fig. B21). This difference suggests that dissolution of the dolomite rock occurs on rainwater-washed surfaces. Whewellite originates probably from the metabolism of microorganisms. Isotopic composition of S and O in gypsum from both groups of samples (dry and wet + dry deposition environments) is very similar, indicating common origin of sulphate ion (Wilczyńska-Michalik *et al.*, 2004; Wilczyńska-Michalik *et al.*, in preparation).

2.4.5 Carpathian flysch sandstone

Weathering features of the Carpathian sandstones in polluted atmosphere are very diversified due to the variations in lithological properties (framework composition, grain size, porosity, presence of matrix, content and composition of cement). The study of sandstones from several localities in the Carpathians differing in the concentration of atmospheric pollution indicates that the relationship between concentration of pollution and weathering processes is evident (Michalik & Wilczyńska-Michalik, 1998; Wilczyńska-Michalik, 2004).

Visual manifestations of weathering of sandstones are numerous and their distribution on surfaces of walls is very complex. Soiling can be commonly observed on surfaces of sandstone building blocks sheltered against direct washout by rain. Intensity of soiling can be different, from delicate grey tint on the rock surface to black, thin black layer, tightly attached to the rock surface. On some sandstone blocks, efflorescence of various salts can be observed on the soiling surface.

Sandstone blocks in buildings in Kraków are often covered by black (or dark grey) crust of gypsum and other secondary minerals (Fig. B22). Gypsum-rich crust surface is uneven and efflorescence of white gypsum crystals could be seen on it. Black gypsum crusts commonly exhibit blistering and exfoliation. The thickness of the exfoliating gypsum-rich crusts is variable (usually about 3–6 mm). The size of exfoliating fragments of the crusts is partly co-related with their thickness. Thick crust exfoliates in bigger fragments (up to several cm). Grains from sandstones are also detached during exfoliation of the thick gypsum crusts. Black gypsum-rich crust is developed mainly on surfaces sheltered against direct washout by rainwater. Exfoliation of gypsum-rich crust can be the reason of significant recession of the rock surface. Recession is especially intense on corners of walls or other protruding elements (Fig. B23).

Granular disintegration is common on surfaces exposed to rainwater washing. Efflorescence of salts is common on the disintegrated surface but secondary salts do not form continuous layer. Salts occur during and after drying of surface after rainfall. Surfaces subjected to granular disintegration devoid of efflorescence of secondary salts can also be observed.

Fig. B23. Disintegration of sandstone block (St. Peter and Paul Church, Kraków).

Layer exfoliation is a relatively common feature of weathering of sandstones in urban environment. The thickness of exfoliating layer varies within range from few mm up to 1–2 cm. Fissures parallel to the surface can be often seen below the exfoliating layer. Set of numerous parallel fissures is very common. The size of exfoliating fragments of layers is variable but usually does not exceed a few cm. The outer surface of exfoliated layers is often covered with a dark pigment layer.

Disintegration of sandstones into irregular fragments is relatively common. Disintegration into bigger blocks occurs rarely. Disintegration into irregular fragments can be noticed usually in the vicinity of edges of sandstone blocks (Wilczyńska-Michalik, 2004).

2.5 Concluding remarks

Surfaces of rocks weathered in the urban atmosphere in Kraków are often covered by the crust of secondary minerals. Gypsum dominates in these weathering crusts but almost 20 other minerals are present. Minerals occurring in the weathering crust originate from crystallization of components of rainwater, reactions between rainwater and rock components, adsorption of various components from the atmosphere on the rock surface and further chemical reactions. Dissolution patterns on components of gypsum crust in Kraków, absent in early 1990s, are recently relatively common. It is related to the lowering of the charge of contamination in rainwater and lowering of the pH value of precipitation. Degree of rocks decay is related mostly to their porosity.

During the relatively long period of very high level of the atmosphere contamination in Kraków and very high charge of dissolved components in atmospheric precipitation, salt weathering was the dominant type of weathering (Wilczyńska-Michalik *et al.*, 2000; Wilczyńska-Michalik, 2004). Opinions about dissolution of rock components by acid precipitations were not justified in this period. Dissolution patterns, observed previously only in rural area, are now noted also in Kraków, which is related to changes in characteristics of atmospheric precipitation.

Because of the progress in renovation of historical monuments, the target of mineralogical and geochemical investigation will move from documentation of weathering features and interpretation of weathering processes to collaboration in preparation of filling materials suitable for various rocks and to studies of changes on rock surfaces after renovation.

2.6 Description of the route

The excursion starts near the remains of the City Walls. Brief introduction will be presented (history of the development of the town, local geology). During the trip we will go along the Royal Route (from the Florian Gate, Market Place to the Royal Castle). Main building stones described above and their weathering features will be presented. Localisation of presented examples of weathered rocks is dependent on the progress of renovation of monuments. Weathering of the Pińczów limestone will be presented near the St. Peter and Paul church (statues of Apostels).

Examples of other building stones used in Kraków used in different historical periods will also be presented. Comparison of weathering processes of the Libiąż dolomite in different environments (dry deposition environment *vs.* wet and dry deposition environment) will be presented on walls of two bridges (Kamienna and Łokietka streets). Weathering of the Upper Jurassic limestone will also be presented in an old quarry (Zakrzówek).

Day 3 (Part C)

Kraków – Wieliczka Salt Mine (12 km) – abandoned quarries of building stones near Krzeszowice (50 km) – Kraków (85 km)

3. Wieliczka Salt Mine

ANDRZEJ ŚLĄCZKA

3.1 Introduction

Exploitation of salt in the Wieliczka region has a very long tradition. It started already in the Neolithic Age (~5,500 years ago) from brine springs. However, the first known documents concerning exploatation of salt in Wieliczka, which was named at that time *Magnum Sal*, are dated from 11th century. The oldest known shaft is dated at the 13th century. The oldest, first level, lies at a depth of 57 m and the deepest one, from the 20th century, at a depth of 327 m. The whole mine is 5.5 km long, around 1 km wide and 327 m deep. During seven hundred years of uninterrupted salt exploitation, labyrinth of galleries, chambers and shafts over 250 km long was created. Commercial exploitations were terminated at the end of the 20th century.

Salt from Wieliczka played a very important role in the economy of the Polish Kingdom, among others, the Jagiellonian University was subsidized from profits of the Wieliczka mine.

Apart from being a source of profit, the Wieliczka salt mine was and still is a world-famous turistic attraction. It was visited by kings, humanists, statesmen, poets, *e.g.* Copernicus, Agricola, Ruggieri, M. German, Goethe, Humboldt, Francis Joseph II and, of course, by hundreds of geologists *e.g.* Hacquet, Townson, Staszic, Pusch and Murchison in the 18/19th centuries. One of a turists from 17th century, Le Laboureur, wrote that the Wieliczka salt-works are not not less splendid but more useful than the pyramids of Egypt.

In the Wieliczka Salt Mine we can observe apart of turistic atractions also the fascinating geology of the salt-bearing deposits (Gaweł, 1962) with a unique pile of halite layers, which show sedimentary structures typical of redeposited sediments (Kolasa & Ślączka, 1985; Ślączka & Kolasa, 1997).

3.2 Geological setting

Wieliczka salt mine is situated within the Carpathian Foredeep Basin (Fig. C1), which developed in front of the advancing Carpathian orogen on the southern edge of the North European Platform (Oszczypko & Ślączka, 1985). This Foredeep Basin can be subdivided into the inner and outer sub-basins. The inner sub-basin, composed of Lower and Middle Miocene molasse deposits, is hidden beneath the overthrusted Northern Carpathians as an effect of Miocene tectonic movements. The outer sub-basin,

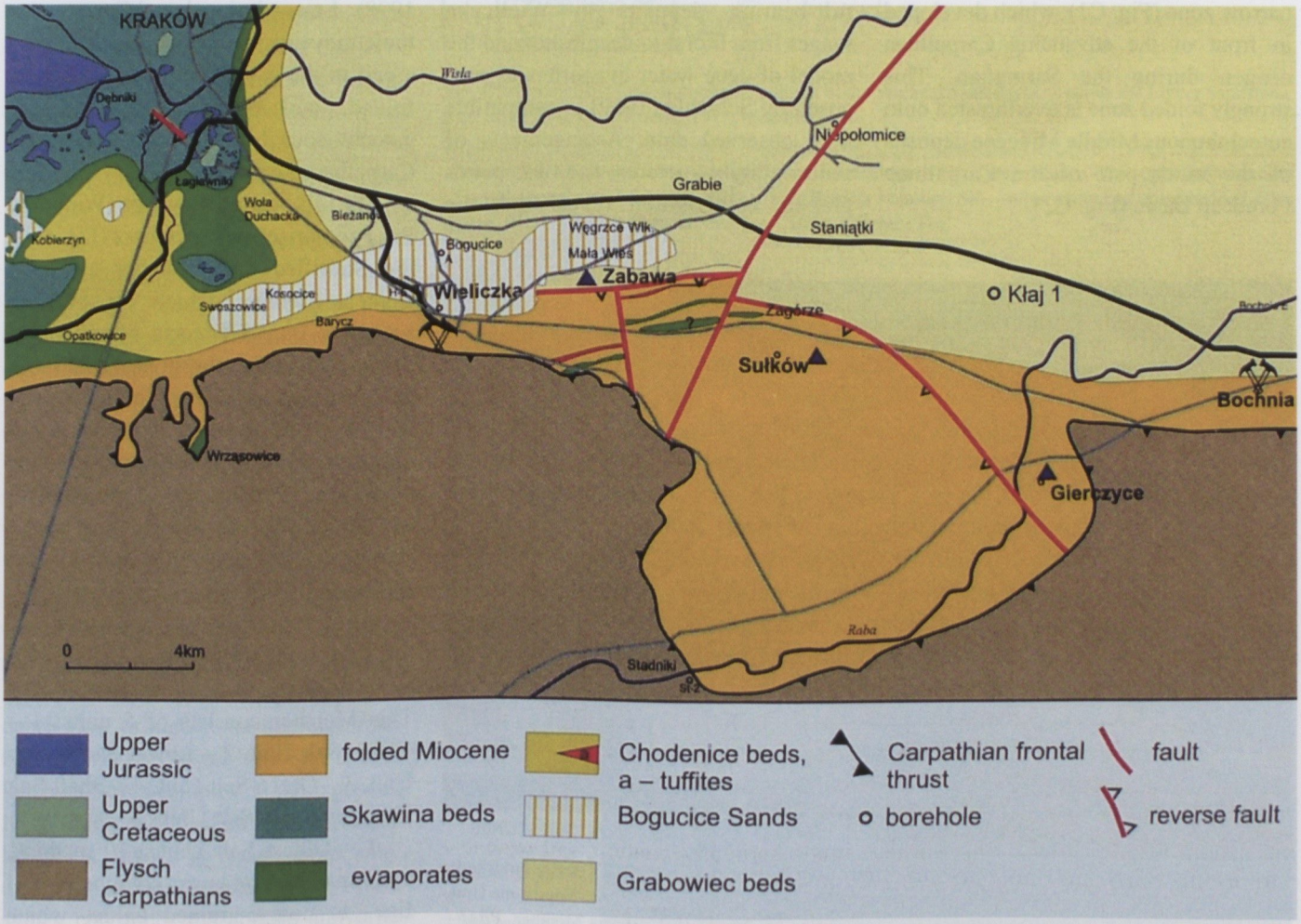

Fig. C1. Geology of the Kraków–Wieliczka area (after Porębski & Oszczypko, 1999; simplified).

filled with mainly marine Middle Miocene (Badenian and Sarmatian) molasse deposits, is generally situated in front of the Carpathian overthrust and only its southern part is hidden below the Northern Carpathians. During the Late Badenian (Serravalian, NN6 and locally NN5; Andreyeva-Grigorovich *et al.*, 2003), as an effect of salinary crisis, evaporitic deposits were formed on wide area of the outer sub-basin. Salt rocks (mainly halite) developed in its southern, deeper part, and sulphates generally in northern, shallower part (Garlicki, 1979; Oszczypko *et al.*, 2006). Fauna (bivalves, echinoderms, Lithothamnium algae, and corals) and plant fragments (mastixioid floras, and paleothropical species), found within salt sequence in Wieliczka salt mine, show Mediterranean-type paleoenvironment (Kowalewski, 1935; Łańcucka-Środoniowa, 1984).

Salt rocks of Wieliczka occur in a narrow zone (Fig. C1), which developed in front of the advancing Carpathian orogen during the Sarmatian. This strongly folded zone is overthrusted onto autochthonous Middle Miocene deposits of the outer part of the Carpathian Foredeep Basin (Fig. C2).

3.3 Wieliczka salt deposits

The main halite sequence of the Wieliczka salt mine is underlain by Lower/Late Badenian (Langhian–Lower Serravalian) siltstones, anhydritic claystones, siltstones and sandstones with sporadic conglomerates and pebbly mudstones with boulders derived from the Carpathian flysch rocks (Skawina Fm.). In the highest part of this sequence, an amphibolic tuffite horizon was found (Bukowski, 1999).

The Wieliczka salt deposit is unique from the point of view of the number and size of chevron crystals of halite (Galamay *et al.*, 1997). Cubic one-phase fluid inclusions are the most common. Those brines belonged to Na-K-Mg-Cl-SO_4 type. The bromine content (67–20 g/t) in halite also indicates the marine source of brines and a relatively low grade of their evaporation.

Depositional paleoenvironment of salt-bearing deposits in Wieliczka ranges from litoral to deep water and the model of deep water evaporites as proposed by Schmalz (1969) is compatible with observed data. Arrangements of sedimentary structures and the petrographic composition reveal that the development of the Wieliczka salt basin was closely related to tectonic movements and the northward advance of the Carpathian nappes. At the beginning of salt sedimentation, when tectonic activity was low, halite was precipitated (Fig. C9). An increase of tectonic movement affecting the southern margin of the salt basin first caused disintegration of the previously deposited salt and afterwards created the proper conditions for density currents. An increase of tectonic activity and earthquakes probably connected with this, led to more and more turbidite currents, which built up submarine fans. Tractional currents played secondary role. The loose salt material could have come from the disintegration of normal precipitated salt layers as an effect of tectonic compression that caused salt behave like brittle material. During the final stage, strong orogenic movements gave rise to submarine debris flows and huge slumps (Ślączka & Kamiński, 1998). Later, during late Miocene tectonic movements, the salt deposits with a part of the substratum were detached, folded, and overthrusted onto the autochtonous Miocene deposits of the Carpathian Foredeep.

The salt-bearing sequence (Wieliczka Fm.) comprises two members (Fig. C3): the Stratified Salt Member and Salt Breccia Member, which are overlain partly by Barren Breccia Member and partly by marine claystones and sandstones (Chodenice Fm.). The lowermost part of the salt-bearing sequence corresponds to the NN5 and higher part to the NN6 zone (Andreyeva-Grigorovich *et al.*, 2003). The Chodenice Fm. corresponds to the uppermost part of the Badenian (NN6/7zone).

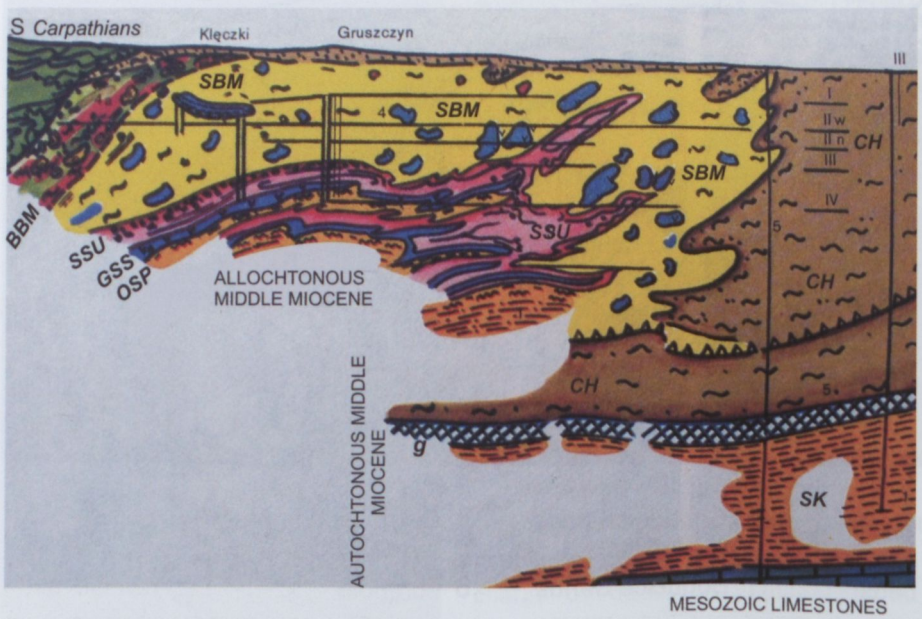

Fig. C2. Cross-section through the Wieliczka Salt Mine (after Kolasa & Ślączka, 1987, partly modified). Explanation of letters: *SK* – Skawina Fm., *g* – gypsum, *OSP* – Oldest Salt Unit & Lower Sandstone Unit, *GSS* – Green Salt Unit & Shaft Salt Unit, *SSU* – Spiza Salt Unit, *SBM* – Salt Breccia Member, *BBM* – Barren Breccia Member, *CH* – Chodenice Fm.

3.3.1 Stratified Salt Member

This Member consists of 5 units: 1 – Oldest Salt Unit, 2 – Lower Sandstones Unit, 3 – Green Salt Unit, 4 – Shaft Salt Unit, 5 – Spiza Salt Unit.

1 – Oldest Salt Unit, ~10 m thick, built up of several layers composed of of fine- to coarse-grained halite, which originated from direct precipitation.

2 – Lower Sandstone Unit (previously called sub-salt sandstone) is represented by a complex of usually graded sandstones, claystones and mudstones. Locally there are lenses of conglomerates that contain boulders, up to 50 cm in diameter, of Carpatian flysch rocks, whitish limestones, and grains of anhydrite and abundant carbonized plant fragments. Blocks of salt also occur. Majority of sandstones was deposited by turbidity currents and, in case of conglomerates, by debris flows. Existence of gypsum layers shows that the water was saturated with $CaCO_3$ (Bukowski, 1997).

3 – Green Salt Unit, ~10 m thick, is represented by four layers composed of coarse halite crystals enclosed in clay material, which originated from direct precipitation (Fig. C4). The salt layers are intercalated with thin sandstone layers cemented by salt and anhydrite, mudstones and anhydrite. Sandstone–mudstone–anhydrite sequences frequently occur. There are also claystone layers, containing in addition to big salt crystals also pebbles of Miocene marls and of anhydrite, which show similarity to pebbly mudstones deposited by dense turbidity currents. Layers are locally contorted, which can be an effect of submarine slumping.

4 – Shaft Salt Unit, up to 2 m thick of pure halite, contain abundant primary cubic crystals. This Unit represents a period of quiet deposition by precipitation.

5 – Spiza Salt Unit is divided by central barren intercalations into two subunits: Lower and Upper. The lower one is built up of layers of pure salt (halite) intercalated by thin clastic layers composed of quartz and anhydrite grains and by clastic salt layers with pebbles of Miocene marls and sandstones representing deposits of debris flow or high-concentration turbidity currents. The Lower Sub-Unit is overlain by a barren complex, built up generally of thin- and medium-bedded, cross-laminated, graded or homogenous anhydritic limestones intercalated by mudstones, claystones and nodular anhydrites (central barren intercalation). Clastic sedi-

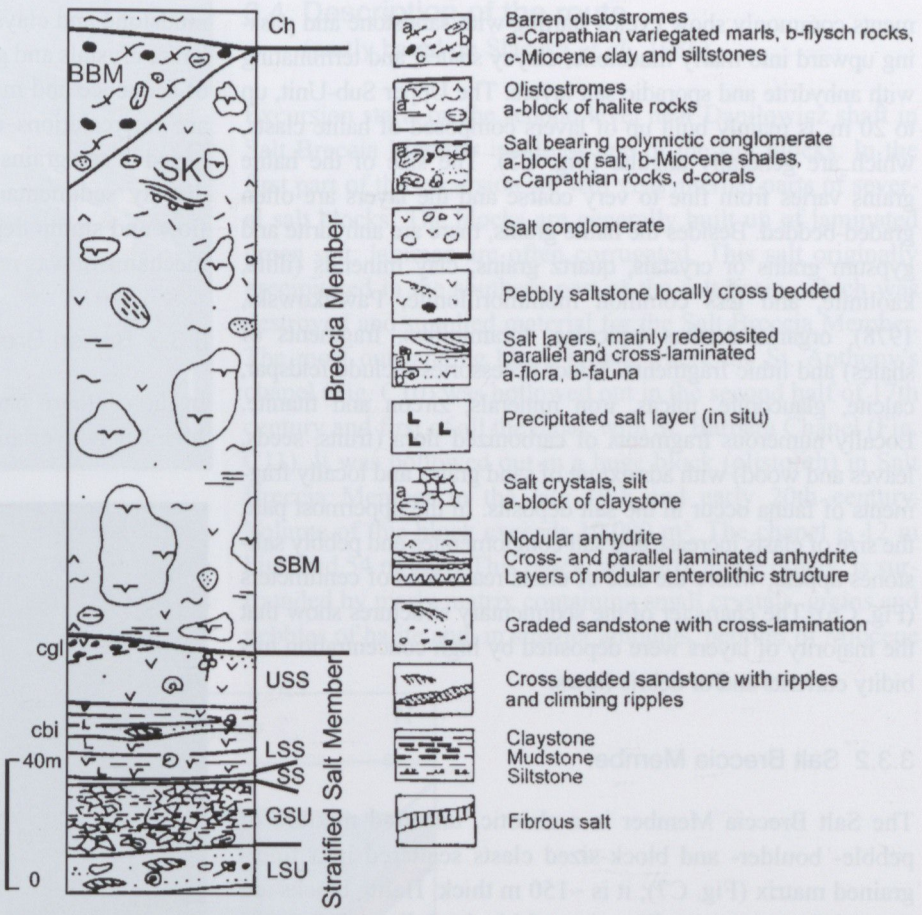

Fig. C3. Generalised lithostratigraphic column of the Wieliczka salt deposits above the Lower Sandstone Unit (after Ślączka & Kolasa, 1977, modified).

Explanation of letters: LSU – Lower Sandstone Unit, GSU – Green Salt Unit, SSU – Shaft Salt Unit, LSS – Lower Spiza Sub-unit, cbi – central barren intercalation, USS – Upper Spiza Unit, cgl – intercalation of conglomerates and debrites, SBM – Salt Breccia Member, SK – intercalation of cross-bedded saltstones, BBM – Barren Breccia Member, CH – Chodenice Fm.

Fig. C4. Coarse-grained salt layer covered by medium-grained salt and laminated salt. Green Salt Unit.

ments commonly show cycles starting with sandstone and passing upward into marly mudstone, clayey shales, and terminating with anhydrite and sporadic salt layers. The Upper Sub-Unit, up to 20 m, is mainly built up of layers composed of halite clasts, which are generally angular (Fig. C5). The size of the halite grains varies from fine to very coarse and the layers are often graded-bedded. Besides the halite grains, there are anhydrite and gypsum grains or crystals, quartz grains, clay minerals (illite, kaolinite, and less common montmorillonite, Pawlikowski, 1978), organic detritus (spiculae, foraminifers, fragments of shales) and lithic fragments. Minor accessories include feldspar, calcite, glauconite, micas, iron minerals, zircon and titanite. Locally numerous fragments of carbonized flora (fruits, seeds, leaves and wood) with admixture of sand grains and locally fragments of fauna occur in the salt deposits. In the uppermost part, the size of clasts increase and salt conglomerates and pebbly saltstones appear, where the size of clasts reach tens of centimeters (Fig. C6). The character of the sedimentary structures show that the majority of layers were deposited by high concentration turbidity currents and/or debris flows.

3.3.2 Salt Breccia Member

The Salt Breccia Member is a chaotic, unsorted mixture of pebble- boulder- and block-sized clasts scattered in a finer-grained matrix (Fig. C7); it is ~150 m thick. Halite blocks are the chief component. The size of blocks (olistoliths) range from a few m^3 to 12,000 m^3, but reach up to 100,000 m^3. They consist of different salt lithologies, but they are usually different than the structures in the Stratified Member. Less common are much smaller fragments of Miocene marls and sandstones and Carpathians rocks. The breccia matrix contains calcareous mudstone and claystone in varying proportions, together with halite crystals and grains. The matrix is marly in the lower part of sequence and more clayey in the upper part. Locally, there are intercalations of graded- and cross-bedded layers composed of salt grains (Fig. C8). Deposits of the Breccia Member display sedimentary structures similar to submarine debris flow and slump deposits and it can be assumed that the same mechamism was responsible for their sedimentation.

3.3.3 Barren Breccia Member

In the southern part of the Wieliczka mine, the Salt Breccia Member is overlain by a breccia that is devoid of salt clasts

Fig. C6. Cross-bedded conglomerates and debrites. Uppermost part of Spiza Salt Unit in the southern part of mine. Gruszczyn Gallery.

Fig. C5. Conglomerate built up of salt grains and pebbles. Salt clasts are angular to subrounded. Size of the pebble up to 5 cm. Spiza Salt Unit.

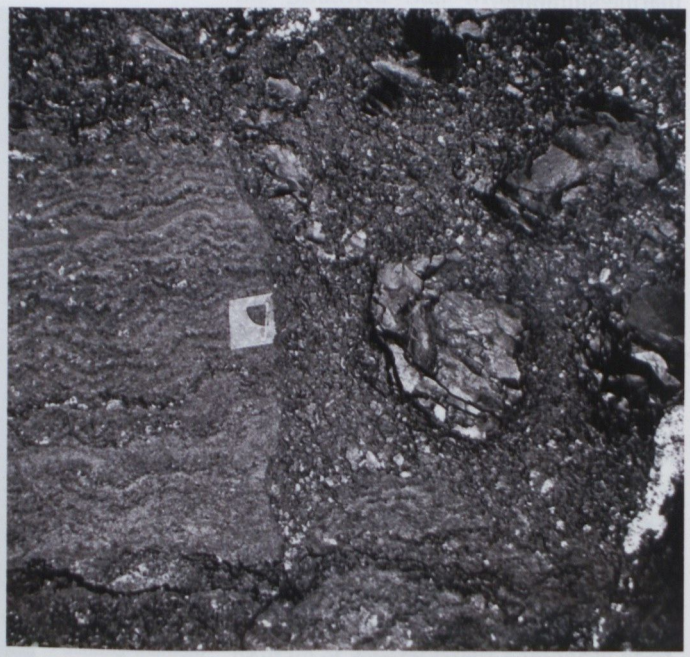

Fig. C7. Debrites composed of blocks of laminated salt and Miocene marls embedded in clay-rich matrix. Salt Breccia Member. Kunegunda Gallery. Scale bar is 10 cm long.

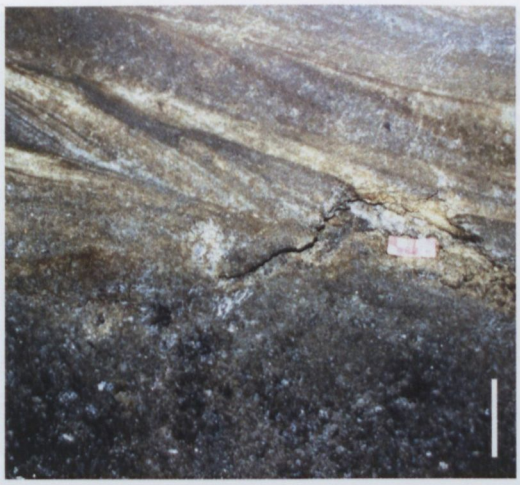

Fig. C8. Cross-bedded coarse grained saltstone on the top of salt debrite. Salt Breccia Member. Klęczki Chamber. Scale bar is 15 cm long.

and blocks. Clasts are represented only by various Carpathians rocks together with Miocene marls. This breccia, similar to the lower one, represents deposits of submarine debris flows and/or submarine slumps.

3.4 Description of the route

(partly based on Ślączka *et al.*, 1986)

Excursion starts on the second level near Daniłowicz shaft in Salt Breccia Member inside of one of the salt blocks. In the first part of the excursion we will visit internal parts of several salt blocks. The blocks are generally built up of laminated green salt; laminae are often corrugated. This salt originally precipitated in the southern part of the salt basin, which was destroyed and supplied material for the Salt Breccia Member. The most outstanding block is that where the St. Anthony's chapel (Fig. C10) was hollowed out in the second half of 17th century and first of all the block with St. Barbara Chapel (Fig. C11). It was hollowed out in a huge block (olistolith) in Salt Breccia Member in the late 19th and early 20th century. Volume of this block exceeds 10,000 m^3. The chapel is 12 m high and 54 m long. This block, similarly to the others, is surrounded by marly matrix containing small crystals, grains and pebbles of halite and, in smaller amounts, pebbles of Miocene

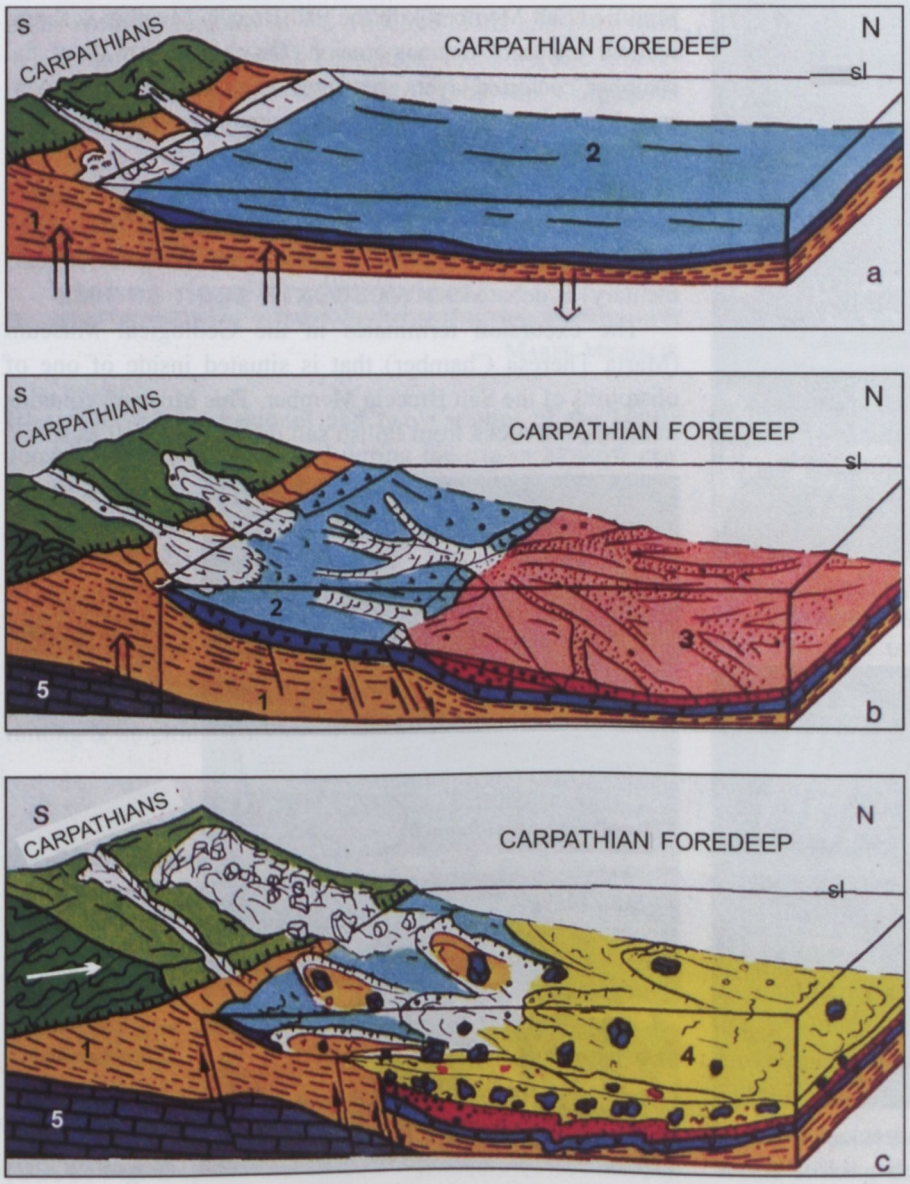

Fig. C9. Schematic diagrams illustrating the evolution of the southern and central part of the Wieliczka salt basin (based on Kolasa & Ślączka, 1987, modified).
1 – Chodenice Fm., 5 – Mesozoic limestones (on a, b and c)
a) first stage: wide 2 – evaporites represented mainly by precipitated halite; 3 – deposits of generally redeposited salt.
b) Beginning of resedimentation of salt in response to tectonic movements in marginal area. Development of submarine fan (3) built up of clastic salt.
c) Final stage: basin is filling up by debrites and slumps with olistoliths (4), derived from the marginal parts of the salt basin and from the Carpathians.

mudstone and sandstones. The contact between the block and matrix can be observed in the exit from the Chapel. The lack of tectonic structures at this contact is noteworthy.

Further on along the galleries we can have a look on the Spiza Salt Unit. They are best exposed in Piaski Chamber. It is represented by conglomerates, which display gradation and are terminated by a horizontal laminated part. The conglomerates are built up almost only from salt clasts and crystals. Some parts of the layers are strongly folded. The origin of some of these folds is uncertain. It is still debated, whether they represent local underwater slumps or they were a product of the Late Miocene tectonism.

Fig. C10. St. Anthony Chapel hollowed out in a block (olistolith) of laminated salt. Salt Breccia Member. Note the strong erosion of the sculptures.

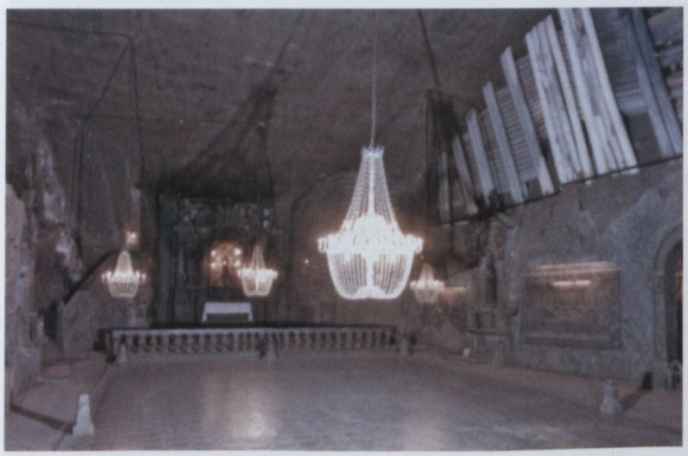

Fig. C11. St. Kinga Chapel hollowed out in a huge block (olistolith) of laminated salt.

Further on we pass a gallery hollowed out in the central barren intercalation (Fig. C12) marking a break in salt sedimentation. It is built up of medium-bedded, cross-laminated, rarely convoluted sandstones, mudstones and layers of anhydrite. Cross-lamination shows, that longshore currents prevailed.

In the next chamber (Warszawa Chamber), the upper part of the Stratified Salt Member – Upper Spiza Unit and the contact with the Salt Breccia Member is visible. It is composed from conglomerates built up of salt pebbles within a matrix of coarse salt. Soles of the layers are sharp, erosive and locally they show flame structures (Fig. C13). The sedimentary structures indicate that these conglomerates were deposited by high-concentration turbidity currents. The conglomerates overlay uneven salt layers without clear evidence of redeposition, these layers may have been formed by direct precipitation. The contact of the Stratified Salt Member with the Salt Breccia Member is sharp, without traces of distinct erosion. On the other wall of the chamber, contorted layers are visible, wich may have been generated by tectonism, although their primary sedimentary genesis (local submarine slump) cannot be excluded.

Leaving Warszawa Chamber, we follow a gallery, where strongly deformed anhydritic mudstones of the Spiza Unit can be observed. The origin of the deformation (tectonic or sedimentary) is debated.

The excursion terminates in the Geological Museum (Maria Theresa Chamber) that is situated inside of one of olistoliths of the Salt Breccia Member. This Museum contains minerals and rocks from Polish salt deposits as well as speci-

Fig. C12. Complex of cross-bedded and convoluted sandstones and mudstones with layers of nodular anhydrite, some having enterolithic structures ("tripestone"). Central barren intercalation.

Fig. C13. Lower part of salt conglomerate with flame structures. Top part of the Upper Spiza Sub-unit. (Warszawa Chamber).

mens with the remains of the Miocene fauna and flora from Wieliczka salt mine. In the exposition, there are also numerous maps of Miocene salt deposits of the Carpathian Foredeep, geological cross-sections and drawings of galleries.

4. Abandoned quarries of building stones near Krzeszowice

MAREK MICHALIK

Black Devonian limestones and two varieties of the Upper Jurassic limestones presented during the trip in Kraków city centre will be shown in abandoned quarries and natural outcrops near Krzeszowice.

Day 4 (Part D)

Kraków – Olkusz (40 km): Pomorzany Zn-Pb mine, Zn-Pb mining & smelting dumps – Kraków (80 km)

5. MVT-type zinc and lead deposits of Upper Silesia, Poland

HARRY KUCHA

5.1 Stratigraphy and lithology of the basement

The Upper Silesian zinc-lead ore deposits lie northwest of Cracow, near the boundary of the Upper Silesian Coal Basin (USCB, Fig. D1) and the Cracow Variscides (Caledonides). The Caledonides are located between the Upper Silesian massif of Precambrian consolidation and the Malopolska massif of Early Caledonian consolidation (Haranczyk, 1979). These massifs may be microcontinents that accreted onto the East European platform during the Caledonian orogenic event (Haranczyk, 1982). The geologic history of the two areas were similar during pre-Devonian, Devonian and Lower Carboniferous, but were very different during the Early Paleozoic and Late Carboniferous, and later, during Mesozoic their geological fate was again similar.

The Upper Silesian Coal Basin is developed on Precambrian schists and gneisses unconformable overlain by terrigenous Cambrian sediments. These in turn, are discordantly overlain by Devonian sandstones and siltstones (up to 410 m thick) and dark limestones and bioclastic dolomites (up to 1.4 km thick). The Carboniferous rests on eroded Devonian and is divided into two horizons: the lower one consists of Lower and Middle Visean limestones and dolomites up to 700 m thick. These are unconformably overlain by 1.5 km of Upper Visean flysch-like mudstones and fine-grained sandstones, tuffites and up to 7 km of Namurian and Westphalian molasse of which the upper 800 m is rich in productive coal seams. Younger formations are preserved only in the USCB troughs (Fig. D1).

During the Sudetic and Asturian phases of the Variscan, the western part of the USCB was intensely deformed and cut by NNW-striking thrust faults, whereas in the eastern part of the USCB, WNW, normal faulting occurred.

The Cracow Variscides (Fig. D2) underlie the Cracow-Silesian Monocline (CSM) and comprise Precambrian schists discordantly overlain by Paleozoic metasediments and sediments. The Cambrian consists of up to 5 km of black quartzites, phyllitic shales, quartzitic sandstones and black claystones with carbonate intercalations (Ekiert, 1978). The Ordovician comprises up to 1.2 km of metamorphic detrital sediments derived from three repeated cycles of deposition starting from coarse-grained sediments and passing into claystones (Ekiert, 1978; Znosko, 1983). The Silurian rests discordantly on the Ordovician, forming up to 5 km of sediments. The Lower Silurian is developed as schist formation 0 to 2800 m thick. The Upper Silurian consists of 300 m molasse sediments and gradually passes into terrigenous Lower Devonian sandstones 0 to 1.6 km thick. The Middle and Upper Devonian as well as Lower Carboniferous comprises carbonate limestones and dolomites 0 to 1.6 km thick (Bukowy, 1974). The remainder of the Carboniferous is composed of carbonate flysch (clay shales, coal seams and limestones) 0 to 1000 m thick. The Permian molasse (conglomerates and siltstones) fills up a WNW-striking depression, which is connected to the main

Permian basin in central Poland (Pokorski, 1981) and consists of 200 to 400 m of conglomerates, sandstones, tuffs, porphyries and melaphyres (Siedlecka, 1970).

The Permian sediments are the lowest unit incorporated into the Cracow-Silesian Monocline (SCM, Bukowy, 1974). The Permian is overlain by the Triassic (Table 1), starting with

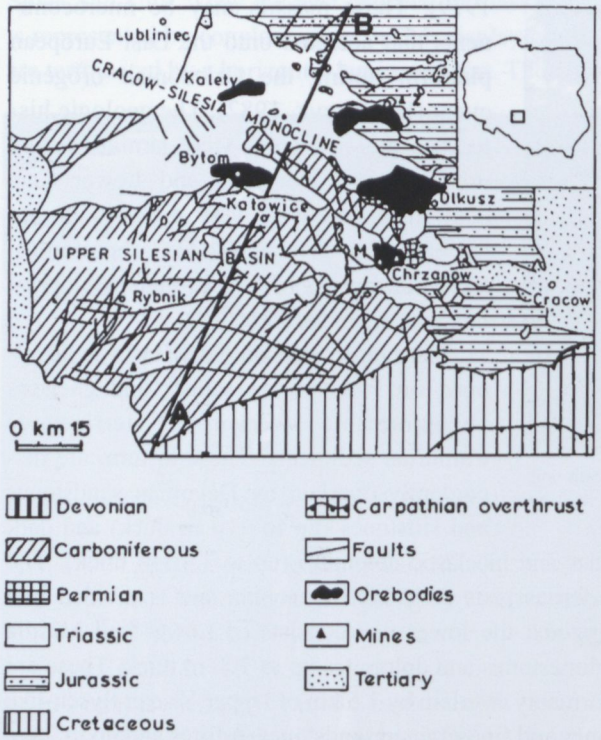

Fig. D1. Geological map of the Upper Silesian Zn-Pb district (after Zartman *et al.*, 1979). Mines: Z – Zawiercie, M – Matylda, T – Trzebionka, J – Jastrzebie colliery. A–B – line of geological cross-section (Fig. D2).

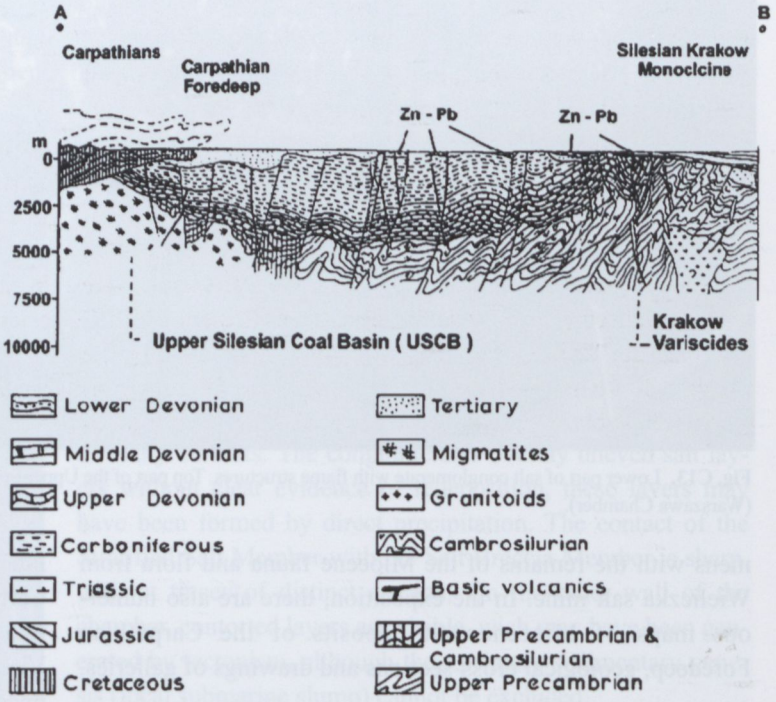

Fig. D2. Geological cross-section including the Upper Silesian Coal Basin, Kraków-Silesian Monocline, Carpathians and Kraków Variscides (after Znosko & Pajchlowa, 1968).

Table 1. Lithology and mineralization in the Upper Silesian Zn-Pb district

STRATIGRAPHY		Thickness (m)	Lithology	Mineralisation			
				Chrzanow	Bytom	Olkusz	Zawiercie
UPPER TRIASSIC	Keuper	0 - 80	Mudstones, clays, dolomite, gypsum				
MIDDLE TRIASSIC (MUSCHELKALK)	Boruszowice Beds	0 - 25	Black shales, sandstone, dolomite				
	Diplopora Dolomites	17 - 40	Dolomite				
	Terebratula & Karchowice Beds	18 - 45	Dolomites, OBD, limestone intercalations				
	Gorazdze Beds	17 - 20	Dolomites, OBD, limestones				
	Gogolin Beds	15 - 55	Dolomites, OBD at the top, limestones, marls				
LOWER TRIASSIC	Roethian	16 – 53	Dolomites, marls, clays, limestones				
PERMIAN		0 – 100	Conglomerates, siltstones				
CARBONIFEROUS		0 – 1800	Gap, shales, marls, limestones, sandstones				
DEVONIAN		0 - ?	Limestones, dolomites, OBD, sandstones, skarns				
SILURIAN		0 - ?	Shales, graywackes, sandstones, porphyries				
Zn : Pb ratio				4.2	5.7	3.0	1.7

Compiled from the data of Duwensee (1929); Sobczynski & Szuwarzynski (1974); Piwowarski & Zeglicki (1974); Wielgomas (1978); Bukowy (1974, 1978); Pawlowska & Szuwarzynski (1979) (OBD – ore bearing dolomite)

locally developed Buntsandstein red sandstones, up to 50 m of argillaceous dolomites, dolomite and gypsiferous beds (Sliwinski, 1969). The Muschelkalk varies in thickness from 50 to 160 m and consists of Gogolin, Gorazdze, Terebratula and Karchowice limestones, Diplopora and Tarnowice dolomites. The Muschelkalk contains very little terrigenous material and was deposited in a shallow marine environment (Bogacz *et al.*, 1972). It is overlain by up to 50 m of non-marine claystones of the Keuper (Table 1).

Jurassic and Cretaceous carbonates (limestones, dolomites, minor sandstones) are 0 to 700 m thick (Bukowy, 1974). The Tertiary of the CSM is 0 to 100 m thick and comprises clays and silts.

The basement rocks of the CSM (Cracow Variscides) were metamorphosed to greenschist facies at temperatures of 400 °C and pressure slightly above 4,000 bars (Ryka, 1978). The Cambro-Silurian basement of the CSM (Fig. D2) contains numerous gabbros, granodiorites, microgranites and monzonites. It also contains andradite-sillimanite skarns, hornfelses with hematite and magnetite, and quartz veins with gold, wolframite, scheelite and Mo-bearing scheelite, Ag-Bi tellurides (Gorecka, 1978; Haranczyk, 1979; Gorecka & Nowakowski, 1979). The intrusives also contain sphalerite and galena.

Variscan volcanism in the CSM basement comprises dykes and related subvolcanic units in zones of greater tectonic activities. Albitisation, sericitisation, propilitisation and carbonatisation are connected with the volcanism (Gorecka & Nowakowski, 1979). The polymetallic hydrothermal deposits are connected with granodiorites, rhyodacite porphyries, and include chalcopyrite, molybdenite, sphalerite and minor galena.

5.2 Main zinc-lead districts

The zinc-lead ores of Upper Silesian District occur in the carbonate Triassic carbonate cover (Figs. D1, D2). The Bytom and Chrzanów troughs are located over sub-outcrops of the Upper Silesian Coal Basin, whilst the Olkusz and Zawiercie ores are located over the Cracow Variscides. Ores occur mainly in the Muschelkalk (Table 1). Only in the area of Zawiercie do more mineralizations occur in the Devonian (Fig. D1, Table 1). The whole of the Ore-Bearing Dolomite (OBD) of the district is enriched in Fe, Zn and Pb (Table 2), and Zn-Pb sulphides are finely dispersed throughout the whole section of the OBD. Several ore horizons are developed within the orebodies. The lower horizons are Zn-rich, while the upper ones have an increased Pb content. Strata-bound mineralization inherited primary features of the parent rock (Bogacz *et al.*, 1973). The main orebodies are present in carbonates deposited in intertidal/subtidal environments characterized by high initial porosities and permeabilities.

An economic orebody is defined by cut-off grade of 3.5 wt% of Zn + Pb for the sulphide ore, or 5.5 wt% of Zn + Pb for the oxide ("galmei") ore.

5.2.1 Chrzanów area (Chrzanów Trough)

The deposits of the Chrzanów area consist of about 90 orebodies of different size (Fig. D3). It is estimated that, from the beginning of documented exploitation in the 14th century until 1992, the Chrzanów area produced about 2.2 Mt of metallic zinc, 0.7 Mt of metallic lead, about 600 t of silver, and several tens of thousands of tonnes of cadmium. At present only one mine in this area is in operation, the Trzebionka mine. It currently produces 2.1 Mt of ore per annum, grading 3.5–3.9 wt% Zn, 1.5–1.8 wt% Pb, ca. 50 g/t Cd and 10 g/t Ag (Szuwarzynski, 1993). The current reserves will permit continuation of mining for the next 10 years at the present rate of production.

In the Trzebionka mine, there are 3 major ore producing horizons located within the OBD – I, II, and III (Figs. D3, D4). There are three other horizons enriched in Zn and Pb located

Table 2. Chemical composition of dolomite from the Upper Silesian Zn-Pb district (wt%)

Dolomite type	*n*	MgO	S	MnO	FeO	ZnO	PbO	Method
Early diagenetic	1	16.29	0.13	0.22	3.46	0.34	0.07	bulk
Ore-bearing (OBD)	16	9.90–19.00 17.21	0.00–0.15 0.05	0.10–0.55 0.14	0.10–4.97 1.67	0.15–0.87 0.20	0.01–0.07 0.02	bulk
Fe-bearing OBD	5	16.89–20.01 19.83	0.03–0.10 0.08	0.11–0.89 0.60	1.89–7.11 5.34	0.34–1.34 0.76	0.05–0.23 0.12	bulk
Zn-bearing OBD	4	16.34–18.99 18.01	0.04–0.25 0.15	0.10–0.78 0.63	0.79–2.01 1.27	1.45–10.12 3.22	0.08–1.11 0.57	bulk
Zoned rhombohedra: core	14	19.55–20.98 20.04	≤0.04	≤0.03–0.21 0.18	0.03–0.34 0.07	0.25–1.51 1.01	≤0.05	electron microprobe
Zoned rhombohedra: Fe-rich zones	9	13.51–17.14 15.14	≤0.04	0.20–1.01 0.68	5.46–9.27 8.05	0.26–1.81 1.11	≤0.05	electron microprobe
Zoned rhombohedra: Zn-rich zones	7	17.28–20.16 19.12	≤0.04	≤0.03–0.81 0.40	0.14–4.01 1.33	0.50–1.85 1.49	≤0.05	electron microprobe
Paragenetic with sulphides	30	14.10–19.40 18.42	≤0.04	0.10–0.98 0.55	0.10–1.30 0.82	0.50–16.00 3.73	≤0.05–2.12 0.12	electron microprobe
Paragenetic with smithsonite–siderite ore	54	13.11–21.03 17.99	≤0.04–0.21 ≤0.04	≤0.04–0.67 0.37	0.16–4.18 1.76	0.18–18.0 6.75	≤0.05–0.42 0.10	electron microprobe

outside the OBD – P, D and B (Fig. D4). The main ores are hosted by the OBD, developed in the Upper Gogolin, Gorazdze and Karchowice Beds, and trend NW–SE along the margin of the Upper Silesian Trough within the ore horizon II (Fig. D5). The Triassic rocks occupy broad synclines and troughs formed during the Early Cimmerian orogeny (Upper Triassic–Middle Jurassic) due to rejuvenation of the Variscan structures in the basement. Some of the faults are synsedimentary (Herbich, 1981; Szuwarzynski, 1988). The latest fault structure was developed in the Miocene during the formation of the Carpathian Foredeep.

The mineral assemblage is simple: sphalerite and galena. In the Chrzanów area, unlike in the other mining areas, pyrite and marcasite are rare. The main textures of the sulphide ores are: replacement of the host rock and filling of primary and secondary porosity, vugs and veinlets. Replacements are the main ore texture in major tabular orebodies of massive sphalerite. Breccia textures are rare, and they are mainly of tectonic origin (Szuwarzynski, 1993).

Mineralization occurs in distinct ore horizons (Fig. D4). Horizons P, B, and partly D have regional extent and are homogeneous, but low in grade. In contrast, horizons I, II and III do not show extensive lateral development, are inhomogeneous and form a series of horizontal Zn-Pb rich orebodies with sharp contacts to the OBD marked by an envelope of smithsonite, siderite and Zn- and Fe-rich dolomite.

Ore Horizon I

Majority of the sulphide orebodies (about 70) occurs in this horizon mainly along the Trzebinia-Bedzin fault zone and in the southern part of the Chrzanów depression. The orebodies form a ~2000 m wide belt in the fault zone. The belt consists of a number of small fold structures cut by faults oriented parallel to fold axes that are in turn cut by a multitude of perpendicular dislocations. All of the orebodies were small in size, with variable metal tonnage varying from about 4,000 to about 50,000 t, but they were rich in silver – about 200 g/t. Most of these orebodies have been deeply weathered and often contain only relics of sulphides incorporated into oxidation products. The size of the orebodies defined by cut-off grade of 5% Zn + Pb were: 400–1600 m along strike, 60–250 m down dip with a thickness of 1.2–1.3 m (Szuwarzynski, 1993). The orebodies are elongated parallel to fold axes and the main ore was formed by metasomatic replacement of the host OBD.

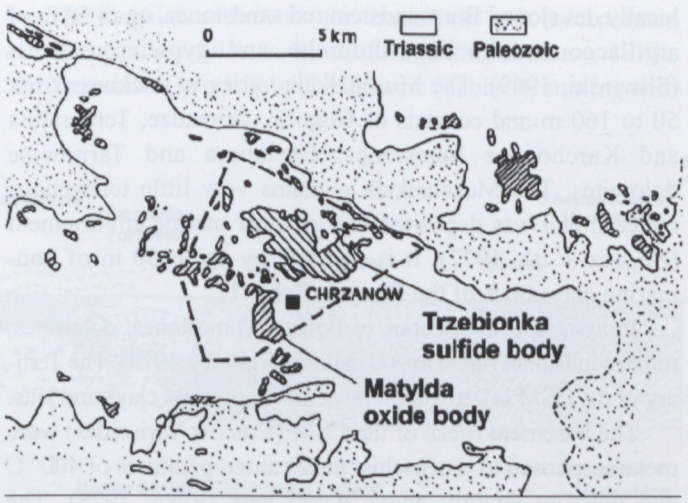

Fig. D3. The zinc-lead deposits in the Chrzanów area (after Szuwarzynski, 1993).

STRATIGRAPHY			ORE HORIZONS	Zn + Pb (WT. %)	ORE MINERALS
MUSCHELKALK	BORUSZOWICE BEDS			0.07	P
			B	0.15	P, G, S
	TARNOWICE BEDS			0.05	G
	DIPLOPORA DOLOMITES			0.06	P, G
			D	0.54	G, S, P, D
				0.07	P, S
	TEREBRATULA & KARCHOWICE BEDS	ORE-BEARING DOLOMITES		0.18	P, S, G, D
			III	8.25	S, G, P, D, SM
				0.29	S, P, D
	GÓRAŻDŻE BEDS			0.37	S, G, P, D
			II	54.00	S, G, P, D, SM
				0.65	S, P, D
	GOGOLIN BEDS	UPPER	I	25.00	S, G, D, SM
				1.04	S, P, D, SM
				0.23	S, P, D
		LOWER		0.05	G, P
			P	1.50	S, P, G
BUNTER	ROETHIAN			0.05	G, S, P

S - SPHALERITE; G - GALENA; P - PYRITE; D - Zn-DOLOMITE; SM - SMITHSONITE - SIDERITE

Fig. D4. Stratigraphy, ore horizons and mineralization in the Chrzanów area (after Szuwarzynski, 1974 and author's data).

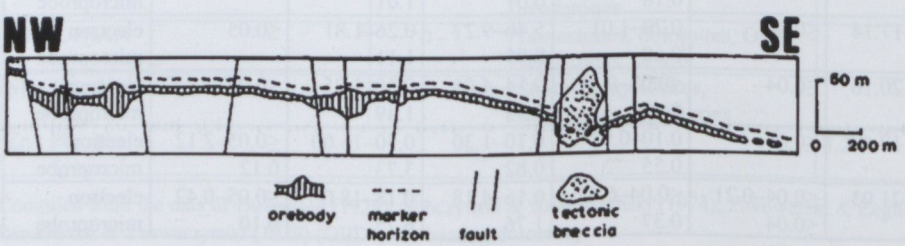

Fig. D5. Schematic NW–SE cross-section through Horizon II in the Chrzanów area (after Szuwarzynski, 1993).

The orebodies of the Chrzanów depression are composed mainly of primary sulphides. The size of the orebodies defined by cut-off grade 2.0 wt% of Zn + Pb was: up to 2,000 m along strike and up to 1,200 m down dip with an average thickness of 1.8 m, but mining stopes locally attained thickness up to 6 m. The main ore texture is represented by a metasomatic replacement of the OBD by sphalerite.

Ore Horizon II

Ore Horizon II contains 10 major orebodies. Many of them resemble orebodies known from Ore Horizon I. However, the two largest have very different features. These are the orebodies exploited by the Matylda and the Trzebionka mines (Fig. D3).

The Matylda orebody (Fig. D3) contained over 150,000 t of Zn + Pb metal, with the Ag content of over 70 g/t. The lead content was high, 5 to 6 wt%, being present in vein- or nest-like galena concentrations within a mass of smithsonite–siderite solid solution series replacing the OBD (Szuwarzynski, 1993). The stratigraphic position of the Matylda deposit is equivalent to that of the Trzebionka mine. The Zn-Fe carbonates occurred in up to 4 ore horizons with ore structures and textures similar to the sulphide body of Trzebionka. The average Zn content in the Matylda ore was about 4 wt%. Mining ceased due to difficulties in processing of Zn-Fe carbonate ore.

The Trzebionka orebody is the largest orebody of the Upper Silesian Zn-Pb district. It contains 3 Mt of Zn + Pb ore with an Ag content of about 10 g/t and Cd concentration of about 300 g/t. The orebody size, defined by a cut-off grade 2.0 wt% of Zn + Pb is over 5000 m along strike and 800–2300 m down dip. The thickness varies from 2 to 6 m, with an average of 4 m. Locally, close to faults perpendicular to the depression axis, there is a thickening of the orebody up to 40 m (Fig. D5; Szuwarzynski, 1993). The orebody is generally parallel to the bedding of the Triassic carbonates and to some dislocations. The main ore texture is represented by a replacement of the OBD by sphalerite and less frequently by fillings of voids or breccia matrix. Breccias seen in Trzebionka orebody are either tectonic or less frequently related to dissolution of the host OBD. A major microtexture in tabular sphalerite orebodies is sphalerite cementing and infilling intergranular porosity of crinoidal grainstones (Fig. D6). The shape of crinoids is preserved and they are converted into single Fe-Mn-Zn-rich dolomite crystals mimicking the shape of crinoids originally built up of high-Mg calcite.

Ore Horizon III

This ore horizon (Fig. D4) contains 7 known orebodies. Two of these bodies were mined by the Matylda mine. Their size varied along strike from several hundred to 2000 m, and down dip from a few tens up to 200 m, with a thickness of up to 1.8 m. The dominant ore texture resulted from the open space filling of voids (veinlets) and lining of cavity walls. Main mineral was smithsonite–siderite solid solution series, and Zn-rich dolomite.

5.2.2 Bytom area (Bytom Syncline and Tarnowskie Gory Syncline)

The Bytom Trough is about 14 km long and 2–4 km wide. As in the Chrzanów trough, the ore deposits are confined mainly to the lower part of the OBD, which is equivalent to the Gorazdze Beds in this area (Table 1). The ore in the Bytom Trough occurred in the form of lithostratigraphically continuous ore horizons, out of which the three lowest have an economic importance (Gruszczyk, 1956; Szuwarzynski, 1996). The thickness of the OBD varies from 20 to 60 m.

In general, orebodies in the main ore horizon I are stratiform with a thickness from 1.5 to 2.5 m, locally up to 5 m. They are tabular, concordant with the host dolomite, with lateral extension up to several km. Smaller orebodies have a lateral dimension of several hundred meters and their thickness stays within 1.5 to 2.5 m. The ore grade varies from 3 to 6 wt% Zn (exceptionally 30 wt% Zn), with sphalerite forming almost monomineralic lenses, pseudolayers, nests, veinlets and only locally breccias, which always stayed within the boundaries of tabular sphalerite bodies. All of the discussed orebodies consisted of poorly cemented banded sphalerite. The thickness of the individual ZnS bands was around a few tens of cm, exceptionally up to 3 m. The top of sphalerite bodies was marked by crackled dolomite breccia cemented with ZnS succeeded by thin, horizontal galena layers. The other two ore horizons are thinner, attain thickness of up to 2 m, and the grade of ore is lower. Sometimes more than 3 ore horizons occur but their lateral extent is limited and the grade is low. In general, the higher the ore horizons number the poorer the ore grade. Locally, the ore horizons merge into a system of sub-vertical veins and breccias cemented by sulphides. Such brecciated ores may attain a thickness of several meters. However, the trough also contains unmineralised breccias, which occur more often than their mineralised counterparts.

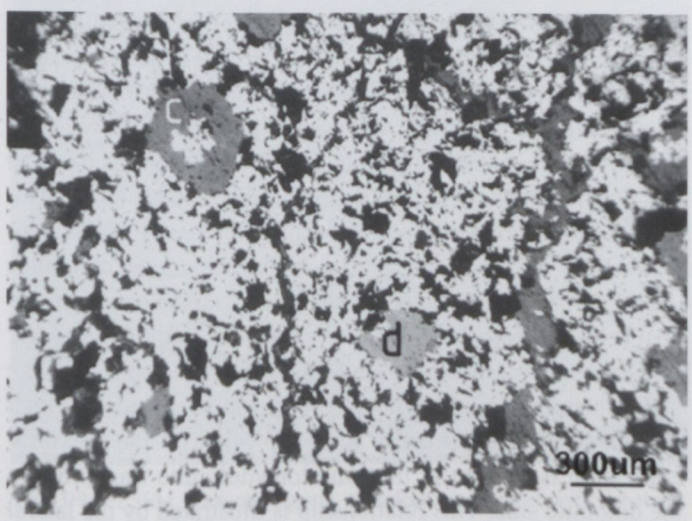

Fig. D6. Photomicrograph of microtexture in tabular sphalerite bodies of the Trzebionka mine. Grey rounded forms (c) are crinoid stems converted into single crystals of Fe-Mn-Zn dolomite (d). Rim cements and filling cements and replacements are represented by sphalerite (white). Reflected light, sample 172, scale bar 300 μm, Trzebionka mine.

Sphalerite dominates in the eastern and the central part of the trough, whilst galena is more abundant in the western part of the Bytom Trough. Galena and sphalerite are accompanied by large, beautifully zoned "melnikovite" accumulations (Ramdohr, 1980). Oxidized ore occurs at the edges of the trough. The Bytom galena is the most silver-rich in the Upper Silesia district and has been mined for Ag since the 12th century, most extensively in the 19th and 20th centuries. The ore rich in silver was mined out first. Mining in the area has now been ceased due to the exhaustion of the economic reserves. The total production was 22–24 Mt of metals, including 3 Mt of lead.

5.2.3 Kalety-Tarnowskie Gory area

The ores of this area were mined out during the 19th and the beginning of the 20th centuries. The production of zinc metal amounted to several Mt and that of lead up to 1 Mt. Ore occurred in the OBD only in the lowest Horizon I as small orebodies, where the main ore minerals were sphalerite and galena, in late-stage veinlets and veins up to 50 cm in thickness. The southern part of the deposit was oxidized and Zn was present mainly as carbonate.

After the Second World War the Miotek-Zielonka deposit was discovered east of Kalety (Fig. D1). Ore nests and pseudolayers occur within an area of approximately 7×2 km within the OBD. Orebodies occur at depths between 80 and 240 m. The main sulphide minerals are sphalerite, galena, pyrite and marcasite. Galena is silver-rich.

5.2.4 Olkusz area

Olkusz area is located near the eastern edge of the Upper Silesian Zn-Pb district (Figs. D1, D2) and occupies an area of about 20×10 km. The deposits of Laski, Krzykawa, Boleslaw, Olkusz, Pomorzany and Sikorka are located in the central part of the area. The Bledow, Klucze and Chechlo deposits occur in the northern part of the area. The orebodies in the central part of the area are composed of several horizons containing ore layers, lenses and nests interconnected by veins and veinlets so that the total thickness of the mineralised horizon is up to 10 m. Less important mineralizations occur at the base of Diplopora Dolomites, in the Roethian and in the Devonian dolomites (Table 1). As a rule the best ore mineralization occurs in the OBD close to vertical and lateral transitions to the limestones.

Statistical treatment of the drillcore data indicates that the best mineralization is connected with those sections, which contain 19–75% dolomite in vertical profile, *i.e.* the best mineralization is present at the limestone/dolomite transition on the dolomite side. This relationship is illustrated by the lateral distribution of dolomite, dolomite plus limestone and Zn-Pb mineralization in a 2 m thick horizon (level B) within the Upper Gogolin Beds in the Olkusz area. This relationship was ignored during the drilling programme of Laski and Krzykawa areas away from the dolomite/limestone transition. The experience was disappointing and costly as no economic mineralization was found despite a very high density of drilling.

The largest deposits of the Olkusz area are Pomorzany, Olkusz, and Boleslaw. The density of drilling around the existing mining leases is variable. The most intensively drilled area is west of Laski and Krzykawa. Very little drilling was done east and north of Sikorka, Klucze and Chechlo, and consequently a good exploration potential may be assigned to these areas.

The Olkusz deposit is slightly smaller than that of Pomorzany. The orebodies consist of layers, lenses, nests and mineralised collapse breccias. Only parts of the collapse breccias are mineralised by sulphides. The sulphides are present as cements and replacements of breccia clasts, composed of dolomite and clasts of earlier sulphides as well. Collapse breccias are developed over hundreds of thousands of square meters and may attain thickness of up to 50 m encompassing entire thickness of the OBD (Sass-Gustkiewicz *et al.*, 1982). The process of brecciation and mineralization alternated so that earlier sulphides form clasts cemented by younger sulphides. The mineralization is developed at several horizons from the Lower Gorazdze to the Karchowice Beds. Some mineralization occurs also in the Roethian and the Devonian (Table 1). The best mineralization occurs towards the base of the OBD, where massive ore is 3 to 6 m thick. In larger karst cavities, sulphides form internal sediments. The main minerals of the Olkusz orebody are: sphalerite, marcasite, pyrite, Fe-Pb-As oxysulphides (Kucha &Viane, 1993; Table 3), galena, Fe-rich dolomite, Zn-rich dolomite and $ZnCO_3$–$FeCO_3$ continuous solid solution series, which predates the main sulphide mineralization (Kucha & Czajka, 1983; Fig. D7). Smithsonite–

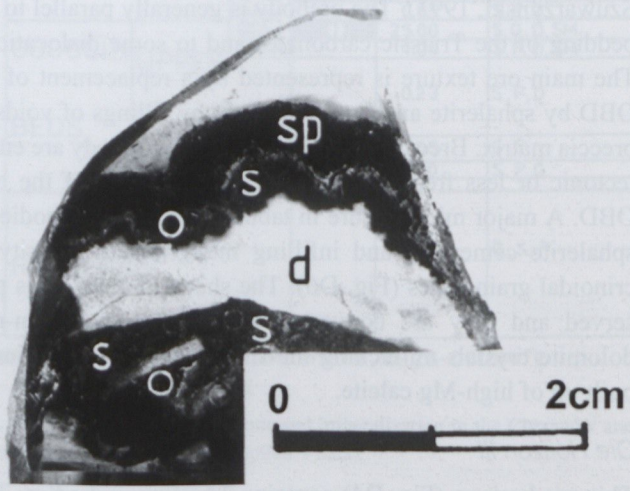

Fig. D7. Photograph of a bleached dolomite clast (d), overgrown first by banded smithsonite–siderite (s) and banded sphalerite (sp). The former is replaced at the contact by the later (Fig. D8) through semimassive bacterial mat (Fig. D9). Dolomite clast rests on fine-grained dolomite breccia and angular sphalerite debris cemented by a continuous solid solution series smithsonite–siderite. Open white circles denote microphotographs of banded smithsonite–siderite overgrowing the top of dolomite clast (Fig. D8), and banded smithsonite–siderite (s) cementing sphalerite clasts below dolomite (d) (Fig. D10). Orzel Bialy mine, sample 169 (sample is bottom-top oriented).

Table 3. Chemical composition of melnikovite-type compounds (oxysulphides), Orzel Bialy mine (after Kucha & Viaene, 1993)

Sample	Si	Ca	S	Fe	Zn	As	Tl	Pb	Σ	$O_{diff.}$	Formula (approximate)
01	0.04 0.8873	0.08	23.48 0.8522	39.28 0.0447	2.41 0.1127	6.97 0.0009	0.15 0.0252	4.33 76.72		23.28 1.7630	$M(S,As)O_2$ sulfoxylane
02	0.04 0.8754	0.11	17.45 1.1522	40.00 0.0578	2.35 0.1246	5.80 0.0015	0.20 0.0274	3.53 69.47		30.53 2.9791	$M(S,As)_3$ sulfite
05	0.29	≤0.03	11.35 1.0434	7.35 0.3889	0.55 0.0226	0.93 0.0332	2.29 0.0332	70.53 1.0000	93.30	6.70 1.1925	PbS + FeOOH fine mixture
06	0.63 0.0224	0.15 0.0037	2.76 0.0861	19.43 0.3480	1.32 0.0202	1.34 0.0179	1.15 0.0056	48.94 0.2362	75.72	24.28 1.5175	Oxides + sulphates
07	0.06	≤0.03	40.89 5.5416	35.51 2.7615	0.07 0.0015	7.92 0.4583	0.20 0.0043	1.67 0.0356	86.32	13.68 3.7147	$1.76Fe(S,As)_2 + 1.24FeS_2O_3$
08	≤0.03	≤0.03	44.69 3.7220	38.39 1.8360	0.07 0.0029	7.84 0.2780	0.20 0.0026	1.81 0.0233	93.00	7.00 1.1682	$1.42\ Fe(S,As)_2 + 0.58\ FeS_2O_3$
09	1.51 0.1189	0.19 0.0104	27.05 1.8645	22.76 0.9006	0.32 0.0102	4.55 0.1355	0.81 0.0087	5.10 0.0543	62.29	33.71 5.1999	pyrosulfite
10	1.42 0.1081	0.19 0.0101	27.60 1.8403	23.93 0.9149	0.24 0.0066	5.60 0.1597	0.81 0.0083	8.23 0.0847	68.02	31.98 4.2732	$M(S,As)_2O_4$ subsulfite
11	0.57	0.23	5.46 0.1703	15.07 0.2698	1.33 0.0203	1.08 0.0144	1.03 0.0050	54.24 0.2618	79.01	20.99 1.3199	Oxides + sulphate
12	0.78 0.2283	0.10 0.0204	10.17 2.6061	23.39 3.4326	1.01 0.1254	3.58 0.3939	0.17 0.0074	36.18 1.4313	75.38	24.62 12.6440	$M_5(S,As)_3O_{12}$
13	≤0.03	≤0.03	12.85 1.0969	3.83 0.1877	0.50 0.0209	0.52 0.0190	2.24 0.0300	75.70 1.0000	95.64	4.36 0.7459	PbS+FeOOH
14	≤0.03	0.13	9.30 0.9195	0.35 0.0228	≤0.03	1.94 0.0805	1.42 0.0219	67.55 1.0330	80.69	19.31 3.8247	$PbSO_4$

upper figure: wt%, lower figure: mol
Sought for but not detected: K ≤ 0.03, Mn ≤ 0.03

siderite solid solution series is replaced by later sulphides, mainly sphalerite and minor pyrite (Figs. D8, D10). Replacement of the former by the latter is controlled mainly by sulphate reducing bacteria forming mats at the contact of smithsonite–siderite / sphalerite layers (Fig. D9).

The main ore mineral textures are replacement of the host OBD due to high Zn content in the dolomite structure (Table 2), and filling cements in collapse breccias. A common texture is also related to the presence of oscillatory zoning controlled by sulphur valency fluctuation from 2– to 6+ parallel to the

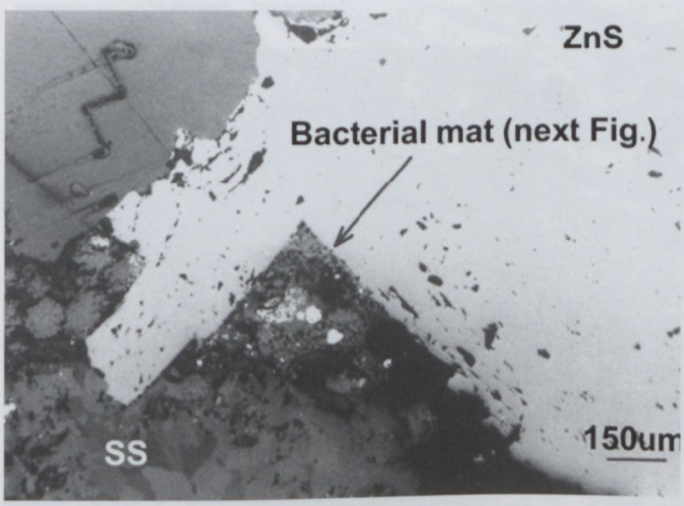

Fig. D8. Microphotograph of banded sphalerite (ZnS) with banded smithsonite–siderite (ss). Sharp corners of smithsonite–siderite (ss) are successively replaced by increasing number of sphalerite dots (arrowed; fossil bacteria) and minor pyrite dots (white framboids). Reflected light, breccia ore, location in white open circle above dolomite clast (d, Fig. D9). Orzel Bialy mine, sample 169, scale bar 150 μm.

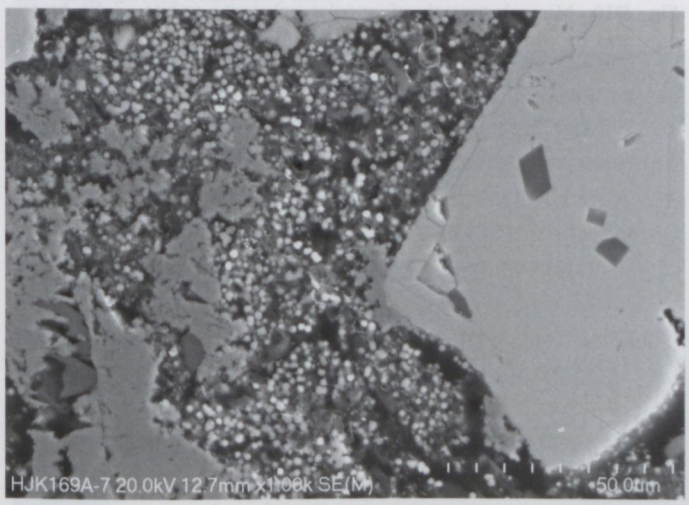

Fig. D9. FESEM photomicrograph of siderite in contact with sphalerite (arrowed on Fig. 8). The contact runs through micro porous area full of small bacterial bodies (now made of ZnS) replacing smithsonite–siderite. Microporosity occurs due to replacement of smithsonite by ZnS, which is resulting in 16.1% of volume reduction (Kucha & Czajka, 1984).

precipitation regime changing from reducing to oxidizing (Figs. D13–D15). Within such oscillatory-banded microtextures, the matrix with mixed S valences re-crystallizes to euhedral crystals having lower valences (Fig. D15). The final stage of replacements of banded oxysulphides by banded sphalerite and/or galena and pyrite takes place (Figs. D13–D15) under reducing conditions, where sulphidic sulphur is stable. The Zn:Pb ratio in the Olkusz area varies from 3:1 to 2:1.

The Pomorzany deposit occupies an area of 12 km^2. The orebodies form layers, lenses, internal sediments in karst cavities and sulphide cemented breccias. The layers may sometimes transgress into breccia bodies. The layers are 300–1000 m long and their thickness varies from centimeters up to several meters (Fig. D11). They are composed of semi-massive sphalerite, and the Zn content varies from a few percent up to 60 wt%. Under the ore microscope, these sphalerite layers show a composite microtexture (Fig. D12). They appear to have been originally crinoidal and oolitic grainstones, where the first sphalerite was introduced as rim cement on bioclasts (Kucha, 1988a; Fig. D12). Subsequently, pore spaces were filled up and a gradual replacement of carbonate allochems resulted in the formation of massive sphalerite layers. Crinoids were preferentially replaced by ZnS due to an increased average zinc content of 0.67 wt%. (This development is similar to that found in Moyvoughly, Ireland, where layers of intertidal/sub-tidal grainstones were precursors of sphalerite layers formed by subsequent infill and replacement of carbonate allochems by ZnS; Kucha, 1988b). The layers and lenses of sphalerite are free of galena and contain only a small amount of pyrite and marcasite. Galena occurs in larger quantities in brecciated ore. To the north-east of Pomorzany, sulphide mineralization appears at increasingly higher stratigraphic levels.

The main ore mineral textures are: i) massive banded sphalerite composed from light-brown to brown sphalerite, which

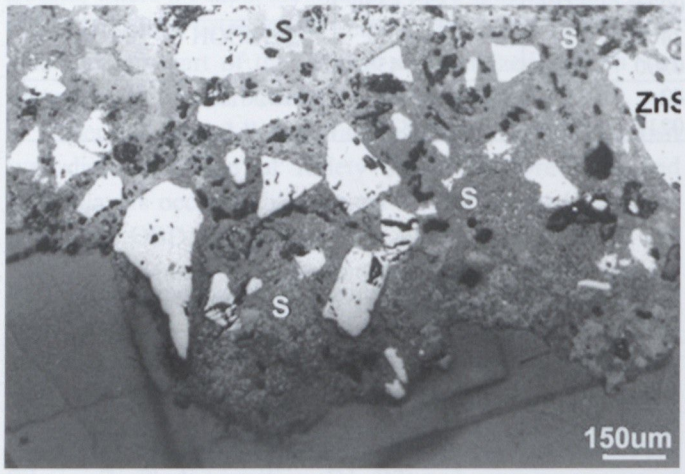

Fig. D10. Microphotograph of angular sphalerite (white, ZnS) breccia cemented by smithsonite–siderite (s). Sphalerite breccia occurs below the large dolomite clast (Fig. D7). Note that smithsonite cement is spotted with myriads of small, brighter ZnS dots representing individual bacteria bodies. Reflected light, breccia ore, location in white open circle below dolomite clast (d, Fig. D7). Orzel Bialy mine, sample 169.

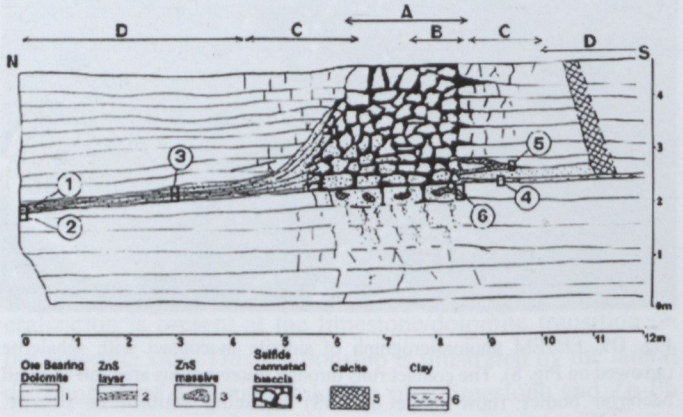

Fig. D11. Sketch of sphalerite layer passing into sulphide-cemented breccia, Mine Drift T-39S, Pomorzany Mine. Detail No 3 is shown on Fig. D12.

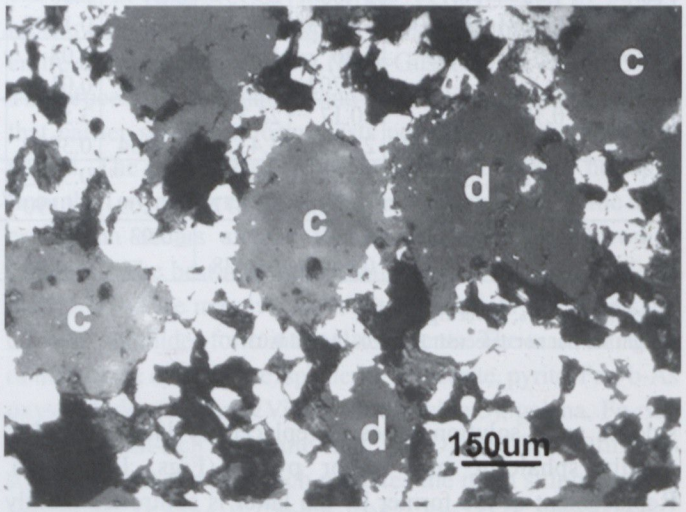

Fig. D12. Details No 3 and 5 from Fig. D11. Sphalerite layer appears to be a layer of crinoidal (c) limestone cemented and replaced by sphalerite and traces of marcasite. Some crinoid stems are recrystallized into dolomite rhombohedra (d). Reflected light, sample 171, Pomorzany mine.

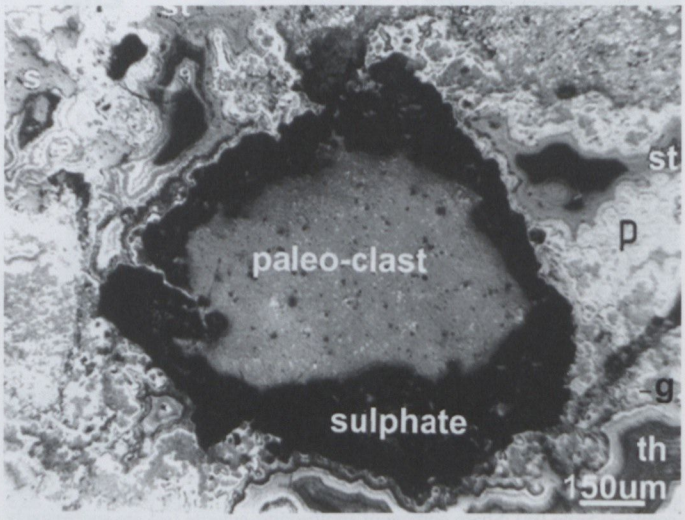

Fig. D13. Photomicrograph of clast of older, partly weathered sulphides (centre of photo) overgrown at first by sulphates and then by younger banded sulphides – pyrite (p), galena (g), thiosulphates (th), sulfites (st) and sphalerite (s). Reflected light, sample 156F, Orzel Bialy mine, scale bar 150 μm.

is often bleached with resultant Fe-loss through microporosity (Kucha & Piestrzynski, 2001). Banded sphalerite is overgrown by black, banded ZnS with abundant oxysulphide inclusions, followed in turn by marcasite bands with/or without PbS (Fig. D16), ii) massive breccia ore composed of bleached dolomite clasts replaced at first alongside the edges by smithsonite–siderite, followed by thick overgrowths of banded sphalerite with abundant oxysulphides in dark bands, and finally overgrown by marcasite layers (Fig. D17), and iii) dolomite breccia with clasts bleached around edges and which may be followed by banded sphalerite and oxysulphide overgrowths (Fig. D18). The Zn/Pb ratio at Pomorzany is 3:1.

The Boleslaw deposit occurs in the OBD equivalent to the Upper Gogolin and in the Gorazdze Beds. The orebody has been fragmented into a mosaic of horst and graben structures. Down-thrown sections remained as sulphides, but uplifted parts were subjected to extensive oxidation. The deposit is developed as several mineralised horizons connected by breccia and vein systems. The thickest deposit, attaining a thickness of 20 to 25 m, was known in the central part of the mine.

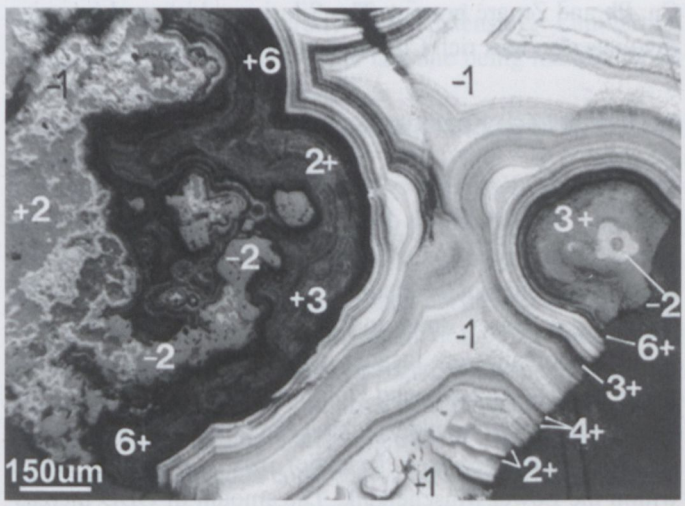

Fig. D14. Microphotograph of oscillatory microbanding in massive mineralization composed of monosulphides (S valence -2; galena: white, sphalerite: grey), disulphides (S valence –1; pyrite: white, melnikovite: various shades of light grey), thiosulphates of Fe, Zn and Pb (average S valence +2; light grey), subsulphites of Fe, Zn and Pb (S valence +3; light grey), sulphites of Fe, Zn and Pb (S valence +4; grey) and sulphates of Fe, Zn and Pb (S valence +6; dark grey). Oscillatory zoning from S +6 to S -2 indicates two major changes from reducing to oxidizing conditions during precipitation of massive sulphides. Reflected light, sample 156F, scale bar 150 μm, Orzel Bialy mine, Upper Silesia.

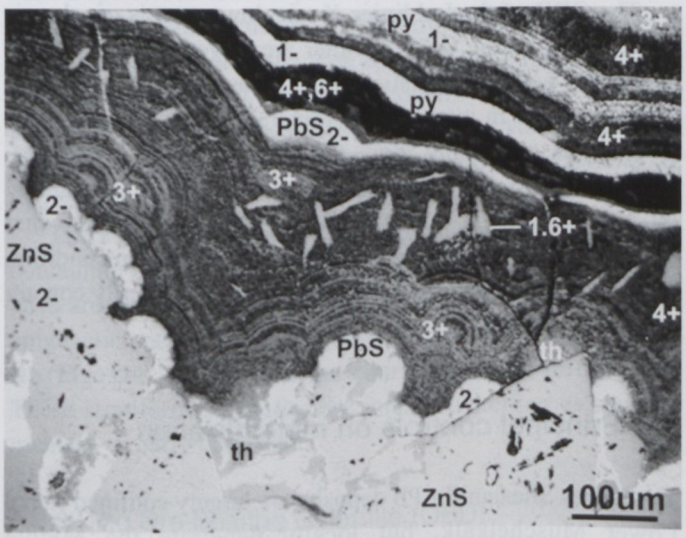

Fig. D15. SEM picture showing oscillatory zoning of sulphur valences from 2– in monosulphides (ZnS, PbS), through 1– in pyrite (py), 1.6+ in oxysulphide recrystallizing from the matrix composed of sulphites (4+) and subsulphites (3+) and thiosulphates (th, S^{1-} & S^{5+}), and dithionate. Sample 156C, Orzel Bialy mine, Upper Silesia.

Fig. D16. Banded mineralization composed of banded ZnS (yellowish to brown), bleached sphalerite (bsf), galena (g), Fe-Zn-Pb-oxysulphides (oxy), and marcasite (m). Pomorzany mine.

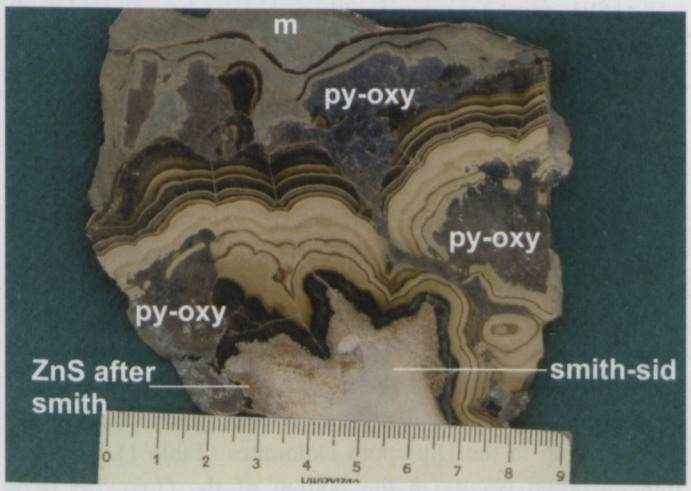

Fig. D17. Complex sulphide mineralization overgrowing dolomite clast (white) replaced first by smithsonite–siderite solid solution series (smith-sid), then replaced by ZnS (ZnS after smith), and subsequently overgrown by Fe-rich sphalerite (black), bleached banded sphalerite (various shades of yellow to brown), pyrite and oxysulphides (py-oxy), and marcasite (m). Pomorzany mine.

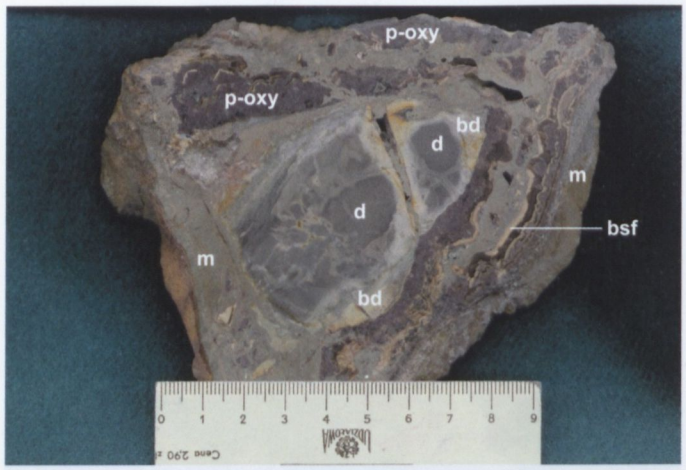

Fig. D18. Breccia ore composed of dolomite clasts (d) bleached alongside edges (bd), and overgrown by black sphalerite, bleached sphalerite (bsf), pyrite and oxysulphides (p-oxy), and marcasite (m). Pomorzany mine.

In the western portion of the mine, the deposit is ~15 m thick, and in the eastern part it is ~10 m thick. The majority of the mineralization is made up of layers and breccias with several stages of brecciation affecting older generations of sulphides. The main ore minerals are: sphalerite, pyrite, Fe-Pb-As oxysulphides replaced by banded sulphides, galena, smithsonite, Zn-rich dolomite, Fe-rich dolomite, and $ZnCO_3$–$FeCO_3$ continuous solid solution series, and traces of jordanite. The Zn:Pb ratio is 8:1.

The deposits of Bledow, Laski and Krzykawa are similar to those in the Pomorzany mine although the size of the orebodies is not that great.

The deposits of Chechlo, Klucze and Sikorka are generally similar to Pomorzany and Olkusz. The mineralization is confined to the dolomite/limestone transition zone. These deposits also have mineralization present at lower stratigraphic levels in the Roethian and Devonian, where the main host is also dolomite developed as a typical OBD type.

5.2.5 Zawiercie area

The Zawiercie area extends from Siewierz to Ogrodzieniec and covers an area of 10×17 km² (Fig. D1). The mineralization occurs at depths of 60 to 140 m below the surface. There are five major orebodies: Zawiercie, Rokitno, Goluchowice, Siewierz-Poreba and Marciszow.

The Zawiercie deposit is the largest concerning size, grade and thickness. These deposits are hosted by the OBD close to its transition into limestone. The main Zawiercie orebody is located in the large horst structure. The mineralization comprises several horizons present in different stratigraphic units, from the Devonian up to the Diplopora Dolomites (Table 1). The best mineralization occurs in the bottom of the Gorazdze Beds (Table 1). The sulphide ore forms layers up to 1 km long and up to 6 m thick with an average thickness from 2 to 3.5 m. Breccia-type mineralization is present locally, but has a limited extent. Many breccias are not mineralised at all. Galena appears mainly in veinlets and in small breccia structures. Since the mineralization is only known from drilling, it is often difficult to characterize the breccia interval due to very poor core recovery.

The main ore minerals are: sphalerite, pyrite, Fe-Pb-As oxysulphides, galena, marcasite and Zn-rich dolomite. Galena is silver bearing. The Zn:Pb ratio is 2.5:1. In the Zawiercie area, the mineralization penetrates lower stratigraphic levels especially Devonian dolomites, where the mineralised zone may be locally up to 90 m thick. At the Devonian/Silurian contact, Zn-Cu mineralization may be observed in the Devonian dolomites, whilst in the underlying Silurian shales increased contents of Cu, Pb and Zn are present. The Silurian schists and intrusive rhyolites also host rich Cu, Mo and W mineralization.

5.2.6 Lubliniec-Kozieglowy area

The Lubliniec-Kozieglowy area is located in the north-west of the Upper Silesian Zn-Pb district (Fig. D1). Drilling within the area was carried out on a regular 1×2 km grid. In zones outlined as anomalous, containing from 0.5 to 1.2 wt% Zn, drilling was denser, down to 250 x 250 m or less. The areas with Zn anomalies are located within the dolomite/limestone transition. The Ore-Bearing Dolomite is developed in a manner similar to that in other highly mineralised areas.

In the Lubliniec area the major part of the OBD occurs within the Lower Muschelkalk. The amount of OBD increases significantly over Paleozoic basement highs. Towards the west, the thickness of the OBD decreases and the OBD gradually vanishes completely as the Triassic carbonates become thicker and they pass into deeper water lithologies. In the Lubliniec area, the thickness of the OBD is bimodal, 0.0–0.5 meters and 40.0–50.0 meters. The thin OBD occurs mainly in the western part of the area, whilst the thickest is observed in the east, where the OBD may attain a thickness of 60 m.

The OBD of the Lubliniec-Kozieglowy area is geochemically similar to the OBD in other areas, yet it only contains anomalies outlined statistically as areas containing 0.5–1.2 wt% Zn over 1 m interval, and mineralised areas defined statistically as containing more than 1.1 wt% Zn. The mineralised areas are generally not larger than 2×5 km and usually do not exceed 0.5–1.5 m in thickness. So, it appears that although the presence of the OBD is a necessary precondition for a good grade mineralization it will not necessarily contain economic mineralization.

5.3 Principal controls on mineralization

The Upper Silesian Zn-Pb deposits are largely confined to the Lower Muschelkalk, but locally penetrate the Middle Muschelkalk, Bunter Sandstone and adjacent Devonian paleo highs (Table 1). Sulphide mineralization occurs almost entirely in the so-called Ore-Bearing Dolomite (OBD) formed by a replacement of limestones and early diagenetic dolomites.

5.3.1 Limestones

The Lower Muschelkalk limestones are hosting the OBD (Table 1), and attain a thickness of up to 60 m (Bogacz *et al.*, 1972). They are composed of limestones of three textural types (Bogacz *et al.*, 1972; Pawlowska & Szuwarzynski, 1979):

1) Crumpled limestones forming 10 to 40 cm thick beds. They comprise crumpled limestone fragments cemented by argillaceous (marly) calcitic or dolomitic cements. This limestone type is often replaced by the later OBD.

2) Laminated limestones forming beds, usually 20 to 50 cm thick, they are laterally very extensive. Lamination changes from fine to coarse, the last one being marked by an increased argillaceous content.

3) Textureless massive limestones forming beds 30 to 40 cm thick, which occur locally.

5.3.2 Early diagenetic dolomites

Four types of early diagenetic dolomites are present in the district:

1) The most common laminated dolomites contain flat pebble conglomerates and intraformational breccias. Laminated dolomites form beds 1 to 2 m thick with lamination parallel to bedding similar to laminated limestones. They may contain horizons with siliceous concretions, and locally dark fossiliferous layers with large amounts of fine pyrite.

2) Textureless, massive dolomites forming beds usually 0.2 m thick, which locally may thicken up to 2 m. This dolomite type is not extensive laterally.

3) Spotted dolomites, which occur locally in the form of lateral and vertical transition between laminated or massive dolomites and oolitic dolomites. The name comes from irregularly distributed, 1 to 2 mm large, interconnected yellow and brown spots, with central parts leached out.

4) Oolitic and pseudooolitic dolomites forming beds from a few cm in the east of the area up to 2.5 m in the west.

Non-recrystallised dolomites contain 0.01–0.2 wt% Zn and 0.001–0.04 wt% Pb, while recrystallised varieties contain 0.01–0.5 wt% Zn and 0.005–0.09 Pb (Pawlowska & Szuwarzynski, 1979).

There are several stratiform anomalies (B, D, K, and P) containing 0.15–1.50 wt% of Zn + Pb (Fig. D4). These anomalies are all on a regional scale, are more extensive than the epigenetic, massive mineralization hosted in horizons I, II and III (Fig. D4), and are not necessarily enclosed in the OBD. These stratiform anomalies are interpreted either as synsedimentary or early diagenetic.

5.3.3 The Ore-Bearing Dolomite (OBD)

The OBD is host to the major Zn-Pb orebodies in Upper Silesia. The OBD is epigenetic and has been formed by recrystallisation of early diagenetic dolomites and by replacement of limestone (Sliwinski, 1969; Bogacz *et al.*, 1972; Pawlowska & Szuwarzynski, 1979). It is considered as a hydrothermally altered envelope around sulphide orebodies.

The OBD differs from early diagenetic dolomites in a few features (Sliwinski, 1969; Bogacz *et al.*, 1972):

i) it is coarser grained,
ii) most of the small-scale sedimentary features has been obliterated,
iii) has cross-cutting relations with respect to bedding, and
iv) it is enriched in iron, zinc and lead (Table 2).

The OBD is developed mainly within the Gorazdze, Terebratula and Karchowice beds (Table 1, Fig. D4). It forms usually discordant, roughly tabular, laterally extensive bodies up to 60 m thick (Sliwinski, 1969; Bogacz *et al.*, 1972). The lower boundary of the OBD is often uneven and is crosscutting the underlying limestones (Bogacz *et al.*, 1972) or marked by residual karst clays (Horzemski, 1962).

The lateral contacts of the tabular OBD to adjacent limestones are commonly irregular with numerous dolomite veins extending into limestones. 'Mottled' structures are typical of the OBD as a result of incomplete dolomitisation. Limestone relicts are common and may be cut by dolomite veins. Silicate accumulations are present in the OBD close to its contacts with limestones (Bogacz *et al.*, 1972).

Vertically extensive forms of the OBD are not common, and occur alongside faults guiding sulphides or around vertically developed karst zones (Pawlowska & Szuwarzynski, 1979). Such vertical OBD forms are confined between the bottom of the Gogolin Beds and the top of the Terebratula Beds. Clasts of the OBD in mineralised collapse breccias are extensively bleached around the margins.

The black Fe-rich dolomite is an important component of the OBD (Table 2). Its color comes from finely dispersed iron sulphides. Fe-rich dolomite is a favorable locus for concentration of sulphide ores and is mostly confined to the lower part of the tabular OBD bodies (Sliwinski, 1969) forming 0.5 to 1.5 m thick halo around sulphide bodies (Kucha & Czajka, 1984). The same seems to be true for Zn-rich dolomite (Table 2), which probably formed precursor layers to which subsequent sulphide ores were confined. The Zn:Pb ratio in Zn-rich dolomite varies from 2:1 to 30:1 (Kucha *et al.*, 1982). The OBD contact with massive banded sphalerite is marked by several millimeters to several centimeters of smithsonite, Zn-rich dolomite and Fe-rich dolomite. The OBD contacts with massive Fe sulphides have an ankerite and Fe-rich dolomite transition zone.

The OBD away from mineralised lateral and footwall contacts with limestone has light gray color and is barren (Pawlowska & Szuwarzynski, 1979).

5.4 Relationship between karst and sulphide mineralization

In the MVT deposits collapse breccias are interpreted either as a result of carbonate dissolution by descending meteoric water

or by ascending hydrothermal fluids (Ohle, 1985; Sangster, 1988; Leach *et al.*, 1996).

In the Upper Silesian MVT deposits four types of breccias are recognized (Leach *et al.*, 1996). They seem always to be in relation with karst:

i) Recent meteoric karst breccias

These breccias occur within the carbonate host rock of the entire district, and are not considered to be related to mineralization. Speleothems may be found in these breccias and in places oxidized debris of ore minerals is present (Bogacz *et al.*, 1973).

ii) Pre-ore breccias

Some researchers assume that the formation of 1) ore-bearing dolomite (OBD) by replacement of pre-existing carbonates, 2) replacement of the OBD by sulphides, and 3) development of mineralized karst cavities and collapse breccias are entirely a simultaneous product of mineralising fluids (Bogacz *et al.*, 1970, 1973; Sass-Gustkiewicz 1975; Dzulynski & Sass-Gustkiewicz, 1989). However, the formation of karst breccias is a multi-stage process and many breccias are not mineralized with sulphides at all (Sass-Gustkiewicz, 1975; Leach *et al.*, 1996). Moreover, mineralization related to the karst breccias controls 20–40% of the total sulphide mineralization in the Pomorzany and Olkusz mines, and only 5–15% in the Bytom trough and Trzebionka mine. The remaining part of the mineralization is controlled mainly by interparticle infill cements and replacements of carbonate grainstone (Kucha, 1988a) forming spectacular, horizontal sphalerite bodies 1.5 to 5 m thick and extending laterally up to 2.5 km (Szuwarzynski & Sobczynski, 1974; Szuwarzynski, 1996). The distribution of these tabular sphalerite bodies follows the original distribution of carbonate grainstones, characterized by high initial porosities and permeabilities, deposited in a shallow marine environment (Kucha, 1988a).

Pre-ore karst breccias might be related to meteoric karst developed prior to sulphide mineralization as suggested by the presence of unconformities at the top of the Muschelkalk, before the overlying deposits of the Keuper (Glazek, 1989).

It is probable that meteoric karst development continued during the time of the sulphide mineralization. This may be suggested by the presence of Zn-rich limonite cementing granular sphalerite at the base of banded sulphides overgrowing on the bleached dolomite (oxidation?) angular clasts in breccia ores.

iii) Replacement breccias

Replacement breccias are observed in the Pomorzany, Olkusz and Orzel Bialy mines. The breccias are formed by the progressive replacement of the fine (Zn- and Fe-rich dolomite) breccia matrix by sphalerite (Leach *et al.*, 1996) so that at the final stage larger dolomite clasts (surviving replacement) are seen embedded into semi-massive sphalerite. Relicts of fine breccia matrix enclosed by replacive ZnS are composed of Zn- and Fe-rich dolomite or smithsonite–siderite (Kucha & Czajka, 1984).

iv) Hydrothermal breccias

There is evidence in some of the sulphide breccia ores that dissolution of the carbonate host and brecciation occurred during sulphide mineralization (Sass-Gustkiewicz *et al.*, 1982; Dzulynski & Sass-Gustkiewicz, 1989). Pre-ore karst breccias have been enlarged by dissolution accompanying sulphide replacements (Leach *et al.*, 1996) and / or replacement of Zn carbonates by sulphides (Kucha & Czajka, 1984), releasing large quantities of CO_2. Dolomite clasts in these breccia are bleached (Figs. D7, D18), their external surfaces exposed to the flowing mineralizing fluids are corroded by overgrowing banded smithsonite–siderite solid solution series (Figs. D7, D10, D17) with strong replacement features of smithsonite–siderite by overgrowing sphalerite (Figs. D7–D9; Kucha & Czajka, 1984). A significant portion of the sulphides in these breccias occur as open space fillings (Leach *et al.*, 1996). Older banded sulphides are often bleached, broken, rotated and re-sedimented as sulphide breccias cemented by younger sulphides. In the Orzel Bialy mine, angular sphalerite clasts in these breccias are cemented by continuous solid-solution smithsonite–siderite series minerals (Fig. D10).

In some of the breccia bodies, weathered clasts of older sulphides overgrown first by sulphates (mainly $PbSO_4$) and then by younger banded sulphides and oxysulphides have been observed (Fig. D13). Some of the banded microtextures provide startling examples of oscillatory zoning of sulphur valences from +6 to –2 (Figs. D14, D15). Recrystallization of laths of compounds containing sulphur +3 and +2 is often visible in the thiosulphate matrix (sulphur –1 and +5). Such fine banding related to sulphur valences and the presence of clasts of paleo-weathered ore embedded into younger banded sulphides can only be explained by mixing of two fluids, one reduced (hotter, with metals) and another oxidized (cooler, with sulphur). The cooler fluid may be related to surficial karst fluids. This may mean that the so-called hydrothermal karst may be a product of different fluids. This is tempting to consider also that in some karst caves the bottom of the collapse rubble was submerged in hydrothermal fluids, while the upper sections of the cave were aerated and subject to weathering. Corrosive weathering caused the loose weathered clasts to fall into submerged bottom rubble, which were under the process of cementation by oxysulphides. Rising and falling levels of the hot fluids could be responsible for complex zoning phenomena (Figs. D14, D15) and overgrowths of banded sulphides on the surfaces of weathered ores (Figs. D13, D17).

5.5 Ore textures and structures

Six major textures can be distinguished in the Upper Silesian Zn-Pb ores:

- Fine disseminations in the OBD external to sulphide orebodies. This takes the form of small sulphide grains dispersed

in a recrystallized dolomite matrix. The typical micro-textures are framboids of pyrite, sphalerite and galena as well as small-scale replacements of carbonates. This texture is associated with low concentrations not exceeding 2.5 wt% of (Zn + Pb) combined.

- Massive texture parallel to the bedding and consisting of single or multiple sphalerite layers with numerous intervening vugs and voids. The overall thickness of the sphalerite layers ranges from a few cm up to a few m and they may extend laterally up to 3 km in the Trzebionka mine. They are assumed to be formed by a metasomatic replacement (Sass-Gustkiewicz *et al.*, 1982). Sphalerite rims around carbonate grains, sphalerite filling up intergranular porosity (Figs. D11, D12) and sphalerite replacing carbonate grains are the typical micro-textures observed (Kucha, 1988a). The discussed sphalerite layers are usually surrounded by a carbonate halo up to 1.5 m thick composed of smithsonite–siderite, Zn-rich dolomite and Fe-rich dolomite (Kucha & Czajka, 1984). Industrial estimations suggest that as much as 65–70 wt% of Zn-Pb resources exploited until now are of this type (Szuwarzynski, 1996).
- Sulphide breccias composed of clasts of previously deposited banded sulphides, which were rotated, displaced and may be cemented by younger sulphides. These textures occur in collapse breccias and are interpreted as a product of hydrothermal karst (Sass-Gustkiewicz, 1975; Sass-Gustkiewicz *et al.*, 1982; Leach *et al.*, 1996). Industrial estimations indicate that as much as 10–20% of total resources of zinc and lead are concentrated in this textural form (Szuwarzynski, 1996).
- Fracture fillings surrounded by metasomatic halo (Kucha & Czajka, 1984). As much as 10–15% of total resources of zinc and lead are concentrated in this textural form (Szuwarzynski, 1996).
- Sulphides in disaggregated (delithified) dolomite (Bogacz *et al.*, 1973). This type of ore probably follows an original distribution of Zn-rich dolomite, which is considered to be a precursor of sphalerite (Kucha & Czajka, 1984; Osman & Piestrzynski, 1989).
- Weathered clasts of older sulphides enclosed by younger massive, banded sulphides (Figs. D13, D14).
- Replacements and recrystallisation of precursor oscillatory zoned oxysulphides (Fig. D15).
- Local bacterial mats composed of fossil microbial sphalerite (Fig. D9).

5.6 Fluid inclusion temperatures

Fluid inclusion temperatures measured for the Upper Silesian Zn-Pb sulphide ores range from 45 to 130 °C (Kozlowski *et al.*, 1980; Kozlowski & Gorecka, 1993). Temperatures of the banded smithsonite–siderite range from 94 to 103 °C (Niec & Bak, 1993), and are similar to the temperature range of banded sphalerite (Figs. D7, D8). The fluids are of hydrocarbon aqueous type. The total salt concentration varies from 0 to 22% NaCl equivalent with the main ions represented by Cl, Na, K and Ca (Kozlowski & Gorecka, 1993) and liquid hydrocarbons. The total gases in fluid inclusions are less than 1.5 mol%. There are two gas groups, $CO_2 + CH_4$ and $CO_2 + H_2S$. The variable proportion of hydrocarbons to aqueous solutions suggests heterogeneous ore-bearing fluids. Metals and sulphur are considered to have been supplied at least partly by different fluids (Kucha & Czajka, 1984).

The OBD is composed of two generations of dolomite. Dolomite I (earlier) contains two populations of inclusions: i) single-phase inclusions formed ≤50 °C, and minor ii) two-phase inclusions displaying temperatures between 50 and 104 °C (Heijlen *et al.*, 2003). The coarser grained Fe-rich dolomite II displays again two populations of fluid inclusions: single-phase aequous inclusions, and another group of two-phase inclusions showing homogenization temperatures 61 to 94 °C. The ion and oxygen isotopic compositions of the crush-leach fluids of the inclusions show them to be more evolved than recent brines of the Upper Silesian Coal Basin. It also shows them to be a product of an extensive mixing with low salinity fluids (Heijlen *et al.*, 2003).

5.7 Sulphur isotopic composition

The Upper Silesian Zn-Pb ores show several generations of sulphides that differ in their sulphur isotopic signature. The sulphur isotopic signature of banded sulphides overgrowing dolomite fragments in breccia ore show progressive enrichment in the heavy isotope (Haranczyk, 1993). Banded pyrite forming the latest bands has $\delta^{34}S$ values ranging from +67‰ (Gehlen & Nielsen, 1969) to +49‰ (Haranczyk, 1993). Coarsely banded, late sphalerites have $\delta^{34}S$ values of +54‰. Sulphide stalactites from the Pomorzany mine have a $\delta^{34}S$ isotopic signature varying from –6‰ to –37.4‰ (Haranczyk, 1993). Similar stalactites at the Trzebionka mine have $\delta^{34}S$ values that vary from +3.40‰ to +2.03, when composed of sphalerite, and –2.90‰, when composed of galena. Stalactites composed of pure, white, soft, powdery ZnS from the Boleslaw mine have $\delta^{34}S$ values varying between –15.6‰ and –18.75‰, whilst pyrite stalactites with recently recognized oxysulphides (Kucha & Viaene, 1993) have $\delta^{34}S$ values of –23.75‰ (Haranczyk, 1993).

Sulphur isotopic composition in banded ZnS showing phenomena of bleaching, affecting some of bands (Kucha *et al.*, 2001a), display negative $\delta^{34}S$ values:

1. the oldest sphalerite "a" replacing dolomite –1.37 to –0.59
2. the first bleached band of sphalerite "b" –4.61 to –3.72
3. sphalerite "c" prior to bleaching –5.10 to –2.54
4. sphalerite "d" ("c" after bleaching) –2.66 to –2.59
5. sphalerite "e" rich in Fe, Ni, As, Pb and oxysulphides –6.01 to –8.56

Such pattern may suggest a preference of light S to be bound to Fe in the sphalerite structure.

5.8 Lead isotopes

The lead isotopic composition of the Upper Silesian zinc-lead ores is very homogeneous (Ridge & Smolarska, 1972; Zartman *et al.*, 1979): $^{206}Pb/^{204}Pb$ 18.406–18.444, $^{207}Pb/^{204}Pb$ 15.599–15.625 and $^{208}Pb/^{204}Pb$ 38.410–38.434. This suggests that parent hydrothermal fluids did not circulate through crystalline basement rocks having variable ages and provenance. This may be further supported by the observation that the Triassic cover is separated from the basement by a shale sequence.

Three lead sources may account for such uniform lead isotopic composition:

- Lead bound in iron oxides in molasse sedimentary rocks (Carboniferous? Permian?). This requires leaching of lead shortly after deposition of sediments otherwise a contribution of radiogenic lead from the silicates would affect the isotopic signature.
- Lead present in evaporatic sequences in the Upper Silesian Coal Basin.
- Lead present initially in carbonates of the OBD displaced and reconcentrated later into sulphide orebodies during sulphidisation (Kucha & Czajka, 1984).

Galena veins are observed in coal mines (Ridge & Smolarska, 1972). In the northern part of the USCB the lead isotopic composition of galena from coal mines is the same as in the MVT Zn-Pb deposits, *i.e.* $^{206}Pb/^{204}Pb = 18.444$, $^{207}Pb/^{204}Pb = 15.619$ and $^{208}Pb/^{204}Pb = 38.418$. However, in the southern part of the USCB, in the Jastrzebie coal mine, galena is remarkably depleted in heavy lead isotopes 18.289, 15.617 and 38.219, respectively (Ridge & Smolarska, 1972).

5.9 The age of mineralization

The horst and graben structures in the Upper Silesian Zn-Pb deposits were reactivated during the Cretaceous–Tertiary Alpine orogeny. The mineralization is hosted in the Ore-Bearing Dolomite formed by an extensive replacement of limestones and diagenetic dolostones (Bogacz *et al.*, 1972). The formation of the OBD postdates sedimentation of Muschelkalk carbonates but predates Jurassic sedimentation and faulting (Kibitlewski & Gorecka, 1988). This faulting has been commonly associated with MVT mineralization (Haranczyk, 1979; Sass-Gustkiewicz *et al.*, 1982). Minor sulphide mineralization occurs along Cretaceous and Tertiary fractures (Haranczyk, 1979).

Recent paleomagnetic dating indicates that OBD containing disseminated sulphides only is older (Middle to Upper Triassic remnance) than coarse sparry dolomite containing the main sulphide ore, both of which indicate Tertiary magnetization age (Symons *et al.*, 1995).

Direct Rb-Sr dating of ore-stage sulphides provides an isochron model age of 135±4 Ma for the main sulphide event. This can be related to the Early Cretaceous crustal extension preceding the opening of the northern Atlantic Ocean (Heijlen *et al.*, 2003).

5.10 Genetic considerations

A wide range of concepts has been suggested to explain the genesis of the Upper Silesian Zn-Pb deposits. At one extreme synsedimentary and early diagenetic models have been proposed (Smolarska, 1974), through polygenetic concepts (Gruszczyk, 1978) to the other extreme of a late hydrothermal formation (Haranczyk, 1978, 1979), or by gravity-driven fluids supplied during the Tertiary from the uplifted Carpathians to the south as deduced from remnant magnetization of sphalerite (Symons *et al.*, 1995). Some researchers over-emphasize one particular feature of the mineralization (Sass-Gustkiewicz, 1975), trying to explain the entire spectrum of mineralization by proposing a simple hydrothermal karst as origin for breccias hosting sulphides. Such breccias may constitute up to 40% of the mineralization at Olkusz mine. However, many breccias are not mineralised at all, and in some of the deposits (Trzebionka) breccias are almost absent or are of tectonic origin. The occurrence of weathered clasts of sulphide ore overgrown by younger banded sulphides suggests that karstification was mainly produced by descending surficial fluids dynamically mixing with ascending hot fluids in some of the karst cavities.

It seems that the genesis of the deposits is related to complex phenomena working in concert. The first mineralization might have been introduced relatively early in the diagenetic history of the host as Zn rim cements (Kucha, 1988a). Zn, Pb and Fe metals were concentrated in the structure of carbonates (early diagenetic dolomites, ore-bearing dolomites, Table 2), and as dispersed sulphides formed extensive anomalies on a regional scale (Przenioslo, 1974; Pawlowska & Szuwarzynski, 1979). These anomalies enclose also stratiform mineralizations containing up to 0.7 wt% of Zn, 0.24 wt% of Pb (Wodzicki, 1987). These sections follow carbonate grainstones that were later replaced by massive, tabular sphalerite bodies (Trzebionka, Pomorzany). Carbonate grainstones, due to their increased permeability and porosity, served as aquifers conducting various fluids that modified the orebodies during later diagenesis.

Faults, fractures and shear zones forming large, interconnected hydraulic systems were important controls on fluid flow and precipitation. Surficial karst phenomena were an important part of this system of fluid circulation. They also provided favorable sites for fluid mixing – one fluid with metals and another with sulphur (Kucha & Czajka, 1984), and for the formation of an extensive system of karstification. Collapse breccias with high domal structures are present (Sass-Gustkiewicz *et al.*, 1982), identical to these found in Tennessee (McCormic *et al.*, 1971). Several stages of breccia-

tion and mineralization may be intertwinned in places so closely that a hypothesis of hydrothermal karst was introduced to explain all these phenomena (Sass-Gustkiewicz *et al.*, 1982). However, only a part of breccias is mineralised, and most of the karst breccias in the OBD are not mineralised with sulphides (Horzemski, 1962). An important role in the formation of the ores was connected with partial remobilisation of sulphur and Zn from the hanging wall into footwall sections of the horst and graben structures leading to a formation of karst fillings by soft sphalerite sediment with light, homogeneous $\delta^{34}S$ (Haranczyk, 1988). This suggests that such a light and homogeneous sulphur was derived from earlier sulphide bodies by paleoweathering and redeposited (Haranczyk, 1988).

In the mineralised breccias, banded smithsonite–siderite, with fluid inclusions temperatures 94–103 °C, forms the first overgrowths on bleached dolomite clasts (Figs. D7, D17). It is followed by banded sphalerite containing at first relicts of replaced smithsonite (Kucha & Czajka, 1984). The same breccia contains clasts of paleoweathered ore overgrown by younger banded sulphides (Fig. D13) and intertwined with sulphates, thiosulphates, sulphites and oxides repeated several times (Figs. D13, D15). Such structures form banded zones extending into macroscopic (hand specimen) size. All these observations suggest that the ores were formed in the process of dynamic mixing of hot ascending fluids with metals with cold surficial descending fluids, probably with sulphur. The surficial fluids were responsible for an extensive karstification most of which is non-mineralized. It is suggested that bottom sections of the karst cavities submerged in ascending fluids were in reducing conditions while upper sections of karst system might have been under oxidising regime. Upward/downward shift of the redox interface probably produced recurrent bands of sulphides, various oxysulphides, sulphates and oxides repeated several times (Figs. D13–D15). Therefore it may be suggested that the present sulphide bodies were partly formed in the cementation zone developed in the lower sections of the karst cavity system. This also implies partial redeposition of already existing mineralization of the hanging wall into a footwall cementation zone, and refinement of Zn from Fe immobilized in higher sections as insoluble iron oxides. The Ore-Bearing Dolomite of Upper Silesia (Table 2) may also be considered as such a precursor ore rich in Fe and containing enough base metals to produce horizons with significant enrichment in metals during the discussed process of mineralization. Reactions of sulphur (sulphidic acid) with Pb and Zn present in the carbonate structure is very fast as compared to carbonate Fe and Mn, which are very slow (Kullerud, 1967).

This feature could have helped to refine Zn and Pb originally residing in the carbonate structure from Fe retained as carbonate.

One of the key mechanisms controlling ore precipitation were sulphide – metal carbonate reactions maintaining high permeability of the ore zone (Kucha & Czajka, 1984; Kucha, 1989). Another key mechanism relied on stepwise reduction of sulphur by both bacterial and abiotic means accumulating banded oxysulphide precursors converted later into banded sulphides (Kucha & Viaene, 1993). Relics of such oxysulphides are still visible in massive banded sulphides (Figs. D13–D15). In some samples, a gradual replacement of the former by the latter may be documented (Kucha & Viaene, 1993).

6. Flotation waste and Zn & Pb metallurgical slags, Upper Silesia, Poland

HARRY KUCHA

6.1 Introduction

There are three active mines of lead and zinc in the area of Bukowno. The average exploited ore contains about 4 wt% of Zn and 1 wt% of Pb. The ore is milled and treated in flotation plants producing separate concentrates of ZnS and PbS. The flotation waste is dumped into 5 ponds. Four ponds are already filled up and occupy an area of 71 ha, the fifths with surface area of 37 ha is currently used to store flotation waste. The total tonnage of waste in all of 5 ponds is 40 Mt.

The main components of mineral dressing waste are: dolomite ~70%, pyrite, marcasite and melnikovite ~13%, ZnS ~1.5%, PbS ~0.5%, $ZnCO_3$ ~0.8%, $PbCO_3$ ~0.4%, gypsum ~5%, quartz ~4%, limonite ~3%, smelting slag ~1% (Gorecka *et al.*, 1994; Szuwarzyński & Kryza, 1993).

The tonnage of heavy metals and sulphur in the four waste ponds was estimated (January 1991; Gorecka *et al.,* 1994) to be: Zn 250,479, Pb 117,710, Fe(total) 1,714,533, S(total) 1,686,448, Cu 4,847, Cd 1,967, Ag 77, As 13,106, Tl 665, Ni 550, Cr 246, ZnO 133 740 and PbO 83,429.

The main metal in the waste is iron, which presents mainly as FeS_2, Fe-rich dolomite and limonite. Zinc is present mainly as ZnS, Zn-rich dolomite and smithsonite. Main minerals of lead are PbS, $PbCO_3$, $PbSO_4$ and Pb-rich melnikovite. Mineralogy of sulphur is controlled by FeS_2, gypsum, ZnS, PbS and $PbSO_4$.

Old smelting slag are located near Bukowno and their tonnage is estimated at a level of 3 Mt. Currently smelting slag are stored at a new dump located near Bolesław mine. Some of smelting slugs were dumped together with flotation wastes (~300,000 t).

A mobility of elements is defined by minerals they form. Earlier studies concerned mainly chemical composition and tonnages of dumped waste (Szuwarzynski & Kryza, 1993; Gorecka *et al.*, 1994). The present study is focused on mineralogy and geochemistry of flotation waste and smelting slugs, and on mobility of metals controlled by mineralogy of the waste.

6.2 Materials and methods

Samples from flotation waste and metallurgical slugs located near Bukowno, Upper Silesia, Poland were studied. Samples were polished and analyzed by reflected light microscopy, which provided a base for further selection of specimens for microprobe study.

Microprobe analyses were made with a JEOL 733 microprobe at the Department of Material Sciences of Katholieke Universiteit Leuven at 20 kV. Two sets of standards were used. The set for metals and sulphides included: S Kα and Fe Kα (FeS_2), Mn Kα, Zn Kα (ZnS), Cu Kα, As Lα, Cd Lα, Ag Lα, Sb Lα, Tl Mα and Pb Mα (PbS). The second set of standards for analysis of aluminum silicates consisted of: oligoclase, leucite, fayalite, forsterite, wollastonite, rhodonite, sapphire, rutile, chromite and hematite. Sulphur valence was measured with spectrometer with the PET crystal calibrated for the purpose of the study (Kucha *et al.*, 1989). S valance was determined from valence related S Kα and S Kβ shifts, valence-characteristic satellites and fine scans of the S Kβ peak top (Kucha *et al.*, 1989).

MicroPIXE analyses were conducted in two modes; i) measurement of Proton Induced X-ray Emission (PIXE) of characteristic radiation of the target, and ii) by RBS (Rutherford Scattering Spectroscopy), using Van de Graff accelerator with proton energy from 2.00 to 2.2 meV, exposure time 30 min, and beam intensity of 10 to 30 nA. Analyses were carried out on surface of 5 mm^2 in pre-selected area on target. Characteristic emission radiation was measured with Li drifter Si detector with resolution of 180 eV at 5.4 keV. Spectrometer has been calibrated with ^{57}Fe. Data reduction was performed with program package for PIXE spoectra evaluation (Kajfosz, 1992), allowing to achieve detection limit of 1g/t.

The RBS spectra has been processes with the 'Sinmra' package. All PIXE measurement has been made in the Institute of Nuclear Physics, Krakow, Poland.

Trace elements in the bulk samples studied has been analysed with ICP-MS and Atomic Absorption Spectroscopy (AAS) in lab of Environmental Protection Unit, Univ. of Mining 7 and Metallurgy, Krakow, Poland (Table 6).

X-ray diffraction (XRD) studies were made with Fe filtered Co Kα radiation in Gandolfi camera attached to a Philips PW-1130 diffractometer at the Department of Geology KU Leuven.

SEM analyses were made with a JEOL JSM-6400 equipped with link EXL-10/EDS system at 15 and 20kV.

Leaching tests were performed on the surfaces of some polished sections in order to assess the mobility of the heavy metals in the dump environment, and to make a correct interpretation of the sequential leaching tests. The etching solutions were applied to polished surfaces as drops encompassing an area of 4–5 mm in diameter. The tested areas were photographed prior to leaching to obtain reference pictures. Five different solutions were applied on polished surfaces. Solution I and II were designed to mimic acid rain water during the initial stage of interaction with dump material. Solution I consisted of water with pH 5 obtained by adding a small quantity of HNO_3 to distilled water. Solution II was similar except for its pH of 2, which increased the speed of etching. Solutions III, IV and V were designed to match the composition of pore waters in the dumps. These fluids have pH ranging between 6.8 and 8.0. The three solutions had the same Cl^- and SO_4^{2-} content (90 µg/l and 82.5 µg/l respectively), but they differed in their pH by addition of NaOH or HNO_3. Leaching solution III had a pH of 7.5, solution IV a pH of 5, and solution V a pH of 4. The solution V was designed to mimic conditions where larger quantities of pyrite are oxidized. Duration of etching varied from 0.5 to 18 hours.

6.3 Flotation tailings

The most important type of dumped waste in the Zn-Pb mining area are flotation tailings because of their large tonnage, ~40 Mt. The threat of different mineralogical components to environment depends on their quantity and amount of poisonous elements present in their lattice either as main elements or as minor and trace admixtures. Minerals constituting flotation waste are described and discussed according to their abundance and poisonous admixtures present in their structure.

6.3.1 Dolomite

Dolomite constitutes about 70% of the flotation waste. There are several types of dolomite (Table 4) characterized by a different admixture of minor and trace elements. Bulk chemical analyses indicate that the major element substituting in dolomite is iron, up tp 1.67 wt% of FeO, the next is ZnO up to 0.87 wt%. Although Fe is not poisonous in oxidizing regimes, it will oxidize to Fe^{3+}, which in turn will cause disruption of dolomite lattice and will cause a release of the poisonous substitutiing elements Zn, Mn, Pb and Cd. The average concentration of the above-mentioned metal oxides is: 0.20 wt% Zn, 0.22 wt% Mn, 0.02 wt% Pb (Table 4) and 0.5–1200 g/t Cd (Zabinski, 1960; Radwanek-Bąk, 1983). The Cd content is always higher in Zn-rich dolomite present in the weathering zones located within horst structures (Zabinski, 1960).

On the microscopic scale, the metal content in different zones of the dolomite rhombs is variable (Table 4), but usually is higher in dolomite grains paragenetic and intergrown with sulphides.

Due to high tonnage of dolomite (29 Mt) in tailings, it is an important carrier of heavy metals. It contains approximately about 56,000 t of ZnO, 5,600 t of PbO and 250 t of Cd. However, dolomite has also a very positive influx on preservation of tailings. It keeps an elevated pH in pore waters which, in turn, lowers or even stops heavy metal dispersion. Under the studied conditions only Cd shows higher mobility (Thornber, 1985).

Table 4. Chemical composition of dolomite from Upper Silesian deposits (wt%)

Dolomite type	*n*	MgO	CaO	S	MnO	FeO	ZnO	PbO	Method
Ore-bearing	16	9.90–19.00 17.21		0.00–0.15 0.05	0.10–0.55 0.14	0.10–4.97 1.67	0.15–0.87 0.20	0.01–0.07 0.02	bulk, wet chemical
Syngenetic	1	16.27		0.13	0.22	3.46	0.34	0.07	bulk, wet chemical
Zoned core	14	19.55–20.98 20.04		≤0.04	≤0.03–0.21 0.18	0.03	0.25–1.51 1.01	0.05	EPMA
Fe-rich zones	9	13.51–17.14 15.92		≤0.04	0.20–1.01 0.68	0.14–4.01 1.33	0.26–1.81 1.11	≤0.05	EPMA
Zn-rich zones	7	17.28–20.16 19.12		≤0.04	≤0.03–0.81 0.40	5.46–9.27 8.05	0.50–1.85 1.49	≤0.05	EPMA
Paragenetic with sulphides	20	14.10–19.40 18.42		≤0.04	0.10–0.98 0.55	0.10–1.30 0,82	0.50–16.0 2.48	≤0.05–2.12 0.09	EPMA
Crinoid ossicles in massive ZnS layers	44	2.31–12.80 10.42		≤0.04–1.75 0.06	≤0.04–0.74 0.38	≤0.02–7.69 2.90	≤0.04–2.04 0.59	≤0.04–8.43 1.13	EPMA
Primary smithsonite–siderite	47	0.10–2.10 0.64	≤0.03–3.18 0.7		0.06–2.25 0.86	0.20–20.51 8.22	25.25–50.06 39.11	≤0.05–8.93 2.25	EPMA

n - number of analyses; upper figure - range; lower figure - average
Compiled from: Sliwinski (1965); Bogacz *et al.* (1972); Osman & Piestrzynski (1989); Kucha *et al.* (1983); Kucha & Czajka (1984), and new data

6.3.2 Pyrite, marcasite and "melnikovite"

These three compounds will be discussed together as they often form tight intergrowths. The amount of these compound in tailings varies from 10 to 16%, with the average close to 13% (Gorecka *et al.*, 1994).

Marcasite is usually free of any admixtures, but pyrite may be enriched in Ni, Zn, As, Pb and Tl (Table 5). The As and Tl content is sufficiently high (1.26 and 0.05 wt% on average, respectively, Table 5) to be of concern, particularly because of high amounts of iron disulphides in flotation tailings. The As and Tl contents are much higher in melnikovite (Table 5).

Table 5. Chemical composition of sphalerite, pyrite and melnikovite from the Zn-Pb ore (wt%)

Sample		S	Fe	Ni	Zn	As	Tl	Pb	O	*n*
Sphalerite	mean	33.02	3.17	0.06	62.14	0.18	≤0.04	0.24		53
	min.	27.32	0.02	≤0.01	46.87	≤0.03	≤0.04	≤0.04		
	max.	34.47	7.39	1.18	67.08	0.62	0.15	2.80		
Pyrite	mean	47.42	36.21	2.62	4.37	1.26	0.05	4.46		17
	min.	40.43	25.42	≤0.01	0.17	0.53	≤0.04	≤0.04		
	max.	52.17	43.59	7.42	15.47	1.69	0.07	9.95		
Melnikovite (Pomorzany)	mean	43.23	43.70	0.06	0.36	0.98	0.48	1.93	10.17	24
	min.	33.88	40.68	≤0.04	0.14	0.05	≤0.04	1.10	2.56	
	max.	49.22	47.24	1.12	0.72	11.12	0.67	1.93	21.42	

n - number of analyses

Melnikovite has been defined as banded substance composed of recurrent darker and brighter spheres built up of sulphites, thiosulphates, dithionates of Fe, Pb, As, Tl, Zn, Ni etc. (Kucha *et al.,* 1989; Kucha & Viaene, 1993). It is suggested that most of Tl (665 t) and As (13,106 t) present in the tailings is connected with melnikovite. This mineral oxidizes much faster than accompanying pyrite and marcasite, and at pH below 6 it is metastable. Therefore, during oxidation, melnikovite may be a locus of a fast release into pore solution of such poisonous elements like As and Tl. Most of the discussed pyrite, marcasite and melnikovite occur in fractions below 0.04 mm. This makes the problem of the fast oxidation very acute due to large surface area available to oxygen. However, high pH in pore fluids controlled by a high dolomite content stabilizes iron disulphides and slows down the release of As and Tl.

The chemical composition of the mineral substance called melnikovite (Table 5) shows a large variation. Sometimes it contains more Pb than Fe. According to Ramdohr (1980), no exact chemical formula can be ascribed to melnikovite. It contains FeS_2, FeS, As (≤8 wt%) as well as H_2O. It is partly or entirely amorphous or cryptocrystalline (Ramdohr, 1980; Uytenbogaardt & Burke, 1985), and shows wide range of reflectance and polishing hardness values. Sometimes it may be as soft as galena. More recent studies show that recurrent darker and brighter spheres constituting melnikovite are composed of alternating zones of pyrite (marcasite), Fe thiosulphate, Fe sulphite and goethite (Kucha *et al.*, 1989). Melnikovite from Zn-Pb deposits shows wide range of compositions, includes various sulphur valences, and may sometimes contain more Pb than Fe (Kucha & Viaene, 1993; Kucha & Barnes, 1995).

Leaching tests indicate that melnikovite dissolves much faster than pyrite and marcasite in all the tested solutions. Melnikovite shows visible dissolution after 2-3 minutes in solutions I, II, IV, and V (see 6.2 for explanation). It suggests that acid rain will cause mobilization of As and Tl from melnikovite mainly in the upper sections of dumps close to aerated surface. In deeper sections of dumps, where pH is higher, dissolution of melnikovite will be much slower.

6.3.3 Sphalerite

Concentration of sphalerite in tailings is about 1.5%. The amount of Zn sulphide in dumps is estimated at a level of 250,000 t (Gorecka *et al.*, 1994). Main admixture in ZnS is Fe (~3.17 wt% on average). Other elements form traces (values in g/t): Ni ~600, As ~1800, Pb ~2400 and Cd ~50-7000. As and Pb are usually connected with small inclusions of melnikovite in banded sphalerite.

Leaching tests indicate that ZnS is inert to solution I. Solution II etches ZnS surface slightly but progress over test time is very weak. The last fluid produces etching pits after 15 minutes. The progress of etching depends strongly on the Fe content in ZnS. The iron-rich varieties become soon coated with a passive iron oxide film, which slows down or even stops visible etching.

6.3.4 Galena

PbS content in tailings is about 0.5 wt%, and reserves of Pb sulphide in tailings are estimatd to 117,710 t (Gorecka *et al.*, 1994). Galena grains are usually coated by passive $PbCO_3$ armour . Etching is visible on galena surfaces after 15 minutes in solution I (in fractured galena the leaching progress is faster), and after 4 minutes in solution II. After 60 minutes in solution I and 20 minutes in solution II, galena is covered by a black coating, which slows down further dissolution. SEM EDS spectra indicate that the black coating consists of Pb sulphate. Galena is etched by solution III, IV and V in a similar manner as described above, and eventually is coated by insoluble Pb sulphate.

6.3.5 Smithsonite and cerussite

In the flotation waste two types of smithsonite are observed:

i) The more common Fe-free smithsonite characterises the oxide ore present on elevations of horst structures. This smithsonite has Fe-free lattice, but may contain minute inclusions of Fe hydroxides, and contains 0.10 to 0.14 wt% of Cd (Kucha & Czajka, 1984; Radwanek & Bąk, B., 1983).
ii) The less common smithsonite forms a continuous solid solution series towards siderite, and contains up to 20.51wt% FeO (Table 4). This is primary smithsonite, predating emplacement of the sulphide ore.

Zn and Pb carbonates are important component of the oxidized ore (Zabinski, 1960; Radwanek & Bąk, 1983). Their reserves in tailings are 177,740 t of ZnO and 31,782 t of PbO.

6.4 Metallurgical slag dumps

Slag mineralogy and geochemistry depends on the technology of Zn and Pb metallurgical recovery. Old slags more often contain metallic Pb, Fe carbides.

Metal content of fresh/old slag on average (wt%, Table 6): Fe 24.26/13.22, S 6.90/0.88, Zn 2.94/1.73, Mg 1.82/6.71, Mn 2.82/1.18, Pb 2.74/1.15, As 0.13/0.10, Tl 0.0033/0.0023, but less Cd 0.0080/0.0127 and Cu 0.4617/0.0572 (Table 6). This pattern seems to depend on remobilization, and washing away of more mobile elements during slag percolation by meteoric fluids. Recently produced slag contains Pb_2SiO_4 due to SiO_2 addition, which is supposed to cut down Pb mobility within dumps.

The slag occurs as fragments of cm to dm in size and sometimes may be coated by gypsum on its surface. The slag is very porous and mineralogically very complex. The main minerals of the slag are Ca, Mg and Fe pyroxenes (Figs. D19, D20). They control not only the majority of iron residing in the slag but also more than half of Zn, which is substituted into

Table 6/1. Metal contents in Zn-Pb slag (wt%)

Type of slag	Sample	Fe	Ca	S	Al	Zn	Mg	Mn	Pb	As	Tl	Cd	Cu	Cr
Fresh slag (2003)	1a	30.4032	5.3137	3.4606	7.2626	2.9384	0.8616	3.8367	1.6172	0.1379	0.0015	0.0008	0.4941	0.0092
	1a d	30.8266	13.3124	8.5834	7.1524	2.9646	2.0155	3.7929	1.6229	0.1339	0.0014	0.0008	0.7085	0.0092
	5a	22.6650	12.5313	8.5922	5.9378	3.6853	2.7169	2.0636	2.9668	0.1396	0.0025	0.0016	0.4440	0.0082
	6a	21.7480	10.1318	6.9985	4.6461	3.8284	2.3623	1.7904	2.7545	0.1161	0.0024	0.0017	0.3924	0.0069
	7a	26.2131	16.5557	7.6950	6.1693	2.8219	3.2542	3.5201	5.9700	0.1760	0.0051	0.0018	0.3187	0.0654
	8a	12.3932	1.6011	6.5762	4.0930	3.0216	0.1834	1.0535	2.4651	0.0428	0.0037	0.0256	0.9835	0.0057
	9a	18.4740	9.3848	7.8039	3.8835	2.3081	1.8679	1.5175	3.0519	0.0929	0.0032	0.0284	0.3175	0.0044
	10a	28.8515	3.9510	4.3751	6.3823	2.6300	1.0932	3.6597	2.2242	0.1532	0.0078	0.0106	0.1269	0.0027
	11a	26.7822	13.0010	8.0432	7.6953	2.2860	2.0296	4.1636	2.0031	0.1733	0.0018	0.0011	0.3694	0.0088
Old slag (~1985)	12a	16.6514	16.5145	0.9035	7.2437	1.5375	7.4445	1.2248	1.0782	0.0886	0.0014	0.0067	0.0524	0.0027
	12a d	16.0937	16.1918	0.8548	7.1195	1.5830	7.1451	1.2146	1.1676	0.1015	0.0016	0.0073	0.0524	0.0022
	13a	12.1326	13.6660	0.6207	6.4488	3.1489	5.8197	1.3761	1.5953	**0.1912**	0.0033	0.0136	0.0770	0.0021
	14a	12.4715	16.5234	0.7835	9.8376	1.7383	5.5147	1.0688	1.8849	0.0881	0.0048	0.0353	0.0636	0.0036
	15a	12.7682	17.4148	0.6101	9.5497	1.6954	6.0904	1.2420	1.0700	0.0996	0.0026	0.0118	0.0572	0.0023
	16a	9.1863	20.0973	1.5380	8.1667	0.6851	8.2267	0.9300	0.1130	0.0601	0.0003	0.0016	0.0407	0.0036

Table 6/2. Metal contents in Zn-Pb slag (wt%)

Type of slag	Sample	Fe	Ca	S	Al	Zn	Mg	Mn	Pb	As	Tl	Cd	Cu	Cr
	17	0.7092	28.0488	19.3977	0.8857	2.4099	1.1510	0.0278	0.8698	0.0368	0.0101	0.1059	0.0055	0.0010
Flotation waste	18	7.3232	18.4245	6.4943	2.0520	1.2698	6.6908	0.2834	4.2665	0.0664	0.0077	0.0078	0.0181	0.0019
	19a	6.2579	17.5053	7.3195	0.3116	1.6881	7.0589	0.2400	0.7976	0.0459	0.0050	0.0076	0.0011	0.0002
Pb dust from furnace gases	20	8.7729	0.5495	12.3305	0.9751	3.7986	0.4552	0.0117	**16.8419**	0.0470	**0.2988**	**0.2393**	0.0232	0.0017
Basic statistical parameters of fresh slag	*min.*	12.3932	1.6011	3.4606	3.8835	2.2860	0.1834	1.0535	1.6172	0.0428	0.0014	0.0008	0.1269	0.0027
	max.	30.8266	16.5557	8.5922	7.6953	3.8284	3.2542	4.1636	5.9700	0.1760	0.0078	0.0284	0.9835	0.0654
	$\overline{x}$	24.2619	9.5314	6.9031	5.9136	2.9427	1.8205	2.8220	2.7417	0.1295	0.0033	0.0080	0.4617	0.0134
	σ	±6.0753	±4.9608	±1.8294	±1.4079	±0.5349	±0.9595	±1.1953	±1.3217	±0.0416	±0.0021	±0.0112	±0.2503	±0.0196
Basic statistical parameters of old slag	*min.*	9.1863	13.6660	0.6101	6.4488	0.6851	5.5147	0.9300	0.1130	0.0601	0.0003	0.0016	0.0407	0.0021
	max.	16.6514	20.0973	1.5380	9.8376	3.1489	8.2267	1.3761	1.8849	0.1912	0.0048	0.0353	0.0770	0.0036
	$\overline{x}$	13.2173	16.7346	0.8851	8.0610	1.7314	6.7069	1.1761	1.1515	0.1049	0.0023	0.0127	0.0572	0.0028
	σ	±2.7659	±2.0772	±0.3416	±1.3811	±0.7956	±1.0615	±0.1551	±0.6043	±0.0448	±0.0016	±0.0118	±0.0123	±0.0007
Detection limit [ppm]		0.06 AAS	0.08 AAS	0.5 ICP-MS	0.39 AAS	0.01 AAS	0.003 AAS	0.03 AAS	0.10 AAS	0.00002 ICP-MS	0.00002 ICP-MS	0.0001 ICP-MS	0.035 AAS	0.05 AAS

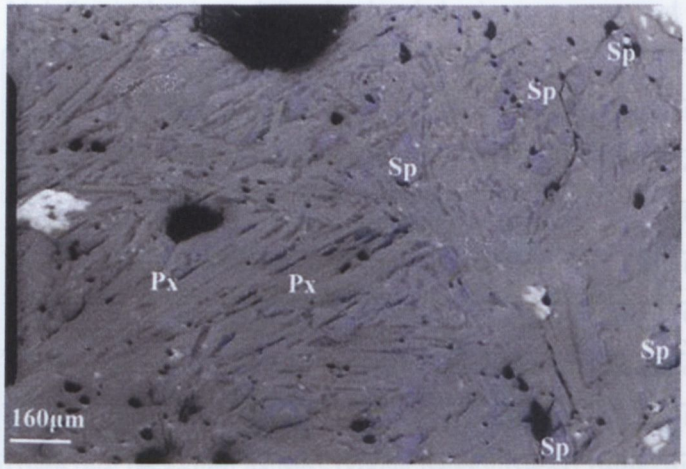

Fig. D19. Photomicrograph of spinels (Sp, isometric) and pyroxenes (Px, elongated) in silicate glass matrix of a slag sample. Reflected light, sample 2b.

the structure of these silicates. The remaining Zn is present as Zn, Zn-Fe alloys, ZnO, spinels and ZnS (sphalerite, wurtzite, ZnS with alabandite structure) (Tables 10–12).

Under reflected light microscope, a complex mineral composition of slag is revealed. Older slags usually contain euhedral pyroxenes and spinels set in glassy matrix (Figs. D19, D20), which contains up to four stages of exsolutions of younger generations of metal silicates, spinels, and fine sulphides (Kucha & Jedrzejczyk, 1995). Younger slags tend to be dominated by glass phase.

The lead budget of the slag is controlled by metallic lead and galena, and in recent slag by Pb_2SiO_4 due to feeding slag with extra SiO_2 to inhibit Pb mobility within dumps (Figs. D23, D24). The last one, however, appears only in samples with higher Pb content. Lead minerals are tightly intergrown with pyrrhotite and chalcopyrite. Therefore, Pb and Cu are usually correlated in the slag.

The Cd budget in the slag is controlled by metallic lead and zinc-rich silicates, which may contain concentrations of Cd, detectable by microprobe. The As budget of the slag is controlled by Fe-rich sphalerite and iron phosphides (Table 11).

6.4.1 Silicate slag (pyroxenes)

Silicate slag constitutes about 75% of the slag minerals. It is very porous and most often it is composed of augite crystals residing in darker Ca-augite matrix (Figs. D19, D20). Ca-augite also forms matrix hosting chromite crystals (Fig. D20). Augite occurs in two forms: augite proper with low contents of MnO, Fe_2O_3 and ZnO but high amounts of TiO_2 (Table 7) and Mn-augite containing high content of Fe in the form of magnetite 'dust' and Zn (Table 7). The augite studied is also rich in zinc (0.56 to 3.51, Table 7). Kirschsteinite (an olivine-group phase) is Zn-rich as well (Table 7). The high ZnO content in the studied silicates, making 75% of the slag, indicates that silicate slag is the most important carrier of zinc.

Leaching tests performed on the silicate slag indicate that augite and kirschsteinite are more resistant than Ca-augite. Incipient etching of Ca-augite occurs in solution II after 15 minutes, kirschsteinite after 30 minutes and augite after 50 minutes. Etching progresses alongside crystal boundaries, and

Table 7. Chemical composition of silicates from metallurgical slag (upper figure: wt%, lower figure: mol)

Sample	Na_2O	MgO	Al_2O_3	SiO_2	K_2O	CaO	TiO_2	MnO	FeO	Fe_2O_3	ZnO	Cr_2O_3	Σ	Phase Σ cations
2FR/E4	≤0.04	14.27 0.7661	4.64 0.0985	50.05 1.8030	0.20 0.0046	22.98 0.8869	0.43 0.0116	2.11 0.0644		3.00 0.0407	0.56 0.0149	≤0.04	98.24	augite 1.8345
E5	≤0.04	12.64 0.6982	4.74 0.1036	48.99 1.8159	0.14 0.0033	22.39 0.8892	0.88 0.0245	2.77 0.0870		3.70 0.1035	0.61 0.0148	≤0.04	97.86	augite 1.8253
F3	≤0.04	12.34 0.6508	9.75 0.2033	45.02 1.5934	0.11 0.0025	23.39 0.8870	1.36 0.0362	2.29 0.0686		2.92 0.0389	0.68 0.0178	0.60 0.0084	96.78	augite 1.9202
F4	1.16 0.0447	8.98 0.5319	5.12 0.1199	42.01 1.6697	0.28 0.0071	33.98 1.4470	0.28 0.0084	2.08 0.0700		3.17 0.0474	0.88 0.0258	0.60 0.0094	101.40	Ca-augite? 2.1703
F5	1.71 0.0652	6.77 0.3966	5.82 0.1348	42,25 1.6610	0.68 0.0170	33.72 1.4203	0.21 0.0024	2.83 0.0942		4.54 0.0671	0.84 0.0244	≤0.04	101.46	Ca-augite? 2.0999
F6	1.72 0.0668	5.37 0.3205	6.68 0.1577	41.07 1.6450	0.79 0.020	32.82 1.4084	≤0.02	3.54 0.0960		6.54 0.0955	1.19 0.0352	≤0.04	99.52	Ca-augite? 2.0215
K8	3.89 0.1721	0.82 0.0558	16.08 0.4324	30.72 1.4019	5.51 0.1604	12.85 0.6283	1.42 0.0487	3.71 0.1434		10.53 0.1800	2.93 0.0987	≤0.04	97.26	Fe-augite?
K7	≤0.04	9.28	3.11	27.96	≤0.04	9.54	≤0.02	15.11		30.38	1.90	0.45	97.68	Mn-augite+ magnetite "dust"
K10	≤0.04	6.03	2.08	27.53	≤0.04	31.97	0.34	7.74		18.73	3.51	0.37	98.29	Mn-augite+ magnetite "dust"
3FR/C3	≤0.04	19.16 0.7868	≤0.04	36.29 1.0000	≤0.04	37.47 1.1062	≤0,02	0.72 0.0168		6.70 0.1543	1.09 0.0221	≤0.04	101.43	kirschsteinite 2.0862
C4	≤0.04	18.05 0.7293	≤0.04	36.88 1.0000	≤0.04	36.54 1.0614	≤0.02	0.75 0.0172		8.02 0.1888	1.21 0.0242	≤0.04	101.45	kirschsteinite 2.0862
D1	≤0.04	9.29 0.5199	12.42 0.2748	38.92 1.4615	0.17 0.0041	36.03 1.4497	≤0.02	0.39 0.0124	0.75 0.0234		≤0.02	≤0.02	97.97	Al-augite 2.0136
D2	≤0.04	9.16 0.5154	11.35 0.2526	39.59 1.4969	0.25 0.0060	36.11 1.4609	≤0.02	0.45 0.0144	0.78 0.0246		≤0.02	≤0.02	97.69	Al-augite 2.0273

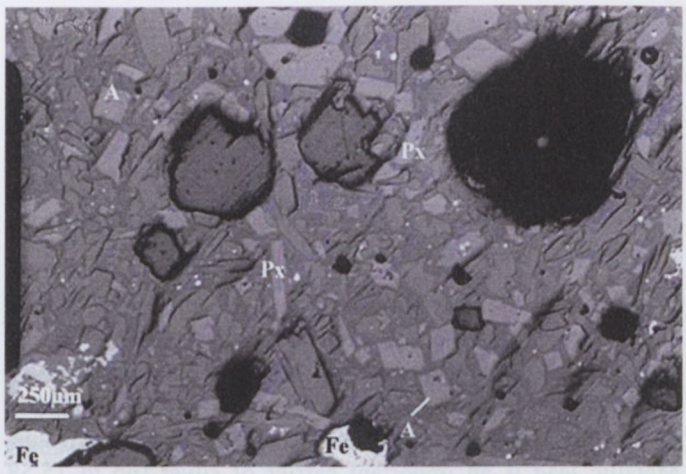

Fig. D20. Photomicrograph of pyroxenes (Px), metallic iron (Fe), and amphiboles (A) in the silicate glass matrix of a slag sample. Reflected light, sample 8b.

is strongly controlled by the crystallographical orientation against the polished surface. Ca-augite rich in alkali-earths may be dissolved after 10 hours of etching. Fe-rich varieties are, however, coated with variegated Fe-oxide coatings, which bring dissolution to a halt.

Dissolution in fluids III, IV and V is faster for Ca-augite than for kirschsteinite and augite. High alkali Ca-augite may be dissolved in fluid V after 10 hours. A prolonged immersion of augite in these etching fluids cause surface coating with Si and Fe – hydrated oxides. This slows down or even stops further progress of etching.

6.4.2 Oxides, excluding wüstite and periclase

Chrome spinels and magnetite

Chrome spinels are common constituents of the studied slag. Most often they occur as euhedral crystals in the Ca-augite matrix. There are two generations of chromite. The first forms large crystals and shows low aluminum content. Some of the large, chromite (spinel) crystals are zoned. The core is Cr-rich, and the outer zone is Fe-rich, with composition close to $MgFe_2O_4$ (Table 8). The second generation of chromite forms small exsolutions in the Ca-augite matrix and it is Al-rich (Table 8). All spinels are Mn-rich.

Magnetite forms ubiquitous exsolutions within the augite matrix. There are three generations of magnetite: i) large (50–300 µm) grains in intracrystalline spaces between pyroxenes, ii) fine-grained magnetite mostly within Ca-augite, and iii) minute inclusions in the second generation of pyroxenes recrystallizing from the glass matrix. Magnetite contains 0.74–1.69 wt% of Cr_2O_3 (Table 8). There are two sources of Cr found in the slag – chromite lining of furnace and clay minerals from karst cavities intergrown with sulphides.

Etching tests indicate that pure chromite is immobile. However, varieties rich in Fe are etched by the fluid II, IV and V. Therefore fluids with lower pH may cause Cr dispersion around the dumps.

ZnO

ZnO occurs as rounded grains with size from a few to 200 µm in spaces of the pyroxene matrix. Another generation of ZnO is present in fractures and oxidation coatings, and may be product of weathering. ZnO contains admixture of Cd 0.05–0.20 wt%, Tl ≤0.06–0.41 wt% and Pb ≤0.06–0.78 wt% (Table 9).

6.4.3 Metallic constituents

Fe

Metallic Fe is common in the slag. Usually it forms intergrown aggregates surrounding graphite-anthracite fragments. Metallic iron also occurs very often as intergrowths with ferroan sphalerite or wüstite both residing within pyrrhotite matrix (Fig. D21). α-iron is much more common than cohenite. Most important admixtures in metallic iron are Cu 0.31–0.42, As 0.89–1.03 and Sb 0.13–0.20 wt% (Table 10).

Table 8. Chemical composition of spinels from metallurgical slag according to EPMA analyses (upper figure: wt%, lower figure: mol)

Sample	MgO	Al_2O_3	CaO	TiO_2	Cr_2O_3	MnO	FeO	Fe_2O_3	ZnO	Σ
2FR/K1	9.41 0.4832	3.52 0.0714	0.74 0.0273	0.22 0.0056	61.51 0.8379	9.77 0.2851	5.37 0.1547	6.57 0.0851	1.95 0.0497	99.05
K3	7.72 0.4232	0.92 0.0199	0.26 0.0102	0.26 0.0071	1.69 0.0245	8.65 0.2694	4.80 0.1476	68.80 0.9520	5.51 0.1496	98.61
K4	9.98 0.5101	3.58 0.0723	0.56 0.0206	0.21 0.0043	59.66 0.8089	10.86 0.3155	5.36 0.1537	9.04 0.1166	≤0.03	99.25
K5	8.10 0.4488	≤0.03	0.37 0.0147	≤0.03	0.74 0.0109	8.42 0.2652	5.68 0.1767	70.71 0.9889	3.45 0.0947	97.47
K6	7.93 0.4328	0.35 0.0075	0.18 0.0070	0.25 0.0068	0.86 0.0125	8.50 0.2636	5.37 0.1646	70.87 0.9765	4.88 0.1320	99.19
K9	9.33 0.4742	7.18 0.1443	1.48 0.0541	0.55 0.0141	55.46 0.7477	9.07 0.2619	5.84 0.1666	7.86 0.1008	1.72 0.0432	98.49
K11	10.27 0.5223	7.22 0.1452	1.01 0.0369	0.53 0.0135	58.14 0.7844	10.26 0.2965	5.05 0.1442	4.94 0.0634	≤0.03	97.42

Sought for but not detected: $K_2O \leq 0.03$

Table 9. Chemical composition of ZnO from metallurgical slag on the basis of six EPMA analyses (wt%)

	S	Mn	Fe	Ni	Cu	Zn	Cd	Tl	Pb
min.	≤0.04	≤0.02	≤0.03	≤0.02	≤0.02	76.11	0.05	≤0.06	≤0.08
max.	0.06	0.09	0.14	0.18	0.05	79.54	0.20	0.41	0.78
mean	0.05	0.06	0.10	0.09	0.03	77.84	0.16	0.20	0.50

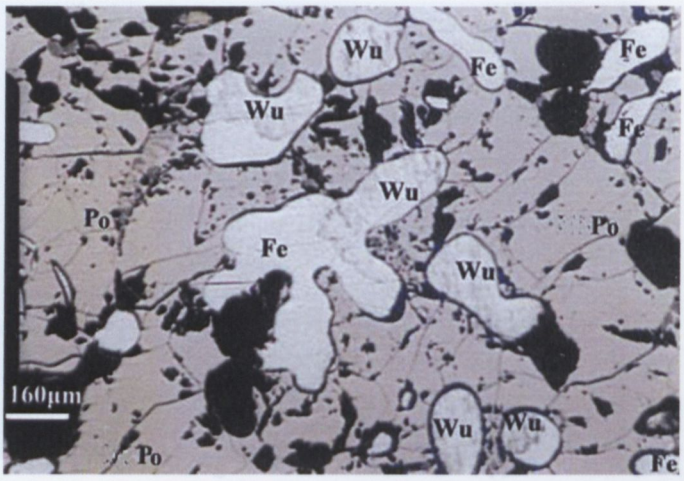

Fig. D21. Photomicrograph of blebs of metallic iron (Fe, white), corroded by wüstite (Wu) in pyrrhotite matrix (Po) of a slag sample. Reflected light, sample 3b.

Zn and its alloys

Metallic Zn is a rare phase, but sometimes may form grains with size up to 500 µm. In this case it occurs as the alloy Fe_3Zn_{10} (Table 10), one of the alloys present in the Fe-Zn binary system (Brandon *et al.*, 1974). This alloy is much more resistant to oxidation than pure Zn metal. Metallic Zn contains Cd, Tl and Pb as main traces (Table 10).

Pb

Metallic Pb forms small but ubiquitous inclusions in pyrrhotite. The size of metallic lead inclusions is below 20 µm in recent slags but may be up to 1 mm in some old slags. Metallic lead is an important carrier of silver (up to 15.58 wt%, Table 10). It also contains significant amounts of Cd, Sb and Cu (Table 10).

Table 10. Chemical composition of metallic zinc, lead, iron and Zn-Fe alloys from metallurgical slag according to EPMA analyses (wt%)

Phase		Fe	Ni	Cu	Zn	Cd	Ag	Tl	Pb	As	Sb	*n*
Zn	min.	≤0.03	≤0.03	≤0.03	99.54	≤0.05		≤0.07	≤0.09	≤0.05	≤0.04	
	max.	≤0.03	0.14	0.12	100.04	0.34		0.28	1.19	≤0.05	≤0.04	
	mean	≤0.03	0.09	0.07	90.79	0.14		0.13	0.37	≤0.05	≤0.04	4
Pb	min.	0.05	≤0.03	≤0.04	≤0.04	≤0.07	1.39	≤0.07	74.50	≤0.07	2.18	
	max.	0.36	≤0.03	0.15	0.06	≤0.07	15.58	≤0.07	96.11	0.19	4.29	
	mean	0.22	≤0.03	0.07	0.05	≤0.07	5.50	≤0.07	95.18	4.80	3.30	5
Fe	min.	98.99	≤0.03	0.31	0.09	≤0.03		≤0.07	≤0.04	0.89	0.13	
	max.	100.09	≤0.03	0.42	0.10	≤0.03		≤0.07	≤0.04	1.03	0.20	
	mean	99.54	≤0.03	0.37	0.10	≤0.03		≤0.07	≤0.04	0.96	0.17	3
Zn-Fe alloy	min.	6.90	≤0.03	≤0.03	79.12	≤0.05		≤0.07	≤0.09	≤0.05	≤0.04	
	max.	20.40	0.31	≤0.03	92.85	0.38		0.31	≤0.09	≤0.05	≤0.04	
	mean	12.27	0.17	≤0.03	87.08	0.19		0.12	≤0.09	≤0.05	≤0.04	5
Fe_3Zn_{10}		20.30	0.29		79.60							

n - number of microprobe analyses. Sought but not detected: S ≤ 0.06, Mn ≤ 0.03

6.4.4 Carbides, phosphides

Cohenite (Fe_3C)

Cohenite forms elongated, harder laths intergrown with metallic Fe (Fig. D22). Cohenite laths within metallic iron reach size 35 x 350 μm. Main admixtures in cohenite are: P, Cu, Zn, and As (Table 11).

Iron phosphides (Fe_3P)

Iron phosphides are minor constituents of intergrowths formed by other minerals with metallic iron. Iron phosphides are more common in the older slag. Microprobe analyses (Table 11) suggest that studied phosphides contain significant admixture of S. It is not clear to which extent S can substitute for P in phosphides. Under SEM, the studied phosphides appeared homogeneous and free of inclusions of other minerals. Phosphides are rich in Ni, Cu, As and Pb (Table 11).

6.4.5 Arsenides, sulphides

(Fe,Ni)As

(Fe,Ni)As occurs together with metallic iron and Fe carbides. It forms small grains from a few μm up to 30 μm. Ni content in this alloy may reach 7.02 wt% (Table 11). Other admixtures are S, Sb and Pb. Ni comes from ore minerals enriched in Ni: some Fe-rich sphalerite, pyrites and melnikovite.

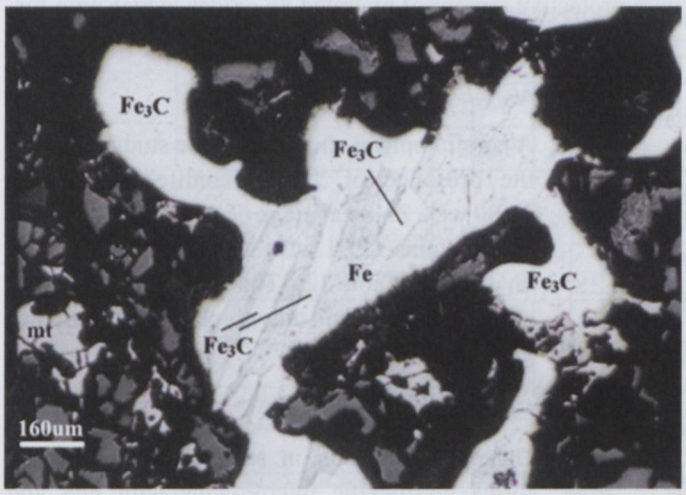

Fig. D22. Photomicrograph of large blebs of metallic iron (Fe) intergrown with Fe carbide (Fe_3C), and minor magnetite (mt) within silicate glass matrix (black) of a slag sample. Reflected light, sample 9b.

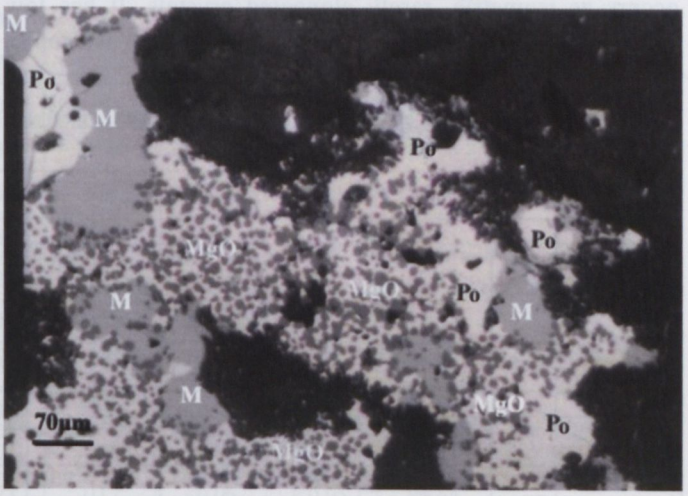

Fig. D23. Photomicrograph of small exsolutions of MgO (grey) in pyrrhotite (Po, light with pink hue), and less often in magnetite (M, light grey). Silicate glass matrix is black. Reflected light, slag sample 13b.

Table 11. Chemical composition of Fe3C, Fe3P and FeAs from metallurgical slag according to EPMA analyses (wt%)

MINERAL		Ni	Bi	P	S	Mn	Fe	Cu	Zn	As	Sb	Pb	*n*
Fe_3C*	min.			≤0.04	≤0.03	≤0.01	92.40	0.10	0.08	0.06	≤0.04	≤0.04	
	max.			1.03	≤0.03	0.08	94.56	2.06	1.56	0.95	0.41	0.10	
	mean			0.37	≤0.03	0.06	93.56	1.08	0.68	0.63	0.16	0.05	7
Fe_3P	min.			15.81	0.23	≤0.01	80.61	≤0.03	≤0.03	0.21	0.05	≤0.04	
	max.			16.30	0.30	0.03	81.24	1.27	1.29	0.66	0.13	0.07	
	mean			16.11	0.27	0.02	80.94	0.45	0.80	0.46	0.08	0.05	3
(Fe,Ni)As	min.	5.26	0.50		0.41	≤0.03	34.21	0.08	≤0.02	54.11	0.90	0.30	
	max.	8.11	0.97		0.58	≤0.03	36.11	0.16	≤0.02	55.04	1.12	0.48	
	mean	7.02	0.80		0.52	≤0.03	34.49	0.13	≤0.02	54.51	1.01	0.36	3

n - number of microprobe analyses. Sought but not detected: Ag ≤ 0.04, Cd ≤ 0.03. *contains also ±4-5 wt% C(diff)

Pyrrhotite

Pyrrhotite is common constituent of the slag. It forms aggregates up to macroscopic size *i.e.* 2 mm. Usually, pyrrhotite is intergrown with metallic iron and wüstite (Fig. D21), but it also forms intergrowths with magnetite, and MgO (Fig. D23). In some samples it is rich in lead and it is intergrown with galena. Small inclusions of metallic lead are present in the fractures of pyrrhotite. The studied pyrrhotite, unlike its natural counterparts, is enriched in Mn, Cu, and sometimes contains also Sb, Zn and Pb (Table 12).

Sphalerite and wurtzite

Sphalerite is usually intergrown with metallic iron and occurs as isometric, rarely elongated crystals. It has low reflectance of about 20% and is optically isotropic. Microprobe analysis revealed that it contains more Fe (11.60 wt% on average) than its counterpart from the Zn-Pb deposits (Table 12). XRD Gandolfi study indicates that this compound is true sphalerite. The studied sphalerite contains also high admixtures of Cu (Table 12). No Cd was detected by microprobe in the studied ZnS.

Wurtzite forms agglomerations of needles with length up to 70 μm. The average Fe content in wurtzite (32.78 wt%) is higher than the amount of Zn. Presence of wurtzite has been confirmed by XRD Gandolfi study. Specimens containing more Fe than Zn need electron diffraction study to clarify the crystallographical status of this "Fe-wurtzite".

Etching tests indicate that these iron-rich zinc sulphides are resistant to dissolution. After 1-2 hours they are coated with protective armour of hydrated Fe oxides, which stop further oxidation and dissolution.

Table 12. Chemical composition of primary sulphides from metallurgical slag according to EPMA analyses (wt%)

Phase		Mn	Fe	Cu	Zn	Ag	Cd	Pb	As	Sb	*n*
Pyrrhotite	min.	≤0.01	59.64	0.78	≤0.01	≤0.04	≤0.03	≤0.04	≤0.04	≤0.05	
	max.	0.20	61.52	1.09	0.14	≤0.04	≤0.03	4.56	0.14	0.35	
	mean	0.12	60.52	0.95	0.05	≤0.04	≤0.03	1.64	0.09	0.16	3
Sphalerite	min.	0.08	9.52	0.04	52.74	≤0.03	0.05	≤0.04	≤0.04	≤0.04	
	max.	0.33	13.40	1.78	58.95	≤0.03	0.08	0.15	≤0.04	≤0.04	
	mean	0.17	11.60	0.53	55.25	≤0.03	0.06	0.06	≤0.04	≤0.04	7
Wurtzite	min.	0.37	32.35	0.57	29.98	≤0.04	0.04	≤0.05	≤0.04	≤0.04	
	max.	0.53	33.00	1.07	31.36	0.06	0.13	≤0.05	≤0.04	≤0.04	
	mean	0.46	32.78	0.83	30.80	0.05	0.10	≤0.05	≤0.04	≤0.04	3
Alabandite	min.	1.17	5.44	0.22	29.81	≤0.04	≤0.03	≤0.05	≤0.04	≤0.04	
	max.	24.60	32.70	0.58	45.55	≤0.04	0.13	≤0.05	≤0.04	≤0.04	
	mean	12.91	15.46	0.40	37.00	≤0.04	0.07	≤0.05	≤0.04	≤0.04	4
Galena	min.	≤0.04	0.27	0.18	≤0.04	≤0.04	≤0.07	84.41	≤0.07	0.09	
	max.	≤0.04	0.91	0.52	0.13	≤0.04	≤0.07	85.87	≤0.07	0.17	
	mean	≤0.04	0.53	0.38	0.07	≤0.04	≤0.07	85.04	≤0.07	0.12	4
Chalcopyrite	min.	0.06	30.18	24.59	0.41	≤0.03	≤0.04	≤0.04	≤0.04	≤0.04	
	max.	0.12	36.67	34.33	1.42	0.06	≤0.04	≤0.04	≤0.04	≤0.04	
	mean	0.08	34.32	28.33	0.83	0.05	≤0.04	≤0.04	≤0.04	≤0.04	3
Bornite		0.12	14.32	58.05	0.15	0.07	≤0.04	≤0.04	≤0.04	≤0.04	1

n - number of microprobe analyses. Sought but not detected: As ≤ 0.04, Sb ≤ 0.04

Alabandite

A careful optical and microprobe study indicates the presence of "Zn-alabandite" containing 37.00 wt% Zn on average (Table 12). Zn-alabandite contains 12.91 wt% Mn and 15.46 wt% Fe on average (Table 12). This compound needs an electron diffraction study to clarify its crystallographic status.

Galena

Galena is common in samples rich in Pb. It forms myrmekitic intergrowths with FeS and does not contain silver (Table 12).

Chalcopyrite

Chalcopyrite fills up small fractures and interstitial spaces in pyrrhotite, and is rare. Unlike natural chalcopyrite, the studied variety contains significant admixture of Mn and Zn (Table 12). Copper in the slag probably originates from Cu sulphate added during flotation as flotation activator. This conclusion comes from the observation that copper minerals are not observed in the Silesian Zn-Pb ores.

6.4.6 Metal silicides

In some of the studied slag pieces, silicides are common compounds, in other samples they are absent. They are usually associated with coke particles surrounded by Si carbides, where they form inclusions. Si carbides were confirmed by XRD Gandolfi study. Most of the discussed Si compounds are Si carbides. Less abundant are Fe silicides ($FeSi_2$, FeSi) and (Al, Fe)Si compounds. The presence of metallic Si was confirmed by XRD study. The above-discussed Si compounds do not contain admixtures jeopardizing environment

(Table 13). They are, however, interesting as regards equilibria in the smelting furnace, especially concerning defected Al silicides. This problem requires further study, which is beyond the scope of this contribution.

6.4.7 Wüstite and periclase

Both minerals are common constituents of metallurgical slag. Wüstite forms larger, massive accumulations bordered directly by metallic iron (Fig. D21), or present as inclusions in pyrrhotite and magnetite (Fig. D23). Varieties rich in Mg (periclase) often form agglomerations of isometric crystals in pyrrhotite (Fig. D21). Wüstite forms continuous series towards periclase from almost pure FeO to periclase containing 30.3 wt% of FeO (Table 14). Mg-rich wüstite contains high amounts of of MnO, ZnO and CaO admixtures (Table 14). Etching of wüstite is much faster in fluids I and II (acid rain) than in solution III, IV and V (saturated pore fluids).

Table 13. Chemical composition of iron silicides from metallurgical slag (wt%)

Sample	Al	Si	S	Fe	Cu	Zn	Ni	Σ
A2/2	≤0.05	46.30	≤0.05	51.96	1.44	0.75	≤0.05	101.70
2a	≤0.05	46.87	≤0.05	50.40	≤0.07	≤0.07	≤0.05	97.27
3	≤0.05	22.39	≤0.05	73.73	1.81	≤0.07	≤0.05	97.93
3a	≤0.05	22.61	≤0.05	73.08	1.87	≤0.05	≤0.05	97.55
3b	≤0.05	22.00	≤0.05	74.49	2.06	≤0.05	≤0.05	98.55
4	≤0.05	37.32	0.56	56.60	2.21	≤0.05	≤0.05	96.70
4a	≤0.05	41.43	0.47	53.86	2.03	0.75	≤0.05	98.55
A3/2	43.93	37.15	≤0.05	17.21	1.05	≤0.05	≤0.05	99.33
2a	44.44	38.83	≤0.05	17.40	1.32	≤0.05	≤0.05	98.76
A5/1	≤0.05	26.82	≤0.05	70.69	1.75	≤0.05	0.41	99.67
2	≤0.05	25.96	≤0.05	71.48	1.88	≤0.05	≤0.05	99.32
A4/1	44.48	35.96	≤0.05	18.01	1.05	≤0.05	≤0.05	99.71
La	45.01	35.74	≤0.05	17.73	1.17	≤0.05	≤0.05	99.64
3	≤0.05	65.57	≤0.05	32.90	1.08	≤0.05	≤0.05	99.55
4	0.80	47.90	≤0.05	51.20	≤0.07	≤0.05	≤0.05	99.50

Table 14. Chemical composition of wüstite and periclase from metallurgical slag (wt%)

Sample	MgO	SiO_2	CaO	MnO	FeO	ZnO	Σ
3FR/A5	6.58	0.53	2.43	≤0.08	89.32	1.15	100.02
A6	≤0.08	≤0.05	2.48	≤0.08	94.63	0.89	98.00
A7	≤0.08	≤0.05	1.80	≤0.08	95.95	≤0.05	97.75
A8	≤0.08	0.45	1.27	≤0.08	95.91	≤0.05	97.63
A8a	1.44	≤0.05	1.84	≤0.08	95.54	≤0.05	98.82
A9	59.20	≤0.05	≤0.08	1.40	33.59	2.46	96.65
A9a	63.68	≤0.05	≤0.08	1.18	32.01	2.11	98.98
A10	63.21	≤0.05	≤0.08	1.12	30.30	4.03	98.66
All	59.62	0.32	0.23	1.44	33.84	3.08	98.53
A12	11.24	3.57	1.95	3.72	72.74	4.68	99.26
A13	62.65	≤0.05	0.47	1.38	32.40	1.95	98.86
CI	55.28	1.08	2.31	1.06	35.72	3.89	99.35
C2	56.20	≤0.05	0.82	1.62	36.55	3.90	99.10

6.4.8 Anthracite–graphite

Coke particles as large as a few mm are common constituents of slag constituting in some samples up to 10% of the sample surface (Fig. D24). As a rule, they are surrounded by an assemblage composed of metallic iron, pyrrhotite and ferrous sphalerite. Coke-anthracite is enriched in S, Ca, Fe, Cu and Zn, but also contains 1.20 wt% of Hg on average (Table 15).

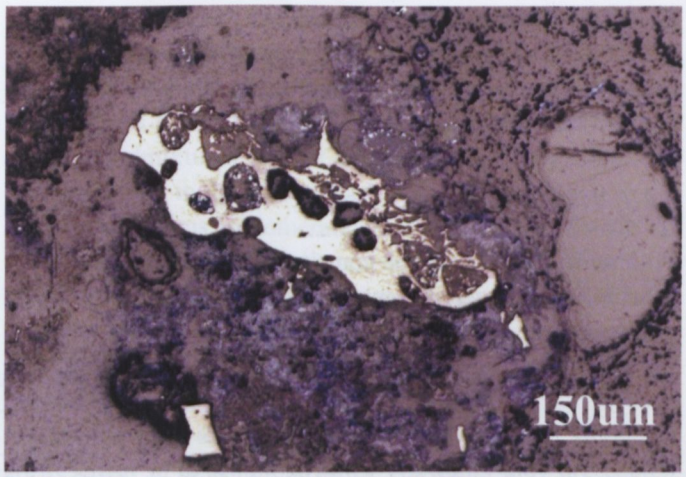

Fig. D24. Photomicrograph of graphite–anthracite (light) with preserved cellular organic microtexture of black coal. Reflected light, slag sample 8b.

6.5 Summary of leaching tests

Solution I (see 6.2 for the dscription of solutions) affects only some minerals. The surface of metallic lead and galena are coated with a black precipitate stopping further dissolution after 30 minutes and 3 hours, respectively. This solution also slowly dissolves iron carbides and iron phosphides. Other minerals were not affected by fluid I over a test period of 18 hours.

Leaching medium II (pH 2) etches faster the same minerals that are affected by fluid I. It also dissolves some of sphalerite along crystal boundaries. This fluid etches pyrrhotite, but after 40 minutes, the surface of FeS is coated by passive brownish film, which stops the progress of etching. Solution II etches also silicates, especially those containing less iron. A prolonged exposure of silicates to this fluid causes precipitation either of a Fe oxide coating or a Si oxide armour stopping further progress of etching. The etching tests with fluids I and II show that these type fluids (acid rain) will mobilize metals which form soluble oxides/hydroxides or sulphates (Zn, Cd), while those forming insoluble salts (Fe, Pb, Si) will remain within the dump.

The etching capacity of fluids III, IV and V containing Cl^- and SO_4^{2-} is different. The action of these fluids mimicking waters of dumps strongly depends on pH, but in general they are capable of leaching silicates as well as sulphides.

Table 15. Chemical composition of coal-anthracite-graphite from metallurgical slag according to EPMA analyses (wt%)

	Mg	Al	Si	P	S	Mn	Fe	Ni	Cu	Zn	As	Hg	Pb	*n*
min.	≤0.01	0.06	0.34	≤0.02	0.26	0.26	0.59	≤0.01	≤0.01	0.19	≤0.01	0.35	0.15	
max.	0.08	0.33	0.61	0.30	0.61	0.58	18.66	0.29	0.11	1.25	0.05	1.89	5.73	
mean	0.05	0.18	0.48	0.10	0.46	0.38	8.09	0.09	0.04	0.83	0.03	1.20	3.88	8

n - number of microprobe analyses
Sought but not detected: Ag ≤ 0.02, Cd ≤ 0.02, Sb ≤ 0.02

Table 16. Chemical composition of wüstite and periclase from metallurgical slag (wt%)

Sample	MgO	SiO_2	SO_2	CaO	MnO	Fe_2O_3	CuO	ZnO	PbO	TiO_2
3FR/B3	0.73	7.68	15.14	15.14	1.01	57.78	2.71	2.84	2.14	≤0.05
B4	0.74	8.61	6.15	12.09	0.86	57.46	1.69	2.65	8.19	0.79
B5	0.09	6.73	9.66	10.46	1.06	59.73	2.35	6.08	1.55	≤0.05
B9	0.10	5.01	4.21	7.08	0.42	60.01	0.55	12.18	6.24	0.22
B10	≤0.05	3.11	7.22	6.11	0.98	56.34	0.72	5.27	0.92	≤0.05
B11	≤0.05	2.34	1.84	3.05	0.41	48.92	0.31	3.33	0.73	≤0.05
B12	≤0.05	5.11	3.89	1.24	0.93	55.89	1.11	6.54	1.53	≤0.05

The leaching action will be probably controlled by the availability of pyrite in the dump material, because this mineral upon oxidation creates a strongly acidic environment (Neuman-Mahlkan, 1993).

6.6 Discussion

Most of the discussed primary phases are metastable at ambient conditions. The most vulnerable ones are those containing sulphidic S and/or divalent iron. Sulphides will decompose mainly due to sulphur oxidation. In this process, sulphur forms soluble sulphate, which serves as a transporting agent for all of the metals except of Fe^{3+} and Pb, because $PbSO_4$ has low solubility under conditions prevailing in the dumps, where fluids are buffered by dolomite. A high pH of fluids residing in the pore networks of the dumps will slow down dispersion of metals. Oxidation of iron from ferrous into ferric increases a capacity of adsorption of metal ions in general order Cu > Pb > Zn > Co > Ni > Cd > Mn (Thornber, 1985). A release of silica due to acid attack will act in the similar way. The significance of the above adsorption may be illustrated by the composition of newly formed Fe hydrated oxides in slag, where high content of Pb, Cu, Zn, Si and SO_2 is observed (Table 16). Unfortunately, no Cd, Tl and As were detected, which means that these poisonous metals are leached away.

The overall picture concerning Pb mobility may be encouraging due to its low solubility under dump regimes (Thornber, 1985). This picture is, however, misleading. As shown by Swennen *et al.* (1994), large quantities of lead are present in overbank river sediments in similar environment in Belgium, despite low solubilities of Pb. This apparent discrepancy may be reconciled if we accept that lead is transported as a particulate matter. This, however, has to be supported by direct investigation of river sediments with modern FESEM microscopy.

Zinc in the dumps occurs as substitutions in slag silicates, as carbonates and as sulphides. Leaching tests performed on polished sections suggest that sulphate-chloride fluids of pore networks of dumps will leach Zn from all of the described mineral forms. The process is likely to continue until most of available zinc is leached away.

Cadmium is present in metallic lead and in sphalerite in flotation tailings. No Cd was found by microprobe in secondary minerals formed in the dumps. This confirms the opinion that Cd is extremely mobile (Thornber, 1985), and further investigations on Cd mobility in ground and river waters is required. In similar settings in Belgium (Swennen *et al.*, 1994), Cd contamination in river sediments is dangerously high.

Arsenic is present mainly in metastable melnikovite in tailings and in metallic iron and Fe-rich sphalerite in slag. All these compounds are unstable and will release mobile arsenates. A high As contamination has been found in similar settings in Belgium (Swennen *et al.*, 1994).

Thallium in the studied dumps is present in high quantities in metastable melnikovite (Table 6). Concerning the high toxicity of Tl, the observed amounts of this element (estimated to 665 t in tailings, Gorecka *et al.*, 1994) are dangerous. Tl is very mobile in most of natural environments as Tl-bearing sulphides (Vink, 1993). There are no systematic measurements of the Tl abundance in and around Zn-Pb dumps. However, because of the toxicity of Tl and its presence in the tailings, such a study is urgently needed.

Buffering by carbonates present in tailings has a positive effect on retardation of the metal discharge from the dumps for most of metals, but may be regarded as insufficient in the case of Cd and Tl.

6.7 Acknowledgements

This research was supported by the KBN grant No. 9-S602-038-06. The author is grateful to Prof. W. Viaene for access free of charge to research facilities of the Department of Chemical Geology, KU Leuven, Belgium.

7. References

Ahmed, H. & Płuska, I. (2000): Conservation and reconstruction of mascaron "From Sukiennice". In Conference Papers, The International Conference on Conservation; Kraków 2000. Cultural Heritage as Foundation of Civilisation Development, October 23-26, 2000. Cracow: Institute of History of Architecture and Monument Preservation, Faculty of Architecture, University of Technology, 339–344 (in Polish and in English).

Amoroso, G.G. & Fassina, V. (1983): Stone decay and conservation. Amsterdam: Elsevier, 453 p.

Andreyeva-Grigirovich, A.S., Gasiński, N., Savitskaya, N.A., Ślączka, A. & Trofimovich, N.A. (2003): Correlation of Late Badenian salts of the Wieliczka, Bochnia and Kalush areas (Polish and Ukrainian Carpathian Foredeep). Annales Societatis Geologorum Poloniae, **73**: 67–89.

Andrzejewski, R., Wilczyńska-Michalik, W. & Michalik, M. (1992): Accelerated destruction of the stony building materials of the historical monuments in Kraków (Poland) – mineralogical description. Wissenschaft und Umwelt, ISU, **1991** (3-4): 121–126.

Anonymous (1995): Raport o stanie środowiska w województwie Krakowskim w 1994 roku [Report on the environment in Kraków Voivodeship 1994], In Turzański, K.P. (ed.): Państwowa Inspekcja

Ochrony Środowiska. Wojewódzki Inspektorat Ochrony Środowiska w Krakowie. Urząd Wojewódzki w Krakowie. Wydział Ochrony Środowiska (in Polish).

Anonymous (1997): Sucha i mokra depozycja pierwiastków w województwie Krakowskim w latach 1992–1996 [Dry and wet deposition of elements in Kraków Voivodeship in 1992–1996]. In Turzański, K.P. & Godzik, B. (eds). Kraków: Biblioteka Monitoringu Środowiska, 3–39 (in Polish).

Anonymous (2009): Raport o stanie środowiska w województwie małopolskim w roku 2008 [Report on the Environment in Małopolska Voivodeship in 2008]. Wojewódzki Inspektorat Ochrony Środowiska. Biblioteka Monitoringu Środowiska, Kraków 2009.

Bąk, B., Poprawa, D. & Radwanek-Bąk, B. (1998): Mineral resources of the Polish Carpathians and the Carpathian Foredeep and their economic utilisation. Przegląd Geologiczny, **46**: 781–787.

Bogacz, K., Dzulynski, S., Haranczyk, Cz. & Sobczynski, P. (1972): Contact relations of the ore bearing dolomite in the Triassic of the Cracow-Silesian region. Annales Societatis Geologorum Poloniae, **42**: 347–372.

Bogacz, K., Dzulynski, S. & Haranczyk, Cz. (1973): Caves filled with clastic dolomite and galena mineralization in disaggregated dolomites. Annales Societatis Geologorum Poloniae, **43**: 59–72.

Bogacz, K., Dzulynski, S. & Haranczyk, Cz. (1975): Origin of the Ore Bearing Dolomite in the Triassic of the Cracow-Silesian Zn-Pb district. Annales Societatis Geologorum Poloniae, **43**: 59–72.

Brandon, J.K., Brizard, R.Y., Chien, P.C., McMillan, R.K. & Pearson, W.B. (1974): New refinenments on the γ-brass structures Cu_5Zn_8, Cu_5Cd_8 and Fe_3Zn_{10}. Acta Crystallographica, **B30**: 1412–1417.

Brzeźniak, E. (2001): Researches on thermic air structure in Cracow with the help of the Automatic Meteorological Station ASM-94. In Problematyka pomiarów i opracowań elementów meteorologicznych. Supplement. Lublin: Wydawnictwo UMCS, 17–21 (in Polish with English abstract).

Bukowski, K. (1997): Sedimentation of clastic strata associated with Miocene salts in Wieliczka (Southern Poland). Slovak Geological Magazine, **3**: 157–163.

Bukowski, K. (1999): Comparison of the Badenian saliferous series from Wieliczka and Bochnia in the light of new data. Prace Państwowego Instytutu Geologicznego, **158**: 43–56 (in Polish with English abstract).

Bukowy, S. (1974): Silesian-Cracow Monocline and Upper Silesian Foredeep. In Pozaryski, W. (ed.): Geology of Poland, Vol. 4 (Tectonics), part 1. Warsaw: Wydawnictwa Geologiczne.

Buła, Z., Habryn, R., Kurek, S., Krieger, W., Markowiak, M. & Woźniak, P. (2002): Geological atlas of the Paleozoic in the border zone of the Upper Silesian and Malopolska Blocks, scale 1 : 200,000. Warszawa: Państwowy Instytut Geologiczny (in Polish).

Chmura, J. & Godzik, B. (1996): Analiza jonowa pojedynczego opadu [Ion analysis of single atmospheric precipitation]. Rocznik Naukowo-Dydaktyczny WSP 184, Prace Geograficzne, **16**: 37–49 (in Polish with English abstract).

Chrzanowski, T. (2000): Italian Cracow and more. In The International Conference on Conservation; "Kraków 2000". Cultural Heritage as Foundation of Civilisation Development, October 23–26, 2000. Conference Papers. Institute of History of Architecture and Monument Preservation, Faculty of Architecture, Cracow University of Technology, 7–16 (in Polish and in English).

Clarke, A.G. (1996): The atmosphere. In Harrison, R.M. (ed.): Understanding our environment: an introduction to environmental chemistry and pollution. Cambridge: The Royal Society of Chemistry, 3–51.

Dębicka, K. (1999): Occurence frequency of days with persisting inversion in Cracow. Wiadomości IMGW, **22** (3): 93–105 (in Polish with English abstract).

Dobrowolski, T. (1950): The art of Kraków. Kraków: Wydawnictwo M. Kot, 477 p (in Polish).

Duwensee, F. (1929): Die Oberschlesische Blei-Zink-Lagerstätte auf Grund der Ergebnisse der geologischen Untersuchung der Deutsch-Bleischarley-Grube. Metall und Erz, **26** [Neue Folge **17**] (19): 481.

Dzulynski, S. & Sass-Gustkiewicz, M. (1989): Pb-Zn ores. In Bosak, P., Ford, D.C., Glazek, J. & Horacek, I. (eds): Paleokarst, a systematic and regional review. Developments in Earth Surface Processes, **1**. New York: Elsevier, Prague: Academia, 377–398.

Ekiert, F. (1978): Precambrian and early Paleozoic stratigraphy in the northern and north-eastern borderland of the Upper Silesian Coal Basin. In Pawlowska, J. (ed.): Prospecting for zinc and lead ores in the Silesian-Cracow area. Prace Państwowego Instytutu Geologicznego, **83**: 55–62.

Fabryczek, K. (1973): Kamienie budowlane miasta Krakowa. Unpublished manuscript. Archives of the Pedagogical Academy of Cracow, Institute of Geography. 64 p (in Polish).

Fiszer, J. (1990): Threat of surface water by polluted precipitation in the Kraków region. In Gumińska, M. & Delorme, A. (eds): Ecological disaster of Krakow. Kraków: Polish Ecological Club, 420 p (in Polish with English abstract).

Florczyk, R., Lach, J., Michalik, M. & Wilczyńska-Michalik, W. (1998): Wpływ zanieczyszczeń atmosfery na rozwój warstw powierzchniowych na materiałach budowlanych kapliczek przydrożnych w Krakowie [The influence of atmospheric pollution on the development of the superficial layers on building materials of wayside shrines in Kraków]. In Suchecki, T.T., Kapała, J. & Konieczyński, J. (eds): Proceedings of the 2nd International Scientific Conference "Air protection in theory and applications", Section IV, Problems of environmental protection; Prace i Studia, **49**: 131–147 (in Polish with English abstract).

Galamay, A.R., Bukowski, K. & Przybyło, J. (1997): Chemical composition and origin of brines in the Badenian evaporite basin of the Carpathians Foredeep: fluid inclusion data from Wieliczka (Poland). Slovak Geological Magazine, **3**: 165–171.

Garlicki, A. (1979): Sedimentation of Miocene salt in Poland. Prace Geologiczne PAN, **119**: 1–67 (in Polish with English abstract).

Gaweł, A. (1962): Geological structure of the Wieliczka salt mine. Prace Instytutu Geologicznego, **30**: 305–331 (in Polish with English abstract).

Gehlen, K. von & Nielsen, H. (1969): Schwefel-Isotope aus Blei-Zink Erzen von Oberschlesien. Mineralium Deposita, **4**: 308–310.

Glazek, J. (1989): Paleokarst of Poland. In Bosak, P., Ford, D.C., Glazek, J. & Horacek, I. (eds): Paleokarst, a systematic and regional review. Developments in Earth Surface Processes, **1**. New York: Elsevier, Prague: Academia, 77–106.

Godzik, B. (1999): Wet deposition of elements in Kraków. In Turzański, K.P. & Pauli-Wilga, J. (eds): Report on the environment in Kraków 1994–1998, current status and trends. The Voivodeship Inspectorate for Environmental Protection in Kraków; City Office of Kraków. Kraków: The Environmental Monitoring Library, 77–79.

Górecka, E. (1978): Polymetallic mineralization in the Paleozoic formations of the Zawiercie area. Prace Państwowego Instytutu Geologicznego, **83**: 163–169 (in Polish with English abstract).

Górecka, E. (1993): Geological setting of the Silesian-Cracow Zn-Pb deposits. Geological Quarterly, **37**: 127–146.

Górecka, E., Bellok, A., Socha, J., Wnuk, R. & Kibitlewski, S. (1994): Variability of metal contents in Zn-Pb flotation waste (ZGH Boleslaw, Olkusz area): Przegląd Geologiczny, **42**: 834–841 (in Polish).

Górecka, E. & Nowakowski, A. (1979): Ore deposits associated with acid intrusives and related rocks in the Zawiercie region. Prace Państwowego Instytutu Geologicznego, **95**: 97–107 (in Polish with English abstract).

Grabski, W. & Nowak, J. (1958): The problem of formation of patina at the surface of Pińczów limestone. Kraków: Czasopismo Techniczne, **1** (7): 13–18 (in Polish).

Gradziński, R. (2000): Geology of the Kraków area. In Gradzinski, M. (ed.): Guidebook & Abstracts – Climate changes, the karst record II, Kraków (Poland), 30 July – 4 August, 2000. Kraków: Institute of Geological Sciences, Polish Academy of Sciences, Institute of Geological Sciences, Jagiellonian University, 3–4.

Gruszczyk, H. (1978): A hypothesis on a polygenetic nature of the deposits. In Pawlowska, J. (ed.): Prospecting for zinc and lead ores in the Silesian-Cracow area. Prace Państwowego Instytutu Geologicznego, **83**: 307–310 (in Polish).

Haber, J., Haber, H., Kozłowski, R., Magiera, J. & Płuska, I. (1988): Air pollution and decay of architectural monuments in the city of Cracow. Durability of Building Materials, **5**: 499–547.

Haranczyk, Cz. (1978): Isotopic composition of sulphur from the Silesian-Cracow deposits. In Pawlowska, J. (ed.): Prospecting for zinc and lead ores in the Silesian-Cracow area. Prace Państwowego Instytutu Geologicznego, **83**: 237–243 (in Polish).

Haranczyk, Cz. (1979): Metallogenic evolution of the Cracow-Silesian region. In Pawlowska, J., Chidester, H. & Wedow, H., Jr. (eds): Research on the genesis of zinc-lead deposits of Upper Silesia, Poland. Prace Instytutu Geologicznego, **95**: 109–132.

Haranczyk, Cz. (1982): The Cracowides as a Caledonian orogen. Przegląd Geologiczny, **30**: 575–582 (in Polish with English abstract).

Haranczyk, Cz. (1993): Sulphur isotope models of genesis of the Silesian-Cracow Zn-Pb ore deposits. Geological Quarterly, **37**: 307–322.

Heijlen, W., Muchez, Ph., Banks, D.A., Schneider, J., Kucha, H. & Keppens, E. (2003): Carbonate hosted Zn-Pb deposits in Upper Silesia, Poland: Origin and evolution of mineralizing fluids and constraints on genetic models. Economic Geology, **98**: 911–932.

Herbich, E. (1981): Analysis of fault network of the Upper Silesian coal basin. Annales Societatis Geologorum Poloniae, **51**: 383–434 (in Polish).

Horzemski, J. (1962): On the relation of so-called vitriol clays to the ore-bearing limestones and dolomites of the Middle Triassic in Upper Silesia. Bulletin de l'Academie polonaise des sciences. Serie des sciences, geologiques et geographiques, **10**: 237–243.

Kajfosz, J. (1992): Computer program package for PIXE spectra evaluation. Report no 1605/Pl, IFJ Kraków, 15 p.

Karwowski, L., Kozlowski, A. & Roedder, E. (1979): Gas-liquid inclusions in minerals of zinc and lead ores from the Silesia-Cracow region. In Pawlowska, J., Chidester, H. & Wedow, H., Jr. (eds): Research on the genesis of zinc-lead deposits of Upper Silesia, Poland. Prace Instytutu Geologicznego, **95**: 78–96.

Kibitlewski, S. & Gorecka, E. (1988): Tectonic structures in ore-bearing dolomites from Pomorzany mine, Olkusz area of Zn-Pb deposits. Przegląd Geologiczny, **36**: 408–413.

Kolasa, K. & Ślączka, A. (1985): Sedimentary salt mega-breccias exposed in the Wieliczka mine. Acta Geologica Polonica, **35**: 221–230.

Kowalewski, K. (1935): Zur Frage des Alters und der Fauna der Salzfomation von Wieliczka. Sprawozdania Państwowego Instytu Geologicznego, **8**: 218–223.

Kozlowski, A. & Gorecka, E. (1993): Sphalerite origin in the Olkusz mining district: A fluid inclusion model. Geological Quarterly, **37**: 291–306.

Kozłowski, R. & Magiera, J. (1989): Decay of "Dębnik" and Pińczów limestones in monuments in Kraków. In Przewodnik LX Zjazdu Polskiego Towarzystwa Geologicznego. Kraków: Wydawnictwa AGH, 204–209 (in Polish).

Kozlowski, A., Karwowski, L. & Roedder, E. (1980): Parent fluids of the zinc and lead ores from the Silesia-Cracow region. Acta Geologica Polonica, **30**: 147–152.

Kozłowski, R., Magiera, J., Weber, J. & Haber, J. (1990): Decay and conservation of Pińczów porous limestone. Part I. Lithology and weathering. Studies in Conservation, **35**: 205–221.

Kucha, H. (1988a): The significance of diagenesis in emplacement of strata-bound Zn-Pb mineralization in carbonate sediments. In Friedrich, G.H. & Herzig, P.M. (eds): Base metal sulphide deposits, SGA Special Publication, **5**. Berlin: Springer, 109–120.

Kucha, H. (1988b): Zn-Pb sulphides as rim cements, filling cements and replacements of carbonate sediments, Moyvoughly, Ireland – a product of two convective cells. Transactions of the Institution of Mining and Metallurgy, Sect. B: Applied Earth Sciences, **97**: 64–76.

Kucha, H. (1989): Macrotextures, microtextures and carbonate-sulfide relationships in stratiform, carbonate-hosted Zn-Pb orebodies of Silvermines, Ireland. Mineralium Deposita, **24**: 48–55.

Kucha, H. & Barnes, H.L. (1995): Compounds with mixed and intermediate sulfur valences in pyrite from the Amelia mine, Southwest Wisconsin. Mineralium Deposita, **30**: 78–81.

Kucha, H. & Czajka, K. (1984): Sulphide-carbonate relationships in Upper Silesian Zn-Pb deposits (Mississippi Valley Type), Poland, and their genesis. Transactions of the Institution of Mining and Metallurgy, Sect. B, Applied Earth Sciences, **93**: 12–22.

Kucha, H. & Jedrzejczyk, B. (1995): Primary minerals of mining and metallurgical Zn-Pb dumps at Bukowno, Poland, and their stability during weathering. Mineralogia Polonica, **26**: 75–99.

Kucha, H. & Viaene, W. (1993): Compounds with mixed and intermediate sulfur valences as precursors of banded sulfides in carbonate-hosted Zn-Pb deposits in Belgium and Poland. Mineralium Deposita, **28**: 13–21.

Kucha H., Bąk, B. & Wieczorek, A. (1983): Preliminary report on superstructures in zinc-dolomite. Mineralogia Polonica, **14**: 19–27.

Kucha, H., Wouters, R. & Arkens, O. (1989): Determination of sulfur and iron valence by microprobe. Scanning Microscopy Inernational, **3**: 89–97.

Kucha, H., Bak, B., Wieczorek, A. & Fitta, G. (1993): Preliminary report on superstructures in iron dolomite with excess of $CaCO_3$. Mineralogia Polonica, **15**: 21–28.

Kullerud, G. (1967): Sulfide studies. In Abelson, Ph. (ed.): Researches in geochemistry, **2**. New York: Wiley, 286–321.

Kuźniar, W. (1918): Comments on our building materials. Rzeczy Piękne, R. **1** (3): 6–8 (in Polish).

Lach, J., Morawska-Horawska, M. & Ziętara, T. (1996): Tendencies in changes in air pollution in Cracow after the World War II. Kraków: Folia Geographica, series Geographica-Physica, **26-27** (for 1994/1995): 39-57 (in Polish, with English summary).

Leach, D.L., Viets, J.G. & Powell, J.W. (1996): Textures of ores from the Silesian-Cracowian lead-zinc deposits, Poland: Clues to the ore-forming environment. In Gorecka, E., Leach, D. & Kozlowski, A. (eds): Carbonate-hosted zinc-lead deposits in the Silesian-Cracow area, Poland. Prace Instytutu Geologicznego, **154**: 37-50.

Lewińska, J. (1979): Thermic pollution in the Kraków region. Folia Geographica, **12**: 93–101 (in Polish with English abstract).

Lewińska, J. (1996): Genesis, expansion and reduction possibilities of the urban heat island in Cracow. Folia Geographica, series Geographica-Physica, **26-27** (for 1994/1995): 75–87 (in Polish with English abstract).

Livingston, R.A. (1989): Atmospheric deposition and its measurement with regard to air pollution legislation to protect monuments. In Materials of European Symposium "Science, Technology and European Cultural Heritage"; Bologna, Italy, 13-16 June 1989, 18–20.

Łańcucka-Środoniowa, M. (1984): The results obtained hitherto in studies on the Miocene macroflora from the salt-mine at Wieliczka (S Poland). Acta Palaeobotanica, **24**: 3–26.

Małecki, Z., Wilczyńska-Michalik, W. & Macharski, P. (1988): The deterioration of cultural monuments as example on Kraków urban and industrial agglomeration. Kraków: Polska Akademia Nauk. Instytut Podstaw Inżynierii Środowiska. Stacja Badawcza, 1–12 (in Polish).

Małecki, Z., Wilczyńska-Michalik, W., Nessler-Wróbel, A. & Karaszkiewicz, P. (1991a): The deterioration of cultural monuments caused by environmental pollution as shown within the urban-industrial center of Cracow. Report of the U. S. National Park Service Delegation to Poland, Occasional Paper, **1**: 55–58.

Małecki, Z., Wilczyńska-Michalik, W., Nessler-Wróbel, A. & Karaszkiewicz, P. (1991b): The deterioration of cultural monuments by polluted environment; an example of Kraków urban and industrial agglomeration. Kraków : Polska Akademia Nauk. Instytut Podstaw Inżynierii Środowiska. Stacja Badawcza, 1–22 (in Polish).

Manecki, A., Chodkiewicz, M. & Konopacki, S. (1982): Results of the mineralogical investigations of the dimensions and causes of the destruction of stone elements in Cracow's monumental buildings. Zeszyty Naukowe Akademii Górniczo-Hutniczej, Sozologia i Sozotechnika, **17**: 35–68 (in Polish with English abstact)

Marszałek, M. (2004): Deterioration of stone in some monuments exposed to air pollution: a Cracow case study. Air Pollution and Cultural Heritage, **1**: 151–154.

Marszałek, M. (2008): Application of optical microscopy and scanning electron microscopy to the study of stone weathering: A Cracow case study. International Journal of Architectural Heritage, **2**: 83–92.

Marszałek, M. & Skowroński, A. (2010): Black "marble": The characteristic material in the Baroque architecture of Cracow (Poland). In Bostenaru Dan, M., Přikryl, R. & Török, Á. (eds): Materials, technologies and practice in historic heritage structures. Berlin: Springer, 93–106.

Marszałek, M., Skowroński, A. & Gaweł, A. (2006): Anthropogenic components in weathered Dębnik limestones from Cracow historic sites. Gospodarka Surowcami Mineralnymi, **22**: 449–460 (in Polish).

Matuszko, D. (2007): Sunshine duration. In Matuszko D. (ed.): Climate of Cracow in the 20th century. Kraków: IGiGP UJ, 87–97 (in Polish with English abstract).

McCormick, J.E., Evans, L.L., Palmer, R.A. & Rasnick, F.D. (1971): Environment of the zinc deposits of the Mascot-Jefferson city district, Tennessee. Economic Geology, **66**: 757–762.

Michalik, A. (1981): Building stones of the old Kraków, part I. Manuscript. Archives of the Pedagogical Academy of Cracow, Institute of Geography, 89 p (in Polish).

Michalik, M. & Wilczyńska-Michalik, W. (1998a): The influence of air pollution on weathering of building stones in Kraków. In Sulovský, P. & Zeman, J. (eds): Environmental aspects of weathering processes, ENVIWEATH 96. Folia Facultatis Scientiarum Naturalium Universitatis Masarici Brunnensis, Geologia, **39**: 159–167.

Michalik, M. & Wilczyńska-Michalik, W. (1998b): Sulphate minerals and anthropogenic dust particles on the surfaces of sandstones in the Carpathians as the indicators of atmospheric pollution concentration. Roczniki Bieszczadzkie, **7**: 209–225 (in Polish with English abstract).

Mochnacka, K. & Sass-Gustkiewicz, M. (1978): Metasomatic process along the contact of the ore-bearing dolomite with limestones, Olkusz mine, Cracow-Silesian Zn-Pb ore district. Annales Societatis Geologorum Poloniae, **48**: 183–191.

Morawska-Horawska, M. & Lewik, P. (1997): The thermal blocking layers in the 100-meter earthbound layer of the air over Cracow. Folia Turistica, **7**: 53–76 (in Polish with English abstract)

Neuman-Mahlkan, P. (1993): Acidification by pyrite weathering on mine waste stockpiles, Ruhr district, Germany. Engineering Geology, **34**: 125–134.

Niec, M. & Bak, B. (1993): Zinc-lead ore deposit in Lower Triassic (Raethian) dolomites at Boleslaw (Olkusz region, Poland). Geological Quarterly, **37**: 157–174.

Ohle, E.L. (1985): Breccias in Mississippi Valley-type deposits. Economic Geology, **80**: 1736–1752.

Olecki, Z. (1975): Influence of a big urban-industrial centre on the amount of solar radiation (as exemplified by Cracow). Prace Geograficzne, **41**: 37–86.

Oleś, W. (2001): Tendences of changes in the sanitary state of air in the Upper Silesian Region over the last twenty years. In German, J. & Balon, J. (eds): Transformations of the natural environment of Poland and its functioning. Problemy Ekologii Krajobrazu, **10**: 433–437 (in Polish with English abstract).

Osman, M. & Piestrzynski, A. (1989): Mechanism of sulphide mineralization through successive metasomatic replacement stages of zoned host dolomite in Carob-Silesian Zn-Pb deposits (Mississippi Valley type), Pomorzany mine, Poland. Mineralium Deposita, **24**: 56–61.

Oszczypko, N., Krzywiec, P., Popadyuk, I. & Peryt, T. (2006): Carpathian Foredeep Basin (Poland and Ukraine): its sedimentary, structural, and geodynamic evolutions. In Golonka, J. & Picha, F.J. (eds): The Carpathians and their foreland: geology and hydrocarbon resources. American Association of Petroleum Geologists Memoir, **84**: 261–318.

Panek, S. & Szuwarzynski, M. (1974): Oxidised zinc ores in the Matylda mine. Rudy i Metale Nieżelazne, **19** (2): 71–74 (in Polish).

Pawlikowski, S. (1959): Development of technical knowledge and progress in protection of monuments. Ochrona Zabytków, **2**: 84–85 (in Polish).

Pawlikowski, M. (1978): Petrographic studies of the Wieliczka salt deposits. Prace Mineralogiczne Komisji Nauk Mineralogicznych PAN Kraków, **58**: 65–110 (in Polish with English abstract).

Pawlowska, J. (1978): Comments on the views on the origin of the Silesia Cracow zinc and lead deposits. In Pawlowska, J. (ed.): Prospecting for zinc and lead ores in the Silesian-Cracow area. Prace Państwowego Instytutu Geologicznego, **83**: 295–300.

Pawlowska, J. & Szuwarzynski, M. (1979): Sedimentary and diagenetic processes in the Zn-Pb host rock of Trzebionka. In Pawlowska, J., Chidester, H. & Wedow, H., Jr. (eds): Research on the genesis of zinc-lead deposits of Upper Silesia, Poland. Prace Instytutu Geologicznego, **95**: 15–58.

Picha, F. (1996): Exploring for hydrocarbons under thrust belts – a challenging new frontier in the Carpathians and elsewhere. American Association of Petroleum Geologists, Bulletin, **80**: 1547–1564.

Pietrzyk-Sokulska, E. (2001): Impact of rock quarrying on the environment on the example of Cracow area. In German, J. & Balon, J. (eds): Transformations of the natural environment of Poland and its functioning. Problemy Ekologii Krajobrazu, **10**: 418–425 (in Polish with English abstract).

Piwowarski, W. & Zeglicki, J. (1978): Modes of occurrence of ore mineralization in the Bytom Trough. In Pawlowska, J. (ed.): Prospecting for zinc and lead ores in the Silesian-Cracow area. Prace Państwowego Instytutu Geologicznego, **83**: 193–200.

Pokorski, J. (1981): Paleogeography of the Upper Rotliegendes in the Polish lowland. In Pakulska, Z. (ed.): International Symposium on Central European Permian. Warsaw: State Geological Institute, 56–68.

Przenioslo, S. (1974): Zinc and lead in the Triassic carbonate rocks in the vicinity of Zawiercie. Biuletyn Institutu Geologicznego, **278**: 115–200 (in Polish).

Przenioslo, S. (1978): Regularities in distribution of the deposits and guidelines of prospecting. In Pawlowska, J. (ed.): Prospecting for zinc and lead ores in the Silesian-Cracow area. Prace Państwowego Instytutu Geologicznego, **83**: 311–318.

Radwanek-Bąk, B. (1983): Petrographic characteristics of oxidized zinc ores in the Bolesław and Olkusz deposits (Southern Poland). Annales Societatis Geologorum Poloniae, **53**: 235–254.

Rajchel, J. (2002): Rocks of the Carpathians and the Carpathian Fordeep in the architecture of Cracow. In Proceedings of the XVII. Congress of Carpathian-Balkan Association, Bratislava, September 1th-4th 2002. Geologica Carpathica, **53**: CD version.

Rajchel, J. (2004): Stones of Kraków. A geologist's view. Kraków: Uczelniane Wydawnictwa Naukowo-Dydaktyczne AGH (in Polish).

Ramdohr, P. (1980): The ore minerals and their intergrowths, Vols 1–2. 2nd edition. Oxford: Pergamon Press, 440 and 1207 p.

Rembiś, M. & Smoleńska, A. (2003): Characteristics and destruction signs of the sandstones in the Sigismund Chapel of the Wawel Cathedral. Kamień architektoniczny i dekoracyjny: materiały konferencji naukowej: Kraków, 23–24 września 2003 r. Kraków: AGH WGGiOŚ ZZSS, 149–164.

Ridge, J. & Smolarska, I. (1972): Factors bearing on the genesis of the Silesian-Cracowian lead-zinc deposits in southern Poland. In Gill, J.E. (ed.): Proceedings of the 24th International Geological Congress, Montreal, Canada, Section 6, Stratigraphy and Sedimentology, 216–229.

Rodríguez-Navarro, C., Sebastian, E. & Rodríguez-Gallego, M. (1997): An urban model for dolomite precipitation: authigenic dolomite on weathered building stones. Sedimentary Geology, **109**: 1–11.

Rutkowski, J. (1996): Przemiany morfologii Krakowa związane z wydobyciem surowców mineralnych [Transformation of Cracow morphology connected with the minaral raw materials exploitation]. Folia Geographica, series Geographica-Physica, **26-27** (for 1994/1995): 3–15 (in Polish with English abstract).

Ryka, W. (1978): Metamorphic rocks. In Pawlowska, J. (ed.): Prospecting for zinc and lead ores in the Silesian-Cracow area. Prace Państwowego Instytutu Geologicznego, **83**: 69–71.

Sabbioni, C. & Zappia, G. (1992): Atmospheric-derived element traces on damaged stone. Science of the Total Environment, **126**: 35–48.

Sangster, D.F. (1988): Breccia-hosted lead-zinc deposits in carbonate rocks. In James, N.P. & Choquette, P.W. (eds): Paleokarst. New York: Springer Verlag, 102–116.

Sass-Gustkiewicz, M. (1975): Zinc and lead mineralization in collapse breccia of the Olkusz mine (Cracow-Silesian region, Poland). Annales Societatis Geologorum Poloniae, **45**: 303–326.

Sass-Gustkiewicz, M., Dzulynski, S. & Ridge, J.D. (1982): The emplacement of zinc-lead sulfide ores in the Upper Silesian district–a contribution to the understanding of Mississippi Valley-type deposits. Economic Geology, **77**: 392–412.

Schmalz, R.F. (1969): Deep-water evaporite deposition: a genetic model. American Association of Petroleum Geologists, Bulletin, **53**: 798–823.

Siedlecka, A. (1970): The Lower Permian (Rotliegendes) of Silesian-Cracow upland. In Sokolowski, S. (ed.): Geology of Poland, Vol. 1, part 1. Warsaw: Wydawnictwa Geologiczne, 519–524.

Skalmowski, W. (1956): Natural and artificial building materials. Warszawa: Budownictwo i Architektura, 243 p [103–120] (in Polish).

Ślączka, A. & Kolasa, K. (1997): Resedimented salt in the Northern Carpathians Foredeep (Wieliczka, Poland). Slovak Geological Magazine, **3**: 135–155.

Ślączka, A. & Kaminski, M.A. (1998): A guidebook to excursions in the Polish Flysch Carpathians. Grzybowski Foundation Special Publication No. 6, Kraków, 171 p.

Ślączka, A., Kolasa, K. & Doktor, M. (1986): Excursion No. B-9. Miocene sub-marine fans along the active margin of the Carpathian orogeny. In Teisseyre, A.K. (ed.): IAS 7th European Regional Meeting Kraków-Poland, Excursion Guidebook, Wroclaw: Ossolineum, 165–177.

Sliwinski, S. (1969): The development of the ore-bearing dolomites in the Cracow-Silesian area. Prace Geologiczne – Komisja Nauk Geologicznych. PAN, **57**, 124 p (in Polish with English abstract).

Smolarska, I. (1974): Studies on mineralization of Triassic rock series in Poland. Prace Mineralogiczne – Komisja Nauk Mineralogicznych PAN, **37**, 71 p (in Polish).

Smoleńska, A. & Rembiś, M. (1999a): Microstructural changes of Jurassic limestone used in select historical objects as the effect of anthropogenic pollution of the atmosphere. Ochrona Zabytków, **1**: 34–38.

Smoleńska, A. & Rembiś, M. (1999b): The state of the preservation of Pińczów limestone applied in decorative architectonic elements of the Church of the Holy Virgin Mary in Cracow. Ochrona Zabytków, **2**: 122–126.

Sobczynski, P. & Szuwarzynski, M. (1974): The lithologic development and mineralization of the Lower Muschelkalk dolomites, Trzebionka mine. Annales Societatis Geologorum Poloniae, **44**: 545–555.

Swennen, R., Van Ker, I. & De Voss, W. (1994): Heavy metal contamination in overbank sediments of the Geul river (E Belgium); as relation to former Pb-Zn mining activities. Environmental Geology, **24**: 12–21.

Symons, D.T.A., Sangster, D.F. & Leach, D.L. (1995) A Tertiary age from paleomagnetism of the Mississippi Valley-type zinc-lead mineralization in Upper Silesia, Poland. Economic Geology, **90**: 782–794.

Szuwarzynski, M. (1988): Lithology and ore mineralization of the Upper Muschelkalk and Keuper sediments from the Chrzanow area. Rudy i Metale Nieżelazne, **33**: 9–13 (in Polish).

Szuwarzynski, M. (1991): Notes on the geological model of zinc-lead orebodies. Rudy i Metale Nieżelazne, **36** (7): 255–258 (in Polish).

Szuwarzynski, M. (1993): The lead and zinc deposits in the vicinity of Chrzanow. Geological Quarterly, **37**: 209–228.

Szuwarzynski, M. (1996): Orebodies in the Silesian-Cracow Zn-Pb ore district, Poland. In Gorecka, E., Leach, D. & Kozlowski, A. (eds): Carbonate-hosted zinc-lead deposits in the Silesian-Cracow area, Poland. Prace Państwowego Instytutu Geologicznego, **154**: 9–24.

Szuwarzynski, M. & Kryza, A. (1993) Problem of flotation waste related to Zn-Pb mining in the area of the Silesia-Cracow ore district. Przegląd Geologiczny, **41**: 629–633 (in Polish).

Tatarkiewicz, W. (1951): The back marble in Kraków. Sprawozdania PAN, **3** (1): 130–133 (in Polish).

Thornber, M.R. (1985): Supergene alteration of sulphides. VII. Distribution of elements during the gossan-forming process. Chemical Geology, **53**: 279–301.

Trepińska, J. & Skublicka, L. (2001): Synoptic conditions of thermal inversion in Cracow in the autumn-winter season. Przegląd Geofizyczny, **46** (4): 351–361 (in Polish with English abstract).

Turzański, K.P. (1991): Pollution of precipitated water in southern Poland – acid rains and their monitoring. Zeszyty Naukowe AGH, Sozologia i Sozotechnika, **34**: 1–106 (in Polish with English abstract).

Tyczyńska, M. (1968): Relief and geological structure within the territory of Cracow. Folia Geographica, series Geographica-Physica, **1**: 9–34 (in Polish with English abstract).

Uytenbogaardt, W. & Burke, E.A.J. (1985): Tables for microscopic identification of ore minerals. 2nd ed. New York: Dover, 430 p.

Vink, B.W. (1993): The behaviour of thallium in the (sub)surface environment in terms of Eh and pH. Chemical Geology, **109**: 119–123.

Walczewski, J. & Łukaszewski, J. (1986): The elements of climate of Cracow having impact on air quality. Zeszyty Naukowe AGH, Sozologia i Sozotechnika, **22**: 61–81 (in Polish with English abstract).

Weber-Kozińska, M. (1967): Stone types used in the early medieval buildings in Małopolska. In Kamienie w architekturze i rzeźbie. Warszawa: Biblioteka Muzeów i Ochrony Zabytków, Seria B, **19**: 173–184 (in Polish).

Wielgomas, K. (1978): Modes of occurrence of ore mineralization in the Zawiercie area. In Pawlowska, J. (ed.): Prospecting for zinc and lead ores in the Silesian-Cracow area. Prace Państwowego Instytutu Geologicznego, **83**: 201–205.

Wilczyńska-Michalik, W. (1997): Exploitation and usage of black coal – influence on environmental and cultural heritage in Kraków. In Papunen, H. (ed.): Mineral deposits: Research and exploration – where do they meet? Rotterdam: Balkema/Brookfield, 931–934.

Wilczyńska-Michalik, W. (2004): Influence of atmospheric pollution on the weathering of stones in Cracow monuments and rocks outcrops in the Cracow, Cracow-Częstochowa Upland and Carpathians. Kraków: Wydawnictwa Naukowe Akademii Pedagogicznej, 247 p.

Wilczyńska-Michalik, W. & Michalik, M. (1991a): Mineral composition and structure of crusts on dolomitic building materials in urban atmosphere in Kraków. Mineralogia Polonica, **22** (2): 69–78.

Wilczyńska-Michalik, W. & Michalik, M. (1991b): Application of mineralogical and petrographical studies in the conservation of the Berrecci portal at Wawel Castle. In Ogólnopolska Konferencja Naukowa; Poznawcze i praktyczne efekty badań prowadzonych w CPBP 03.11. Zabrze: IPIŚ PAN, 318–325 (in Polish).

Wilczyńska-Michalik, W. & Michalik, M. (1993): Solubility controlled mineral zonation in efflorescences and crusts from building walls. Mineralogia Polonica, **24**: 73–87.

Wilczyńska-Michalik, W. & Michalik, M. (1995): Deterioration of stone material in the buildings of Krakow. Przegląd Geologiczny, **43**: 227–235 (in Polish).

Wilczyńska-Michalik, W. & Michalik, M. (1996a): Weathering processes of sandstones from the areas of different concentration of air pollution. In 1st International Conference "Theory and practice of atmospheric air protection", Polish Academy of Sciences, Institute of Environmental Engineering, 893–903 (in Polish with English abstract).

Wilczyńska-Michalik, W. & Michalik, M. (1996b): Petrographical, mineralogical and geochemical indicators of the impact of anthropogenic air-pollution on rocks. Rocznik Naukowo-Dydaktyczny WSP, Prace Geograficzne, **16**: 71–81 (in Polish with English abstract).

Wilczyńska-Michalik, W. & Michalik, M. (1998): Differences of the mechanisms of weathering of the Jurassic limestones related to the concentration of air pollution. In Sulovský, P. & Zeman, J. (eds): Environmental aspects of weathering processes, ENVIWEATH 96, Folia Facultatis Scientiarum Naturalium Universitatis Masarici Brunnensis, Geologia, **39**: 233–239.

Wilczyńska-Michalik, W. & Michalik, M. (1999): Weathering of the Carpathian flysch sandstones – a natural or atmospheric-pollution influenced process. Geologica Carpathica, **50**: Spec. Issue, 87–89.

Wilczyńska-Michalik, W. & Michalik, M. (2004): Influence of anthropogenic factors on weathering of the Carpathian flysch sandstones. In Smith, B.J. & Turkington, A.V. (eds): Stone decay; its causes and controls. Shaftesbury: Donhead, 225–245.

Wilczyńska-Michalik, W. & Michalik, M. (2006): Celestite in the weathering crust on limestone exposed to an urban atmosphere in Cracow (Poland). Mineralogia Polonica, **37**: 133–142.

Wilczyńska-Michalik, W., Banaś, M. & Michalik, M. (1994): Mineralogical and chemical differentiation of the weathering processes on carbonate rocks in the areas of different concentration of the pollution of atmosphere. Prace Specjalne, Polskie Towarzystwo Mineralogiczne, **5**: 208–209 (in Polish with English abstract).

Wilczyńska-Michalik, W., Pieczara, P., Łatkiewicz, A. & Michalik, M. (2000): Chemical composition of atmospheric precipitation in Kraków as a factor of salt weathering of stony building materials. In Zioło, Z. (ed.): Działalność człowieka i jego środowisko. Krakow: Wydawnictwo Naukowe Akademii Pedagogicznej w Krakowie, 73–91 (in Polish with English abstract).

Wilczyńska-Michalik, W., Michalik, M., Niezgoda, H. & Hałas, S. (2008): Black crust on the dolomite in polluted urban atmosphere differences in dry and wet deposition dominated environments. Geochimica et Cosmochimica Acta, **72**: A 1020.

Wodzicki, A. (1987): Origin of the Cracowian-Silesian Zn-Pb deposits. Annales Societatis Geologorum Poloniae, **57**: 3–36.

Zabinski, W. (1960): Geochemistry of cadmium in the oxidation zone of Silesia-Cracow zinc and lead ore deposits. Bulletin de l'Academie polonaise des sciences. Serie des sciences, géologiques et géographiques, **8**: 251–254 (in Polish, with English abstract).

Zartman, R.E., Pawlowska, J. & Rubinowski, Z. (1979): Lead isotopic composition of ore deposits from the Silesian-Cracow mining district. In Pawlowska, J., Chidester, H. & Wedow, H., Jr. (eds): Research on the genesis of zinc-lead deposits of Upper Silesia, Poland. Prace Instytutu Geologicznego, **95**: 153–151.

Znosko, J. (1983): Tectonics of southern part of middle Poland (beyond the Carpathians). Geological Quarterly, **27**: 457–470 (in Polish with English abstract).